THE STRUCTURAL BASIS FOR *BURKHOLDERIA PSEUDOMALLEI* HCP-INDUCED MULTINUCLEATED GIANT CELL FORMATION

LIM YAN TING

(B. Sci. (Hons), NUS

A THESIS SUBMITED

FOR THE DEGREE OF DOCTOR OF PHILOSOPHY

NUS SCHOOL OF INTEGRATIVE SCIENCES AND ENGINEERING

NATIONAL UNIVERSITY OF SINGAPORE

2013

Declaration

I hereby declare that the thesis is my original work and it has been written by me in its entirety. I have duly acknowledged all the sources of information which have been used in thesis.

This thesis has also not been submitted for any degree in any university previously.

Lim Yan Ting

22th January 2014

感谢父母多年的呵护，
让我如今拥有机会，
写篇属于自己的故事。

Acknowledgements

First of all, I would like to acknowledge the support of my supervisor. I am most grateful to Paul for the past six years of mentorship. He has been very generous, constructive and his door is always open to us. He has allowed me to be curious about subjects apart from the immediate PhD theme, hence giving me the opportunity to be exposed to a breadth of scientific themes before committing to this final piece of work.

I would also like to thank Yunn for her co-supervision. Her devotion to the topic and constant encouragement have sustained our efforts in investigating this question on *B. pseudomallei* Hcp1. I would like to acknowledge the efforts of our collaborators, Dr Jobi, Manfred, Dr Direk, and Nalini Srinivasan, Jocelyn and Yahua. Without their respective inputs, the story would be incomplete.

During this PhD stint, I was also given the opportunity to study the generation of anti-lipid antibodies, hence I would like to thank the mentorship of Andrew Jenner, Markus Wenk, Brendon Hanson, Conrad and Omedul.

I am hugely indebted to Ms Too Chien Tei, Ms Fatimah Bte Mustafa and Ms Isabelle Chen Gek Joo, for their help in numerous occasions. I am also very grateful to be a part of two dynamic labs, the PAM Lab, the GYH Lab, and to be a member of the Immunology Program.

And finally thank you, Amaury. I am very happy that we have found each other.

Contents

Summary

The Type VI Secretion System cluster 1 (T6SS1) is essential for the virulence and pathogenesis of *Burkholderia pseudomallei* in melioidosis, a disease endemic in many tropical regions. In exposed hosts, the bacterium is taken up by mononuclear phagocytes and survives intracellularly. Inside mononuclear phagocytes, *B. pseudomallei* escapes from phagosomes, initiates actin tail motility and induces cellular fusion with the associated development of multinucleated giant cell (MNGC) formation, a process mediated by T6SS1. Here we analyze the structure and function of a component of the T6SS1 termed hemolysin coregulated protein 1 (Hcp1) that is critical for T6SS1 activity. By employing an in-house conformational-dependent antibody, we show that Hcp1 can be detected on the surface of infected host cells. Furthermore, the recombinant exogenous Hcp1 can bind directly to host antigen presenting cells and enhance MNGC formation upon bacterial infection. Although Hcp1 was undetectable in sera of melioidosis patients, these patients had high titers of IgG against Hcp1. Our structural studies confirm that *B. pseudomallei* Hcp forms hexameric rings that stack into a tube-like assembly with an outer diameter of 80 Å and an inner diameter of 40 Å. In comparison to related bacteria, Hcp1 of *B. pseudomallei* has a unique extended loop region (from Asp40 to Arg56) that potentially acts as a key contact point between adjacent hexameric rings within the tube-like assembly. When key residues within the loop are mutated, the recombinant mutant proteins assembled into hexameric rings that failed to stack and they suppress *B. pseudomallei* induced MNGC formation. Moreover, the *in situ* substitution of these *hcp1* residues in *B. pseudomallei* abolishes MNGC formation and Hcp1 secretion. Taken together, these data provide structural and mechanistic insights into the novel contribution of Hcp1 in *B. pseudomallei* immunogenicity and pathogenesis apart from its structural role in T6SS secretion.

List of Tables

List of Figures

List of Symbols

Amp	ampicillin
APC	antigen-presenting cells
BSA	bovine serum albumin
CO_2	carbon dioxide
DAPI	4',6-diamidino-2-phenylindole
dH_2O	deionized water
DLS	dynamic light scattering
DNA	deoxyribonucleic acid
ELISA	enzyme-linked immunosorbent assay
Fab	fragment antigen-binding
FACS	flow activated cell sorting
FBS	fetal bovine serum
FITC	fluorescein isothiocyanate
HAT	hypoxanthine-aminopterin-thymidine
HCP	hemolysin-coregulated protein
His	polyhistidine
HRP	horseradish peroxidase
IgG	immunoglobulin G
IgM	immunoglobulin M
IPI	International Protein Index
IPTG	isopropyl β-D-1thiogalactopyranoside
LAM	lipoarabinomannan
LB	luria broth
LPS	lipopolysaccharide
MNGC	multinucleated giant cells
MOI	multiplicity of infection

OD	optical density
PAGE	polyacrylamide gel electrophoresis
PB	pacific blue
PBS	phosphate buffered saline
PDB	protein data bank
PE	phycoerythrin
PFA	paraformaldehyde
PMA	phorbol myristate acetate
PS	penicillin/streptomycin
RNA	riboxynucleotide
RPMI	roswell park memorial institute medium
T6SS	type six secretion system
TBS	tris buffered saline
TCEP	*tris*(2-carboxyethyl)phosphine
TMB	3,3',5,5'-tetramethylbenzidine
TSAP	thermosensitive alkaline phosphatase
SAD	single wavelength anomalous diffraction
SDS	sodium dodecyl sulfate
SepA	sepharose A
SSF	salt-free LB media supplemented with sucrose
X-gal	5-bromo-4-chloro-3-indolyl-β-D-galactopyranoside

List of Publications

1. Extended loop region of Hcp1 is critical for the assembly and function of Type VI Secretion System in Burkholderia pseudomallei.
   Yan Ting Lim, Chacko Jobichen, Manfred Raida, Direk Limmathurotsakul, Shaowei Li, Jocelyn Wong, Yahua Chen, Nalini Srinivasan, Paul Anthony MacAry, Jayaraman Sivaraman, Yunn Hwen Gan
   Manuscript in preparation

2. Lipid anti-lipid antibody responses correlate with disease activity in systemic lupus erythematosus.
   Jovanović V, Abdul Aziz N, Lim YT, Ng Ai Poh A, Jin Hui Chan S, Ho Xin Pei E, Lew FC, Shui G, Jenner AM, Bowen L, McKinney EF, Lyons PA, Kemeny MD, Smith KG, Wenk MR, Macary PA.
   PLoS One. 2013;8(2):e55639. doi: 10.1371/journal.pone.0055639. Epub 2013 Feb 7.

3. Generation and characterization of a novel recombinant antibody against 15-ketocholestane isolated by phage-display.
   Islam MO, Lim YT, Chan CE, Cazenave-Gassiot A, Croxford JL, Wenk MR, Macary PA, Hanson BJ.
   Int J Mol Sci. 2012;13(4):4937-48. doi: 10.3390/ijms13044937. Epub 2012 Apr 19.

4. Characterization of human umbilical cord lining-derived epithelial cells and transplantation potential.
   Zhou Y, Gan SU, Lin G, Lim YT, Masilamani J, Mustafa FB, Phua ML, Rivino L, Phan TT, Lee KO, Calne R, MacAry PA.

Cell Transplant. 2011;20(11-12):1827-41. doi: 10.3727/096368910X564085. Epub 2011 Mar 24.

5. Fc gamma receptor biology and systemic lupus erythematosus.
   Jovanovic V, Dai X, Lim YT, Kemeny DM, MacAry PA.
   Int J Rheum Dis. 2009 Dec;12(4):293-8. doi: 10.1111/j.1756-185X.2009.01426.x. Review.

6. Suppression of host innate immune response by Burkholderia pseudomallei through the virulence factor TssM.
   Tan KS, Chen Y, Lim YC, Tan GY, Liu Y, Lim YT, Macary P, Gan YH.
   J Immunol. 2010 May 1;184(9):5160-71. doi: 10.4049/jimmunol.0902663. Epub 2010 Mar 24.

7. Differential signal transduction, membrane trafficking, and immune effector functions mediated by FcgammaRI versus FcgammaRIIa.
   Dai X, Jayapal M, Tay HK, Reghunathan R, Lin G, Too CT, Lim YT, Chan SH, Kemeny DM, Floto RA, Smith KG, Melendez AJ, MacAry PA.
   Blood. 2009 Jul 9;114(2):318-27. doi: 10.1182/blood-2008-10-184457. Epub 2009 May 6. Erratum in: Blood. 2013 Apr 4;121(14):2814.

Chapter 1.

Introduction

1.1 Melioidosis

1.1.1 A brief history of the disease and its causative agent *Burkholderia pseudomallei*

Melioidosis, also known as pseudoglanders or Whitmore's disease, is derived from the Greek words *melis* (distemper of the asses), *oeidēs* (resemblance) and *osis* (a suffix indicating an abnormal condition or disease), which reflect the nature of this glander-like illness.[1,2] It is caused by the bacterium *Burkholderia pseudomallei* (previously called *Pseudomonas pseudomallei*). The bacterium is an aerobic, Gram-negative motile bacillus found in moist soil and water, and is endemic to the tropical and subtropical regions. It is an opportunistic pathogen that is capable of producing exotoxins and surviving within phagocytic cells, hence latent infections are a common disease manifestation. It is closely related to *Burkholderia mallei*, its infectious counterpart that affects equine hosts.

The disease was first described in 1912 by the pathologist Captain Alfred Whitmore and his assistant C. S. Krishnaswami in emaciated morphine addicts in Rangoon, Burma.[3] Autopsies of the morphine addicts revealed consolidation in the lungs and abscesses in the liver, spleen, kidneys and beneath the skin. The disease bore similarities to glanders, but the deceased did not have prior

exposure to the equine hosts. Microbiological tests showed that the causative bacterium was distinct from that of glanders; when cultivated on peptone agar and potato slopes, the bacterial colonies grew more rapidly, were motile, and did not elicit the Strauss reaction that was characteristic of *B. mallei* upon injection into the peritoneal cavity of guinea pigs. Ambrose Thomas Stanton, a bacteriologist, and William Fletcher, a pathologist, identified this causative agent as *Burkholderia pseudomallei* in 1917.[4]

Following the identification of *B. pseudomallei*, the disease was recognized in soldiers stationed in endemic areas such as Vietnam, Sri Lanka and Indonesia.[1,5] It particularly affected the French soldiers that were stationed in Vietnam between 1948 and 1954, with over 100 cases diagnosed, and over 300 cases among the US troops during the Vietnam War.[2,5] The majority of the cases were acquired via direct contact with soil and mud. However, an unusual number of cases among the helicopter crews suggested that inoculation could also occur via inhalation.[6] The latent nature of the infection was also discovered as many soldiers had reoccurrence, with the longest documented latent period of 29 years.[7]

1.1.2 Current disease epidemiology

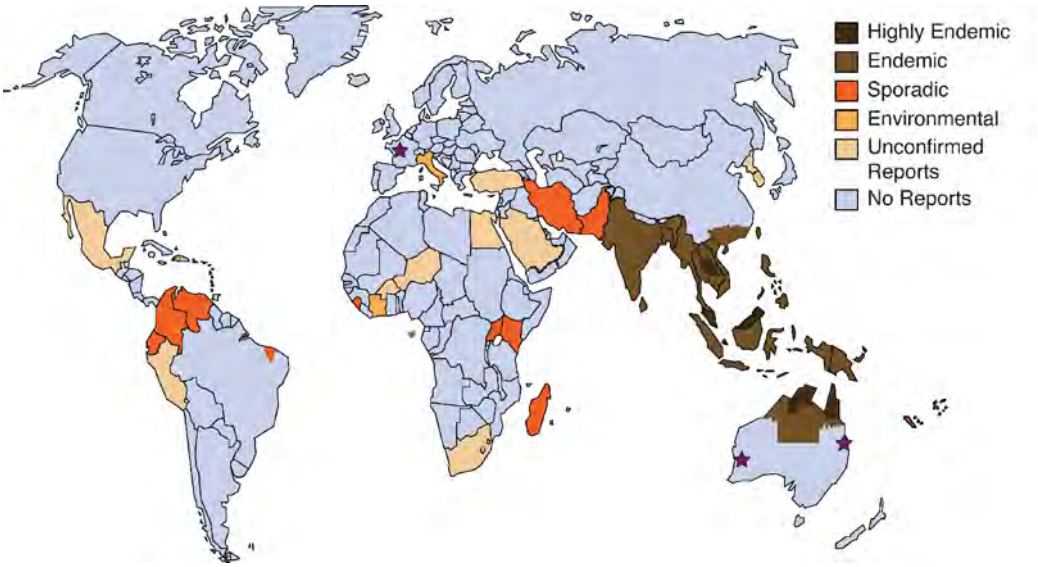

Figure 1: Global distribution of melioidosis and Burkholderia pseudomallei as of the year 2008. Adapted from Dance, 1991, Currie and Cheng, 2005 and Currie et al., 2008.[2,5,8] Purple stars indicate reported temperate outbreaks of melioidosis: France; southeast Queensland, Australia; and southwest Western Australia.

The main endemic foci of melioidosis are Southeast Asia and northern Australia. Northeastern Thailand, parts of Malaysia, Singapore and the 'Top End' of northern Australia are currently recognized as 'highly endemic' locations where many cases are diagnosed each year (Figure 1).[2,5,8] It is most frequently reported from Darwin, northern Australia, where it is the most common cause of fatal community-acquired septicemic pneumonia.[9] The Top End of northern Australia, which is the second northernmost point of the continent, has the highest documented average annual incidence rate of 19.6 cases per 100,000 population between 1989 and 2003.[9] The disease is also the most common cause of community-acquired bacteremia in northeast Thailand.[10,11] Ubon Ratchathani, its largest province, reported a comparable average annual incidence rate of 12.7

cases per 100,000 population between 1997-2006.[11]

Table 1: Comparative epidemiology of melioidosis in Southeast Asia and Australia.

	Australia[9]	Thailand[11]	Singapore[12]	Pahang, Malaysia[13]	Alor Setar, Malaysia[14]
No. of cases	252	2217	693	135	145
Average annual incidence*	19.6	12.7	1.7	6.1	16.4
Average mortality rate (%)	19	42.6	16.2	54	34

Adapted from Hassan et.al (2010).[14] ***per 100,000 population per year***

Several studies have reported increased incidence rates within the highly endemic region. The Alor Setar region of Kedah, Malaysia, reported an average annual incidence rate of 16.35 per 100,000 population between 2005 and 2008[14] (Table 1), as compared to the Pahang state, Malaysia, with an average annualincidence rate of 6.1 between 2000 and 2003.[13] A study performed in northeast Thailand between 1987 and 1991 reported the incidence rate as 4.4 per 100,000[10] but a subsequent follow-up study updated the incidence rate to 12.7 per 100,000 population between 1997 and 2006.[11] Although the incidence rate in Singapore generally decreased from 2.9 to 1.4 per 100,000 population between 1998 and 2007, there was an outbreak of melioidosis in the first quarter of 2004, with a total of 23 cases with onset of illness over a 5 week-period.[12] For most studies, there was a positive association of the disease with severe weather events and rainfall, with the exception to a few study series in Thailand between 1997-2006 (negative correlation) and Singapore (no correlation) in July 1995.[15]

Apart from Singapore, where melioidosis is statutorily notifiable since 1989, and Australia,[2] most human melioidosis cases are underreported, thus obscuring

the true global distribution and incidence rates of melioidosis. Continuing efforts at laboratory strengthening and improvement of global disease surveillance over the last two decades show an expansion in the geographical boundaries of melioidosis.[16] Sporadic and outbreak cases in new geographical regions, such as south and east Asia as well as parts of South America, Papua New Guinea, the Caribbean and Africa were reported.[8,17–21] There is also an increase in number of cases in travellers and returning military personnel.[22–26]

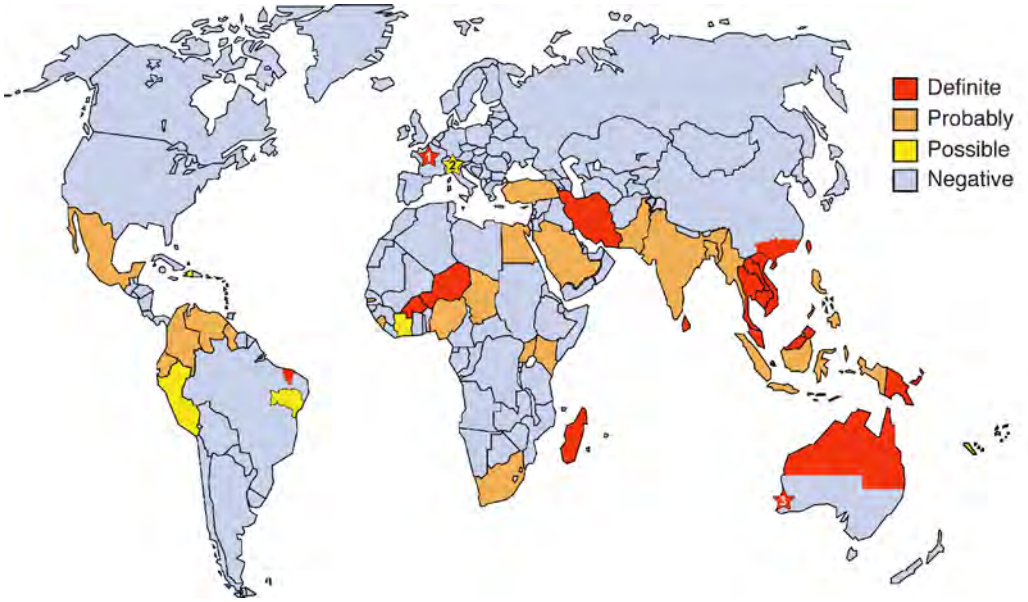

Figure 2: Global distribution of environmental B. pseudomallei as of the year 2013. 'Definite' was defined by the detection of environmental B. pseudomallei using culture or a B. pseudomallei-specific PCR with or without evidence of melioidosis having been acquired in that country. 'Probable' was defined by clinical reports that indicated in-country disease acquisition and in the absence of published literature of environmental sampling. 'Possible' was defined as the detection of environmental B. pseudomallei using culture or a B. pseudomallei-specific PCR that did not distinguish between B. pseudomallei and the highly related Burkholderia thailandensis. (1) and (3) highlight the definite detection of environmental B. pseudomallei in Paris,[153] and Chittering, Australia.[151] (2) highlight the possible detection of environmental B. pseudomallei in Bologna, Italy.[155] Adapted from Limmathurotsakul et al., 2013.[17]

An international working party (Detection of Environmental *Burkholderia pseudomallei* Working Party (DEBWorP) was formed in 2010 with the aim

reviewing the literature on the detection of environmental *B. pseudomallei* and formulating a consensus guideline for environmental sampling of the bacteria.[17] The study reported that as of the year 2013, there was definite evidence for the presence of environmental *B. pseudomallei* in 17 countries (Figure 2), which was defined by the detection of *B. pseudomallei* from the environment using culture of a specific polymerase chain reaction (PCR) for *B. pseudomallei* with or without evidence of melioidosis having been acquired in that country. A comparison of the global distribution of melioidosis (Figure 1) against that of environmental *B. pseudomallei* (Figure 2) highlights the countries that have sporadic melioidosis cases but also have the definite presence of environmental *B. pseudomallei* such as Brazil. It is possible that the sporadic cases are merely the "tip of the iceberg",[5] hence these countries should consider increasing surveillance of the disease and improving access to diagnostic laboratory facilities. The true global distribution of environmental *B. pseudomallei* and the actual risk map of melioidosis continues to be redefined.

1.1.3 Clinical features

The clinical features of melioidosis have been reviewed in detail. In summary, these include associated risk factors, mode of transmission, its clinical presentation, diagnosis and treatment.[2,28,29]

1.1.3.1 Risk factors

Type II diabetes is by far the strongest comorbity associated with

melioidosis.[11,30] Other comorbidities include chronic lung disease, chronic renal failure, and liver disease.[29] Conditions that cause immune suppression such as corticosteroid therapy, thalassemia, systemic lupus erythematosus, malignancy and alcoholism are also implicated.[29] In addition, occupational or recreational exposure to moist soil or surface water also increases the risk of acquiring the disease. People that fall into this high-risk category include rice farmers, other agricultural workers, construction labourers, adventure travellers, military personnel and a variety of indigenous groups.[2]

1.1.3.2 Mode of transmission

Infection by *B. pseudomallei* can be acquired in three possible ways, i.e., inoculation, inhalation and ingestion.[6,27,31]. Of the three, inoculation by means of direct contact with contaminated soil and water through penetrating wounds is considered the major mode of acquisition. Extreme weather that generates heavy rainfall and winds may cause a shift towards inhalation as the major route of infection.[32] Ingestion as a mode of infection was observed in animals, through the discovery of an infected gastrohepatic node in pigs.[33] However a recent study in Thailand, which is the first evidence-based study, examined the activities of daily living associated with melioidosis, together with routes of infections.[34] There is increased risk of acquiring melioidosis with working in rice fields, washing in water pooled in the rice field, working without protective clothing, barefooted walking, having an open wound, direct application of herbal remedies to open wound.[34] In addition, they showed that the consumption

of food contaminated with soil or dust, and drinking untreated water also increased the risk of acquiring melioidosis, demonstrating for the first time that ingestion was also an important route of human *B. pseudomallei* infection.[29] All other modes of transmission such as person-to-person transmission,[35,36] neonatal transmission,[37–40] and epizoonotic human infections[41] are rarely observed.

1.1.3.3 Clinical presentation and mortality rate

The clinical features of melioidosis reported thus far are illustrated in Figure 3. The disease presentation varies from asymptomatic infection and localized skin ulcers or abscesses without systemic illness to fatal septicaemia with lung and multiple organ abscesses.[3] The Infectious Disease Association of Thailand summarized 345 cases into these four categories[42] 1) disseminated septicaemic melioidosis, defined as positive blood culture and multiple organs involvement, 2) non-disseminated septicaemic melioidosis, defined as positive blood culture with one or no apparent focus of infection, 3) localized melioidosis, with a single focus of infection, and 4) transient bacteremia.[43,44] In all series of cohort studies on melioidosis, pneumonia and bacteremia are the most common presentations of melioidosis and are present in about 50% of all cases.[11,15,30,39,45,46] Important clinical differences were observed from the cohort studies based in the Royal Darwin Hospital, Australia and Sappasithiprasong Hospital, Thailand. The incidence of genitourinary infection and prostate melioidosis is higher in Australian male patients (approximately to 20%),[30] as opposed to 7% and 0.3% for the respective presentations in Thai male patients.[31] There is an absence of

supparative parotitis in Australia,[47–50] but this presentation accounts for 30-40% of pediatric melioidosis in Thailand.[51] Encephalomyelitis is seen in 3% of adult melioidosis presentations in northern Australia[30] and in small numbers of children in Australia and Thailand.[47,52] Internal organ abscesses are common, but spleen and liver abscesses (74% and 46% for the respective foci) predominate the Thai cohort,[46] whereas prostate abscesses were extremely common in the Darwin series, being present in 20% of the males patients.[30]

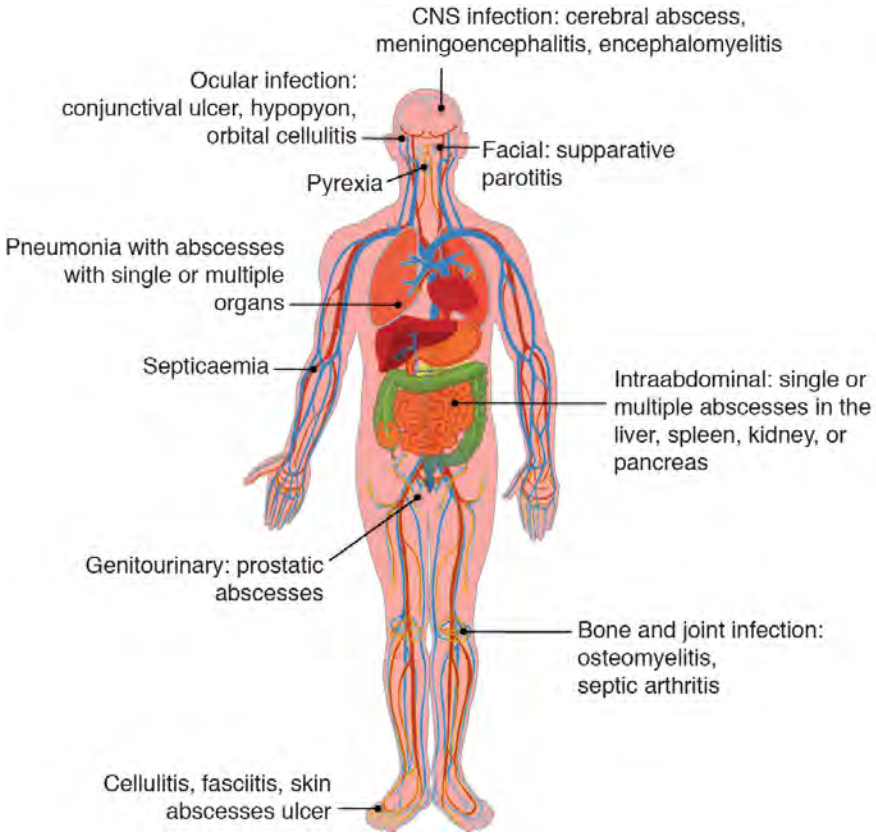

Figure 3: Clinical presentation of melioidosis.[28,29]

The absence of any risk factors associated with melioidosis is strongly predictive of survival.[30] With early diagnosis, availability of resources to provide appropriate antibiotics and critical care, it is unlikely for a healthy

person to die from melioidosis.[30] In the cohort studies from Thailand and Australia, the decrease in average mortality rate (49% in 1997 to 40.5% in 2006 in Thailand, and 30% in 1989 to 9% in 2009 in Australia) have been attributed to these factors.[11,30] The mortality rate in Thailand is double that reported for patients with melioidosis in Australia, and it has been attributed to the limited availability of intensive care facilities.[11]

1.1.3.4 Diagnosis and Treatment

Culturing the organism from any clinical sample remains as the gold standard for diagnosing melioidosis, but these established methods are time consuming, with a median time to culture positivity of 48 hours.[53] A few other techniques have been employed in the attempt to reduce the time required for diagnosis, including antigen detection on specimens or on culture supernatants, antibody detection, molecular techniques and rapid culture techniques.[54] However, few are sufficiently sensitive or specific for routine clinical use and only indirect hemagglutination, latex agglutination and immunofluorescence are currently in use clinically.[55–59]

Therapy for melioidosis requires a combination of prolonged antibiotics and intensive care medicine to cure the infection and prevent relapse. The current guidelines for treating melioidosis are based upon the results from several clinical trials.[60,61] It is divided into two stages, an intravenous high intensity phase, and an oral eradication phase to prevent recurrence. For the intensive

phase, intravenous ceftazidime or the carbapenem antibiotics (imipenem and meropenem) are given for a minimum of 10 to 14 days.[60,61] This is followed by the eradication phase therapy, which consists of oral administration of the antibiotics trimethoprim-sulfamethoxazole for three to six months.[61] In the most recent study on the oral antibiotic regimen duration, 20 weeks chosen as the minimum duration, but the authors stated that the optimal duration remains to be determined.[61] The treatment and management of severe clinical presentations are also critical in determining the outcome of the disease.[60] The rate of recurrent infection due to relapse of an unsuccessfully eradicated infection was 5.4%, with a median time to relapse of 8 months from initial admission in the Darwin study,[30] and 9.7% with a median time time to relapse of 6 months from commencement of oral therapy in the Thailand study.[62] In both studies, the choice, duration of and compliance with antibiotic therapy were the most important determinants of relapse.

1.2 *Burkholderia pseudomallei* and the role of the type six secretion system (T6SS)

B. pseudomallei is a facultative intracellular bacterium that is capable of invading and replicating within host cells, especially phagocytes and epithelial cells.[28,63] *B. pseudomallei* invasins, which are yet to be identified, facilitate actin-dependent internalization of the bacteria into single membrane primary endosomes.[64] The activity of its *Burkholderia* secretion apparatus (Bsa) type III secretion system cluster 3 ($T3SS_{Bsa}$) then directs bacterial escape from the

primary endosome, but is otherwise dispensable for subsequent intracellular events.[64] The bacterium has two independent motility systems, flagellar (Fla2) or actin based (BimA), and at least one of these two systems is required for intracellular motility.[64] Its type six secretion system cluster 1 (T6SS1) facilitates subsequent cell fusion events leading to the formation of multinucleated giant cells (MNGCs) and eventually cell death.[64]

With respect to pathogenic mechanism employed by the bacterium, the induction of MNGC formation in infected phagocytic or epithelial cells is a feature unique to *B. pseudomallei*[65] and *Mycobacterium tuberculosis*.[66] The presence of granulomas and giant cells in mouse models[67] and in melioidosis patients[68] suggests the relevance of MNGC in disease pathogenesis. It is unclear whether MNGC formation is induced by the pathogen to evade the immune system or as a protective host response.[67] The mechanism for *B. pseudomallei*-induced MNGC formation is not well understood, but previous studies have suggested that the process requires an intermediate direct cell-to-cell fusion stage.[65] Specific host adhesion proteins such as integrin-associated protein (CD47), E-selectin (CD62E), a fusion regulatory protein (CD98) and E-cadherin (CD324) were shown to be involved in *B. pseudomallei*-induced MNGC formation, and CD47 and CD62E were upregulated upon infection.[69] As aforementioned, it has been shown that MNGC formation requires a functional Type VI Secretion System cluster-1 (T6SS1) of *B. pseudomallei*.[70,71] Thus, it is likely that the components involved in MNGC formation are found within this gene cluster.

1.2.1 The discovery of T6SS

Hemolysin co-regulated protein (Hcp), a hallmark protein of the T6SS, was first identified as a protein whose *in vivo* expression was coordinately regulated with the hemolysin HlyA from *Vibrio cholerae.*[72] The lack of a hydrophobic signal peptide indicated that Hcp was secreted by a novel mechanism independent of the general secretory Sec pathway.[72] The cluster of genes that encode for this novel secretory pathway in *V. cholerae* were originally named IAHP, IcmF-associated homology proteins because one of its genes, subsequently named *icmF*, is highly homologous to IcmF from the Type IV protein secretion system of *Legionella pneumophila.*[73] The gene cluster, termed as *imp* (impaired in nitrogen fixation) locus in *Rhizobium leguminosarum*, was important for nodulation and symbiosis between the bacteria and *Pisum* sativa. The gene locus was subsequently found in several other animal pathogens such as *Pseudomonas aeruginosa*, *Vibrio cholerae*, *Edwardsiella ictaluri* and was required for the secretion of proteins into the environment.[74]

This locus also encodes for a virulence-associated secretion (VAS) system of *V. cholerae* towards *Dictyostelium* amoebae and was predicted to be responsible for mediating extracellular export of virulence factors and their translocation into target eukaryotic cells.[75] The authors proposed to name this gene locus as the type VI secretion system (T6SS) because it was a novel ensemble of genes that was linked to a secretion pathway of proteins without N-terminal signal peptides. Its homolog in *Pseudomonas aeruginosa* was the Hcp1 secretion

island (HSI-1), which was responsible for the export of Hcp1, a hexameric protein that formed rings with a 40 Å internal diameter.[76]

1.2.2 The type six secretion system (T6SS)

The T6SS appears to be the most widespread specialized secretion system, with putative T6SSs gene clusters predicted to exist in 25% of all Gram-negative bacteria, such as *Escherichia coli*, *Salmonella typhimurium*, *Yersinia pestis*, *P. aeruginosa*, *V. cholerae*, *Aeromonas hydrophila*, *Edwardsiella tard*a and the *Burkholderia* species.[77] Comparative genomic analyses revealed that the T6SS gene clusters, which generally consists of 15-20 genes, are in a specific conserved genetic organization.[78] In many instance, a single organism could possess multiple copies of the T6SS gene cluster, whose expression levels are distinctly regulated under different milieu.[70,71,79–81] Although it was initially discovered as a virulence factor in several pathogens, cumulative studies to date provide a more complete and nuanced view on the role of T6SS as an important mediator of antagonistic or non-antagonistic interbacterial interactions in both pathogenic and non-pathogenic bacteria.[82,83] The unifying theme to date on the role of T6SS is the delivery of bacterial effectors into the target eukaryotic and prokaryotic cells. Hence current models of T6SS often orientate the bacterial T6SS secretion system from the extracellular milleu towards the membrane the target cells, giving the impression of the T6SS penetrating the target membrane from the outside inwards.

1.2.3 Regulation of T6SS1 in *B. pseudomallei*

In the case of *B. pseudomallei* K96243 strain, its genome encodes six T6SS clusters, designated as T6SS1 (BPSS1496-BPSS1511), T6SS-2 (BPSS0515-BPSS0533), T6SS-3 (BPSS2090-BPSS2109), T6SS-4 (BPSS1660-BPSS0185), T6SS-5 (BPSS0091-BPSS0117), and T6SS-6 (BPSL3096-BPSL3111).[72] Its T6SS1 contributes to the pathogenic interactions of the bacterium with the host.[60,61,8]

Figure 4: Genetic organization of T6SS1 in B. pseudomallei (BPSS1490 to BPSS1514). Genes and their direction of transcription are represented by arrows. Annotation of the tss genes are adapted from Schell et. al (2007). Shown in green is the bim clusters where bimA is required for actin tail motility. The T6SS genes are shown either in their corresponding colours from Figure 6 or in black. Shown in light blue are virA and G homologs, the two-component system that regulates the T6SS cluster. Genes of unknown function are in purple. Adapted from review by Jocelyn Wong and Yunn-Hwen Gan (unpublished work).

It was first discovered via in vivo expression technology that *B. pseudomallei* T6SS1 was only expressed when the bacterium is inside host cells.[85] The expression of T6SS1 is tightly regulated by VirAG, a two-component histidine sensory kinase, and an AraC-type regulator BprC, an AraC regulator located within the adjacent T3SS3,[71] which is also true for *B. mallei,* its equinine pathogenic equivalent.[70,79] In free-living *B. pseudomallei*, the expression of T6SS1 is driven by BprC alone.[71] However inside host cells, VirAG becomes the major regulator of all T6SS1 genes starting from *hcp1*.[71] The *tssAB* operon remains as the exception, which remains mainly regulated by BprC (Figure 5).[71]

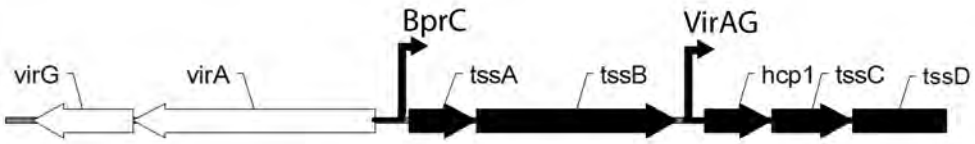

Figure 5: Promoter sites in the T6SS1 gene cluster. Bent arrows indicate promoter sites and their regulators. Block arrows indicate transcription directions. Adapted from Chen et al., 2011.[71]

Intracellular host signals that are sensed through VirAG to drive the transcription of T6SS1 genes have yet to be determined. It was thought that the source of these intracellular signals were derived from the phagosomal compartment from which the bacteria escapes,[79] but experiments that bypass the phagosomal trafficking suggest that these signals could come from the host cytosol instead.[64] However, a model on the orientation of the T6SS1 from *B. pseudomallei* would have to differ from current reported models of T6SS1.[78,86] It would originate from within the eukaryotic host towards the extracellular millieu, as the T6SS1 is only expressed when the bacteria is within host cytosol.

1.2.4 Structural biology of T6SS

It has been proposed that the T6SS is a macromolecular nanomachine that facilitates the transport of bacterial proteins across both the inner (IM) and outer bacterial membrane (OM) in a single step (Figure 6).[75,76,83,87]

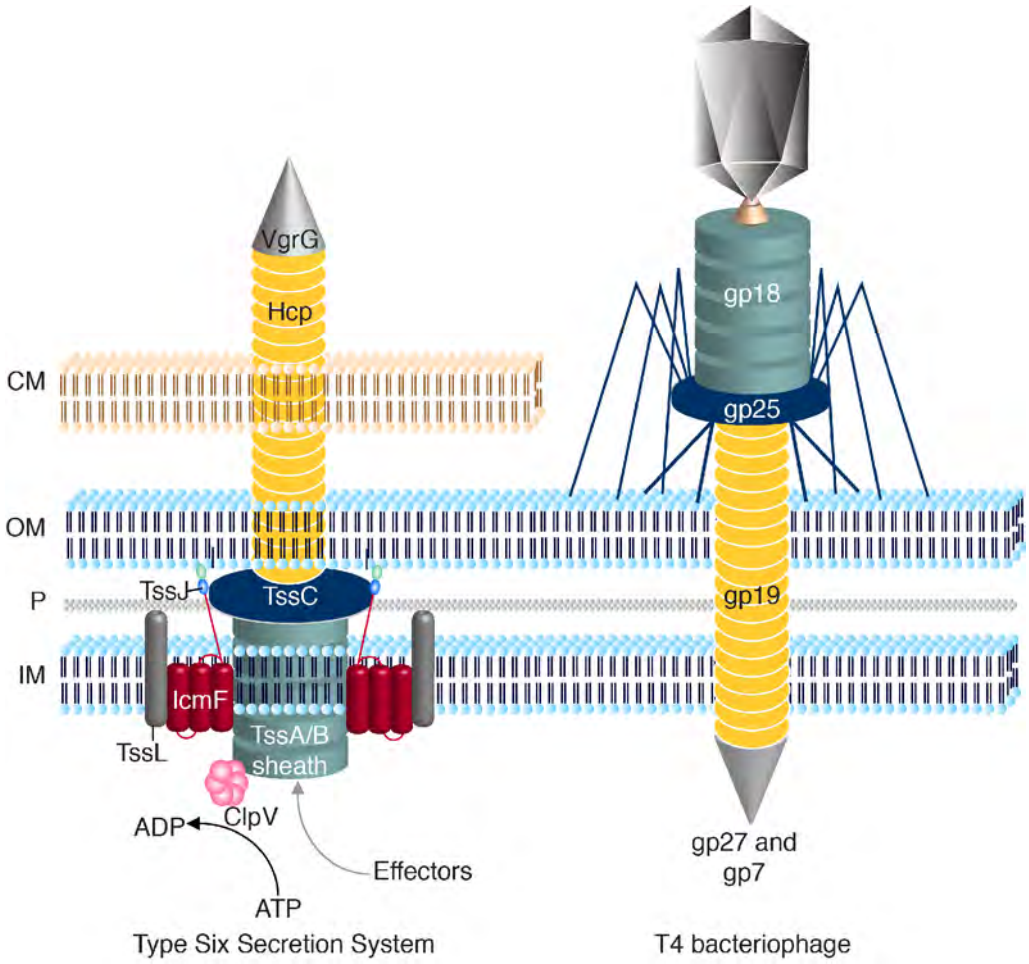

Figure 6: The type six secretion system (T6SS) and the T4 bacteriophage tail. The schematics illustrate the localization and topologies of the T6SS core proteins. The proteins are labelled with their gene products. Homology between T6SS and phage protein sequences, and predicted subcellular localization of proteins form the basis of the T6SS model. T6SS proteins sharing homology with phage proteins are coloured the same as their T4 phage counterparts. CM, host cell membrane; OM, bacterial outer membrane; P, peptidoglycan; IM, bacterial inner membrane. Adapted from Records, 2011.

Approximately fifteen core genes within the cluster encode the T6SS and studies on their gene products suggest that T6SSs are anchored contractile syringes that use a mechanism similar to the injection device of bacteriophages (Figure 4 and 7).[77,88,89] The T6SS protein components can be divided into two groups: membrane or membrane-associated proteins that form the anchor complex required for coupling the energy generated by contraction of the

tubular sheath to protein export across the membranes, and soluble proteins that share a common evolution history with subunits forming the bacteriophage's injection tail.[90]

The basic anchor complex requires TssL, an IM protein that can be associated or fused with TagL (not illustrated), an IM protein that has a peptidoglycan binding domain, IcmF, an IM protein with a periplasmic domain that forms a complex with TssL, and TssJ, a lipoprotein anchored to the OM that binds to IcmF's periplasmic domain (Figure 6).[91] The interactions between these proteins effectively link the peptidoglycan and both membranes to provide an anchored housing to the contractile hypodermic portion of the T6SS apparatus.

The hypodermic device of a typical bacteriophage comprises of a baseplate and a contractile sheath that houses an inner noncontractile tube attached to a tail spike complex (Figure 6). Contact with the host cell surface induces conformational changes to the baseplate that triggers the contraction of the sheath, leading to the expulsion of phage's inner tube and tail spike complex.[92] The protein TssC from the T6SS gene cluster shares high sequence homology with the T4 bacteriophage's baseplate protein gene product (gp) 25.[88,93]

ClpV-interacting proteins TssA and TssB are structural homologs of the T4 tail sheath proteins.[94,95] TssA and TssB form tubular complexes up to 500 Å in length, and their dynamic remodelling permits the reuse of the injection machinery. Their disassembly is powered by the AAA+ ClpV ATPase under

adenosine triphosphate (ATP) consumption, which specifically binds to contracted TssA/B.

TssA/B complexes have an outer diameter of 300 Å and an inner diameter of 100 Å, which is sufficient to harbour the shaft of the inner tube, formed by haemolysin co-regulated protein (Hcp). Hcp, together with the protein valine-glycine repeat protein G (VgrG), are two structurally conserved proteins that form the shaft and the needle tip respectively.[76,96,97] The contraction of TssA/B is thought to be responsible for their ejection into the extracellular milieu.[96,98] The export of Hcp and VgrG orthologues represents the universal activity of all T6SSs.[99]

1.2.5 The structure of VgrG and Hcp

Structural studies of Hcp1 homologues from other bacteria showed that the Hcp1 is able to form hexameric rings with an outer diameter of 80 Å and inner width of 40 Å, and structural models suggest that these rings are able to polymerize in a head-to-head or head-to-tail fashion to form filamentous tubes.[76,96,100] Crystal structures of Hcp from *P. aeruginosa* and *E. tarda* consistently highlight its remarkable structural semblance to components of a bacteriophage tail.[76,101,102] It has high structural homology to the major tail protein gpV of bacteriophage λ, or gp19 of bacteriophage T4. These tubes form the inner shaft of the T6SS and are proposed to serve as a conduit for other canonical T6SS protein substrates to diffuse through.[100]

The sequence and structure of the N-terminal fragment of VgrG from the uropathogenic *E. coli* CFT073 was compared against the gp5-gp27 of the T4 bacteriophage. Despite the low sequence identity (13%) between VgrG and the gp5-gp27 complex, the N-terminal portion of VgrG is well superimposable on gp5-gp27 as a single connected polypeptide chain. Current models propose that the trimeric VgrG protein is harboured at the tip of the Hcp tube and they function as the puncturing device towards target cells.[96] The surface assemblies of Hcp and VgrG are mutually dependent, as VgrG is absent in the culture supernatant of *hcp*$^{-}$ cells and Hcp is absent in *vgrG*$^{-}$ cell supernatant.[75,89,103,104] One may hypothesize that Hcp assembly is triggered by VgrG recruitment to the apparatus, and the polymerization of the Hcp tube subsequently pushes the VgrG protein towards the external medium to puncture target cells.[78,105]

1.2.6 The immunobiology of Hcp to date

B. pseudomallei carries six copies of Hcp (Hcp1-Hcp6), each corresponding to its six T6SS clusters. Hcp1 is not constitutively expressed in both wild type *B. pseudomallei* and *B. mallei* but the overexpression of *virAG* regulatory genes would drive its expression and subsequent secretion, making it detectable in the supernatant.[71,84] The *Δhcp1 B. pseudomallei* mutants were highly attenuated in mice,[70] confirming the critical role of T6SS1 for bacterial virulence in mammalian hosts. It is not known whether *B. pseudomallei* Hcp1 exerts any function apart from its structural role in the assembly of the T6SS needle for secretion of T6SS substrates. However, the function of Hcp is more extensively

explored in other bacteria. Hcp has the ability to adhere to the surface of mammalian cells, and the functional consequence of this binding had been investigated in *A. hydrophila*[106] and meningitis-causing *Escherichia coli* K1 strain RS218.[107]

When exogenously complemented in the *A. hydrophila ΔvasH* mutant, Hcp reduced uptake of bacteria by macrophages, increased bacterial virulence in a septicaemic mouse infection model. Furthermore, it inhibited production of proinflammatory cytokines by stimulating release of immunosuppressive cytokines such as interleukin-10 (IL-10) and transforming growth factor-beta (TGF-β).[106] *E.coli* K1 strain RS218 has two hcp-like gene designated *hcp1* and *hcp2*,. The protein Hcp2 is responsible for cellular invasion and adhesion, but Hcp1 is the secreted effector that has the ability to cause changes to the host cells on its own, such as inducing actin cytoskeleton rearrangement, apoptosis and release of IL-6 and IL-8 in human brain microvascular endothelial cells.[107]

In the context of cystic fibrosis, Hcp1 was found in the sputum of a patient infected with *P. aeruginosa* actively secreting Hcp1 *in vitro*.[76] Anti-Hcp1 response was also detected in patients chronically infected with *P. aeruginosa*. With respects to *Aeromonas hydrophila SSU*, circulating antibodies against Hcp were detected after infection in mice. These findings suggest that Hcp is highly immunogenic.[108] In *B. pseudomallei*, anti-Hcp1 antibodies could be detected via immunoblotting from pooled patient sera.[70] This means that Hcp1 protein was available for immune processing during bacterial infection. A recent study

showed that the inner ring of Hcp from *P. aeruginosa* interacts specifically with Tse2, a cognate T6SS effector, and serves as a exported chaperone and receptor protein to T6SS effector molecules.[109]

1.2.7 Aims of the project

The principle objective of this project was to determine whether Hcp1 from *B. pseudomallei* is able to exert any effects on host cells apart from its structural role in supporting T6SS substrate secretion, including its own secretion. This objective can be broadly summarized in the following specific aims:

Aim I. To generate biochemical tools and reagents that detect the interaction of Hcp1 with host cell.

Aim II. To determine the structure of *B. pseudomallei* Hcp1 so as to define the structure-function relationship of Hcp1 in *B. pseudomallei*-infected host cells.

Chapter 2.

Materials and Methods

2.1 Primers and Bacterial Strains

2.1.1 List of primers

Table 2: List of primers.

Primer (PCR)	Sequence (5'-3')	T_a (°C)
Hcp1F	CATATGCTGGCCGGAATATATC	55
Hcp1R	CTCGAGTCAGCCATTCGTCCAGTT	55
Hcp1UpF	CCATGATTACGAATTCGTACGTCGTCGACATGGAC A	60
Hcp1UpR	TACCCGGGGATCCTCGATGTGGATTTTCCCGTCAT	60
Hcp1DnF	GAG GAT CCC CGG GTA TCA CGT TGA CGA AGG AAA TG	60
Hcp1DnR	CCAAGCTTGCATGCCTGCAGCGATCTGCGCTTCG ATTT	60
Hcp1Up3	GGAGCCTTTGATTTCCCCCT	60
Hcp1Dn3	GAAATCAAAGGCTCCGCGGGCGCCGCAAACTGG AC	60
Hcp1FH	GGCCAGTGCCAAGCTTGCAGATCGTCGTGTCGGA	60
Hcp1RB	CGGTACCCGGGGATCCGATCAGCCATTCGTCCAG T	60
TssCRB	CGGTACCCGGGGATCCGCGCTTCAGGAAATCGTT	60
Hcp1Q46AE47AF	GCGGCGGGCCTGACGCCCGCCGCCGCCGCTCGC	60
Hcp1Q46AE47AR	CGTCAGGCCCGCCGCGAGCCTGGCAGGCATGTC	60
Hcp1L49AT50AF	CAGGAAGGCGCGGCGCCCGCCGCCGCCGCTCGC	60
Hcp1L49AT50AR	CGCCGCGCCTTCCTGGAGCCTGGCAGGCATGTC	60

Abbreviations: T_a, annealing temperature.

Primer (realtime PCR)	
Gene	
hcp1	CACATCCTCGCCTTCAA TCTCGAACTCTTCCATCATCT
rpoB	GTTCCATCGTTCACCAAGTG TTGCAGAAATGTGCTGAATG

2.1.2 List of plasmids and bacterial strains

Table 3: List of plasmids and strains.

Plasmid/Strain	Relevant characteristic(s)[a]	Reference
Plasmid		
pET28a-*hcp1*	pET28a containing codon 1-169 of BPSS1498	This study
pET22b-*hcp1*	pET22b containing codon 1-169 of BPSS1498	This study
pK18*mobsacB*	Conjugative, suicide vector, Km^r	[110]
pFRTT1	pGEM-T contains a *tet* cassette with FRT sites and tetRA genes, Ap^r, Tc^r	[111]
pMLBAD	Broad host range vector, Tm^r	[112]
pUCP	pUCP28T empty vector	[113]
pUCP-*hcp1*	pUCP28T containing codon 1-169 of BPSS1498	This study
pUCP-*hcp1-tssC1*	pUCP28T containing codon 1-169 of BPSS1498 and codon 1-153 of BPSS1499	This study
B. pseudomallei		
KHW	*B. pseudomallei* wild type strain	[114]
ΔvirAG::tet	*B. pseudomallei*, codon 56-614 of BPSS1495 and codon 1-233 of BPSS1494 were replaced with the *tet* cassette from pFRTT1	This study
Δhcp1::tmp	*B. pseudomallei,* nucleotide position 335 to 446 of BPSS1498 was replaced with the trimethoprim resistance gene from pMLBAD	This study
Δhcp1	*B. pseudomallei,* nucleotide position 335 to 446 of BPSS1498 was removed	This study
Δhcp1inf	*B. pseudomallei,* codon 1-20 of BPSS1498 joined to 161.	This study
KHW hcp1^{L49AT50A}	*B. pseudomallei*, codon 46 and 47 of BPSS1498 substituted with alanine.	This study
E. coli		
S17-1	Donor strain for conjugation	[115]

[a] *Abbreviations: Ap^r, ampicillin resistant; Km^r, kanamycin resistant; Tc^r, tetracycline resistant, Tm^r, trimethoprim resistant.*

2.2 Screening for anti-Hcp1 monoclonal antibodies

2.2.1 Generating recombinant Hcp1

The *B. pseudomallei hcp1* gene (BPSS1498) was amplified using Polymerase Chain Reaction (PCR). The primers used were Hcp1F and Hcp1R (Table 2). A NdeI restriction site was introduced at the 5' end of the forward primer, and a XhoI restriction site at the 5' end of the reverse primer. The template DNA was the genomic DNA from *B. pseudomallei,* strain KHW. The PCR reaction mixture contained 2X GoTaq® Green Master Mix (Promega, Madison, WI, USA), 0.2 mM of forward and reverse primers, 100 ng of genomic DNA and 5 % dimethyl sulfoxide (DMSO), to a volume of 50 µL. The cycling parameters were 95 ^{o}C for 4 min, followed by 30 cycles at 95 ^{o}C for 1 min, 56 ^{o}C for 1 min, and 72 ^{o}C for 2 min and a final extension at 72 ^{o}C for 10 min. The PCR product was separated by 1 % agarose gel to verify the presence of a single band of the desired size (516 bp) and purified using DNA Clean & Concentrator (Zymo Research, Irving, CA, USA).

The purified PCR product was ligated to pGEM®-T Easy Vector (Promega). The ligation mixture contained 50 ng of vector, 25 ng of PCR product, 5 µL of the 2X ligation buffer, and 1 µL of the T4 ligase, to a final volume of 10 µL. The mixture was incubated at room temperature for 2 hr. 2 µL of the ligation product was added to 50 µL of electrocompetent Tg1 *E.coli* cells (ECC) and electropulsed using Gene Pulser® II Electroporation System. 1 mL of LB was

added to the transformed cells and the cells were incubated at 37 °C for 1 hr at 140 rpm for recovery. The recovered cells were plated on LB agar with 100 µg/mL of ampicillin, 40 µg/mL of IPTG and 40 µg/mL of X-gal for the selection of successful transformants. A few white colonies were selected and cultured overnight in 5 mL LB broth with ampicillin. The plasmids from these clones were extracted using Wizard® Plus SV Minipreps DNA Purification System (Promega). A small-scale restriction digest was performed to verify the presence of the *hcp1* gene insert in the plasmid. The digest reaction contained 1 µL plasmid DNA, 2 µL of 5X buffer D (Promega), 5 units of NdeI and XhoI (Promega) each, to a final volume of 20 µL. The reaction was incubated at 37 °C for 3 hr. The digest was separated by 1 % agarose gel and the positive plasmids pGem®-T-*hcp1* would give the desired bands of ~516 bp (*hcp1*) and ~3000 bp (pGEM®-T Easy vector).

A positive pGEM®-T-*hcp*1 plasmid was digested to generate the insert for ligation into the protein expression vector pET-28a. The pGEM®-T-*hcp*1 plasmid digest reaction contained 5 µL of buffer D, 2 µg of plasmid, 10 units of NdeI and XhoI to a final volume of 50 µL. The pET-28a plasmid digest reaction contained 5 µL of buffer D, 1 µg of plasmid, 10 units of NdeI and XhoI and 1 µL of thermosensitive alkaline phosphatase (TSAP) (Promega), to a final volume of 50 µL as well. The cut plasmids were purified QIAquick® PCR Purification kit (QIAGEN) and eluted with 10 µL of nuclease-free water. Ligation of the *hcp1* insert to pET-28a was undertaken in a 10 µL reaction of the following composition: 5 µL of 2X rapid ligation buffer (Promega), 1 µL of T4

DNA ligase, 100 ng of vector, 50 ng of insert, to a final volume of 10 µL and incubated at room temperature for 3 hr. The resulting plasmid was transformed into Tg1 electro-competent cells and selected on LB agar with 25 µg/mL of kanamycin. The success of the ligation was verified by restriction digestion, and the cloning of the *hcp1* gene in-frame with the N- terminal 6x His-tag of pET-28a was verified by sequencing.

The pET-28a-*hcp1* plasmid was harvested and re-transformed into BL21 (DE3) for protein expression and purification. The glycerol stock of BL21-pET-28a-*hcp1* was cultured at 37 ºC overnight in 250 mL of LB broth with 50 µg/mL of kanamycin. The overnight culture was subcultured in 2 L of LB broth with 50 µg/mL of kanamycin at 37 ºC for 2 hr to achieve log phase. 0.5 mM of IPTG was added to induce protein expression for a further 4 hr. The induced bacteria were pelleted at 6000 rpm for 15 min and kept frozen at -80 ºC overnight.

The bacterial lysis buffer contained B-Per® Bacterial Protein Extraction Reagent (Thermo Fisher Scientific Inc., Rockford, IL, USA), 200 µg/mL of lysozyme (Sigma-Aldrich, St. Louis, MO, USA), 25 µg of DNase (Sigma-Aldrich), 1x cOmplete EDTA-free protease inhibitor (Roche Diagnostics GmbH, Mannheim, Germany), in a final volume of 40 mL. The bacterial pellet was thawed, resuspended in the lysis buffer and the suspension was shaken at room temperature 15 min. The mixture was distributed into 1.5 mL microcentrifuge tubes, centrifuged at maximum speed to remove the insoluble proteins and the supernatant was pooled.

A 3 mL HisPur™ Cobalt Resin column was equilibrated with an equilibration/wash buffer of the following composition: 50 mM sodium phosphate buffer, 300 mM sodium chloride, 10 mM imidazole; pH 7.4. The supernatant was ran through the column twice and washed with two resin-bed volumes. Elution was done with 3 resin-bed volumes, with an elution buffer of the following composition: 50 mM sodium phosphate buffer, 300 mM sodium chloride, 150 mM imidazole; pH 7.4. The column was regenerated according to manufacturer's instructions for repeated use. The eluate was dialyzed against 1X phosphate-buffered saline (PBS) and ran on a 12 % SDS-PAGE gel to verify the presence of the desired protein (~18.4 kDa).

2.2.2 Immunization schedule

125 µg of Hcp1 in 500 µL of 1X PBS was emulsified with an equivalent volume of complete Freund's adjuvant (Sigma-Aldrich). 25 µg of emulsified protein was injected intraperitoneally per mouse; 6-8 weeks old female Balb/c. 2 subsequent boosts (25 µg of protein per mouse) in incomplete Freund's adjuvant were given on day 21 and day 35. The final boost (25 µg of protein per mouse) in 1X PBS was delivered intravenously on day 42. At day 45 the mice were euthanized with CO_2 and spleens were aseptically removed for fusion.

2.2.3 Preparation of NS1 myeloma fusion partner and macrophage feeder layer

The myeloma fusion partner NS-1 was cultured for two weeks in R10, which contained 10 % FBS, 1 % penicillin/streptomycin and 1 % L-glutamine in

1X RPMI. They were cultured till approximately 250 x 10^6 cells for fusion.

4 naïve 6-8 weeks old female Balb/c mice were euthanized with CO_2 and a tiny incision was made to the abdominal skin. The skin was pulled back to reveal the intraperitoneal cavity. 10 mL of RPMI 1640 (RPMI) was injected into the cavity with 18 ” needle syringe, and the media was gently withdrawn and injected several times to recover the intraperitoneal macrophages. This was repeated till 20-30 mL of RPMI with macrophages was harvested. The cells were pelleted and resuspended per spleen in 100 mL of hypoxanthine-aminopterin-thymidine (HAT) media, which contained 1X HAT (Sigma-Aldrich), 1 % penicillin-streptomycin (PS), 20 % fetal bovine serum (FBS) and 1 % L-glutamine in 1X RPMI. 100 µL of cells were pipetted into each well of a 96-well flat bottom tissue culture plate to give approximately 1000 cells per well. The cells were incubated overnight at 37 ^oC.

2.2.4 Pre-fusion preparation

On the day of fusion, the feeder layers were first checked for viability. 50 x 10^6 of NS-1 were harvested per fusion in a round-bottomed tube, pelleted and resuspended in 10 mL of R10. They were incubated at 37 ^oC until fusion.

2.2.5 Fusion

The spleens from the immunized mice were washed once in RPMI and gently homogenized with the base of a rubber plunger through a 70 µm nylon mesh

into 50 mL falcon tubes in RPMI. The resulting single cell suspension of splenocytes was fused directly with NS1 using the protocol developed by Milstein and Kohler.[116] Splenocytes from each spleen were washed once in RPMI, resuspended in 10 mL of RPMI and mixed with the prepared NS-1. The cell mixture was pelleted and its supernatant decanted. The pellet was gently agitated and 1 mL of warm polyethylene glycol (titrated until a pink colour development with 2 M NaOH) was added at a rate of 1 mL/min. It was incubated at 37 ^{o}C for 1 min, and was diluted with pre-warmed RPMI at a rate of 1 mL/min to final volume of 4 mL. The sides of the tubes were further rinsed with 2 mL of RPMI. The fused cells were centrifuged washed once and resuspended in 20 mL of HAT medium. They were incubated for 2 hr at 37 ^{o}C to allow recovery from the fusion. 80 mL of HAT medium was added to give a final volume of 100 mL, and 100 µL of fused cell suspension was cultured per well in microtitre plates for 7-14 days.

The resulting hybridoma clones were then scored microscopically. Supernatants were harvested in 96-well cell culture plates over the next 21 days from the resulting hybridomas.

2.2.6 Anti-Hcp1 hybridoma screen by indirect ELISA and FACS

Maxisorp^{TM} plates (Thermo Fisher Scientific Inc.) were coated overnight at 4^{o}C with 100 ng of Hcp1 per well. The negative control protein in the ELISA was recombinant TssM, a deubiquitinase from *B. pseudomallei*. The protein was generated and purified by Isabelle Chen Gek Joo. They were washed 4 times

with 0.05 % Tween 20 in PBS (PBS-T) and blocked with 5 % skim milk in PBS at room temperature for 1 hr. The supernatant harvested from the hybridomas were diluted 1:1 with the blocking buffer and added to the blocked Maxisorp™ plates at room temperature for 1 hr. The plates were washed 4 times and 100 µL of secondary antibody (goat anti-mouse antibody conjugated with house-radish peroxidase (HRP), Thermo Fisher Scientific Inc.) was added per well at a dilution of 1:5000 in blocking buffer. The wash was repeated and 50 µL of 3,3',5,5′-tetramethylbenzidine (TMB) (Thermo Fisher Scientific Inc.) was added per well. 50 µL of the stop solution 1N H_2SO_4 was added upon achieving the desired colour development and the plates were read at 450 nm (415 nm as the reference wavelength) using Bio-Rad Model 680 Microplate Reader (Bio-Rad Laboratories, Hercules, CA, USA). Wells with absorbance of optical density (O.D.) 1 and above were scored as the hybridomas that yielded anti-Hcp1 supernatants.

Anti-Hcp1 response from the selected hybridomas was further assayed using Hcp1-coated U937 by flow cytometry. The harvested supernatants were first diluted 1:1 in the FACS buffer, which contained 1 % FBS in 1X PBS, and were each distributed into 5 mL FACS tubes. The target cells U937, a myelomonocytic cell line, were incubated with 3 ng of Hcp1 per 0.5 x 10^6 cells at 37 ^oC for 1 hr, under gentle rotation in R10. The coated cells were washed once in 1X PBS and resuspended at a concentration of 10 x 10^6 per mL in the FACS buffer. The cells were distributed into the prepared FACs tubes at 50 µL per tube and incubated at 4 ^oC for 1 hr. The stained cells were washed once with

4 mL of PBS and stained with the goat-anti-mouse Alexa Fluor® 488 antibody (Life Technologies, Carlsbad, CA, USA) at the dilution of 1:200 in the FACS buffer. The cells were washed once more and fixed with 1 % paraformaldehyde (Sigma-Aldrich) in 1X PBS. The fixed cells were analyzed with CellQuest Pro Software on a BD FACSCalibur™ flow cytometer (BD Biosciences, San Jose, CA, USA).

2.2.7 Subcloning positive hybridomas

The selected hybridomas were progressive expanded from their 96-wells to 48-wells, 24-wells, and finally 6-wells. They were re-assayed for their anti-Hcp1 response, and those that remained positive were subcloned to achieve monoclonality. The cells were serially diluted in HT medium, which contains all that was found in HAT medium minus aminopterin. The cells were diluted to 5 cells/mL and 10 cells/mL, each 100 mL. They were distributed in 20 96-well cell culture flat-bottomed plates, 100 µL per well, and cultured for 7-14 days. Growing colonies were screened once more as aforementioned and the subcloning was repeated until the selected hybridoma clones became monoclonal.

2.2.8 Validation of monoclonality

1 x 10^6 hybridoma cells were harvested and resuspended in 1X PBS. The RNA was extracted with High Pure RNA Isolation Kit (Roche Diagnostics GmbH), according to manufacturer's instructions. The heavy and light chain sequences

were amplified using QIAGEN® OneStep RT-PCR kit (QIAGEN) with the Mouse IgG-Primer Set (Merck KGaA, Darmstadt, Germany). The reaction mix per primer was as follows: 12.5 µL of dH_2O, 5 µL of 5X OneStep buffer, 1 µL of dNTP, 1.25 µL of forward and reverse primer each, 1 µL of OneStep enzyme mix, and 3 µL of extracted RNA. The cycling parameters were 50 ºC for 30 min, 95ºC for 15 min, followed by 34 cycles at 95 ºC for 1 min, 50 ºC or 60 ºC for 1 min (depending on the primer, according to manufacturer's instructions), and 72 ºC for 2 min and a final extension at 72 ºC for 6 min. The PCR products were separated by 1 % agarose gel to visualize the amplified bands of the desired size (500 bp) and purified using QIAquick® Gel Extraction Kit (QIAGEN). The purified PCR products were sent for DNA sequencing to determine their precise nucleotide sequence.

2.2.9 Specificity of anti-Hcp1 antibody

The mutants *Δhcp1::tmp* and *ΔvirAG::tet* were generated by Jocelyn Wong and Yahua Chen respectively (Table 3). 2 mL of overnight culture of wild type *B. pseudomallei, Δhcp1::tmp* mutant and *ΔvirAG:tet* mutant were pelleted, lysed in B-Per®, and filter-sterilized. The lysates were concentrated to 200 µL using Vivaspin® protein concentrators with MWCO 5 kDa (Sartorius AG, Göttingen, Germany). 40 µg of lysate was resolved with 12.5 % SDS-PAGE, transferred onto a polyvinylidene fluoride (PVDF) membrane and blocked with 5 % skim milk in PBS-T at room temperature for 1 hr. The blot was incubated overnight at 4 ºC with 56-1 at a dilution of 1:10000 in blocking buffer. The membrane was

washed thrice with PBS-T, incubated at room temperature for 2 hr with a goat-anti-mouse secondary antibody conjugated with HRP at 1:5000 dilution in blocking buffer, and the wash was repeated. All blotting steps were done with gentle agitation, whilst all washing steps were done with agitation at 80 rpm. The substrate used was Western Lightning ECL (PerkinElmer) and the blot was exposed for 10 s using CL-XPosure Film (Pierce).

2.3 X-ray crystallography of Hcp1^{BP}

The solving of Hcp1^{BP} structure was done in collaboration with Dr Chacko Jobichen from the Protein Structure Laboratory, Department of Biological Sciences, NUS. Cloning and generation of both the recombinant native and L-selenomethionine (L-SeMet) incorporated- Hcp1 protein was done by the thesis author with Dr Jobichen, and the crystallization and resolution of the structure by Dr Jobichen.

2.3.1 Plasmid and strain construction

Hcp1 with a N-terminal His-tag did not yield diffraction quality crystals, hence *hcp1* was further cloned between NdeI and XhoI restriction sites of pET22b vector with a C-terminal 6x His-tag. Site-specific mutations in *hcp1* were introduced by overlapping PCR as previously described.[117] The template DNA was pET28a-*hcp1*. For each mutant, two fragments of *hcp1* are amplified separately with the following pairs of primers: Hcp1F with Q46AE47AR and Hcp1R with Q46AE47AF (for Hcp1^{Q46AE47A}), and Hcp1F with L49AT50AR and Hcp1R with L49AT50AF (for Hcp1^{L49AT50A}). The resulting two fragments per mutant were the template DNA for a subsequent PCR with Hcp1F and HcpR. Each PCR reaction mixture contained 2X GoTaq® Green Master Mix (Promega, Madison, WI, USA), 0.2mM of forward and reverse primers, 100 ng of genomic DNA and 5 % dimethyl sulfoxide (DMSO), to a volume of 50 µL. The new *hcp1* fragments containing mismatched bases were cloned into pET22b between NdeI and XhoI restriction sites, in frame with the C-terminal His-tag,

and verified with DNA sequencing.

2.3.2 Purification, crystallization and structure determination

The plasmid was transformed into *E. coli* BL21 cells and grown in defined M9 medium supplemented with 25 mg/L L-SeMet at 37°C until log phase.[118] 1 L culture was induced with 500 μM IPTG and growth continued at 37 °C for 5 hr. Cells were then harvested by centrifugation at 6000 rpm for 15 min and re-suspended in 40 mL of lysis buffer (B-Per® Bacterial Protein Extraction Reagent (Thermo Fisher Scientific Inc., Rockford, IL, USA), 200 μg/mL of lysozyme (Sigma-Aldrich, St. Louis, MO, USA), 25 μg of DNase (Sigma-Aldrich), 1X cOmplete EDTA-free protease inhibitor (Roche Diagnostics GmbH, Mannheim, Germany). Hcp1 was purified using B-PER 6xHis Fusion Protein Purification Kit (Pierce), followed by size exclusion (Superdex 75, GE Healthcare Life Sciences).

Crystallization conditions for the protein were screened using Index Screens (Hampton Research) using the hanging drop vapour diffusion technique. Drops containing 1 μL of Hcp1 solution at 8 mg/mL and 1 μL of reservoir solution were equilibrated at 25 °C. The optimized crystallization condition consisted of 0.1 M Na HEPES pH 7.5, 1.4 M tri-sodium citrate, 200 mM NaCl and 5 % (w/v) glycerol, with Hcp1 in 20 mM Tris-HCl (pH 7.0). Crystals selected for data collection were flash-cooled at 100 K in the reservoir solution supplemented with 25 % glycerol for cryoprotection.

Three homolog structures of $Hcp1^{BP}$ were available, but molecular replacement did not yield a solution to the crystal structure. Thus the structure was solved by single wavelength anomalous dispersion (SAD) using L-SeMet-labeled protein crystals instead.[119] X-ray diffraction data were collected at 13B beamline at National Synchrotron Radiation Research Centre (NSRRC), Taiwan, using a Quantum-315r CCD area detector (ADSC) and analysed with HKL2000.[120] Twelve expected 12 Se positions were found using the program Phenix.autosol.[121] RESOLVE was used to further improve the phases by density modification,[122] which gave a final overall figure of merit of 0.70, and was also used to build over 50% of the backbone atoms of the model.[122] COOT was used to manually built the remaining residues,[123] phenix.refine was used to refine the model.[121] An analysis using the phenix.xtriage program during the refinement process indicated the presence of merohedral twinning, hence refinement was undertaken with the twin refinement. Refinement was continued until the R-value converged to 0.239 (R_{free} = 0.289) for reflections $I>\sigma$ (I) to 2.63 Å resolution (Table 5).

2.3.3 Dynamic light scattering

Dynamic light scattering studies were undertaken on a DynaPro Light Scattering instrument (Protein Solutions, USA) at different protein concentrations in a buffer containing 20mM Tris pH 7.0, 200mM NaCl and 5mM DTT.

2.4 Functional studies on Hcp1

2.4.1 Imaging endogenous Hcp1 during *B. pseudomallei* infection *in vitro*

12 mm glass coverslips were rinsed for 10 min with 2 N HCl, and copiously washed with dH_2O. They were flamed sterilized using 100 % ethanol, and incubated with 40 µg/mL of poly-L-lysine (PLL) (Sigma-Aldrich) for 1 hr or overnight at 37 ^oC. They were copiously washed once more with dH_2O and allowed to dry upon sterile filter paper disks. The dried coverslips were stored in 24-well plates (Thermo Fisher Scientific Inc.).

U937 cells were activated with 200 ng/mL of phorbol-12-myristate-13-acetate (PMA) in R10 and plated upon the coverslips at 0.25 x 10^6 per coverslip. They were activated for 24 hr, and were given fresh R10 without PMA and antibiotics for another 24 hr. They were infected with log phase wild type *B. pseudomallei*, the negative control strain *Δhcp1,* or KHW *hcp1*^{L49AT50A} for at the MOI of 10:1. Kanamycin was added at a final concentration of 25 µg/mL per well 1hr after the infection and the infected cells were fixed with 1 % PFA after a further infection of 6-8 hr.

The fixed cells were washed thoroughly with 10 mM glycine in PBS. They were stained with a rabbit anti-*B. pseudomallei* lipopolysaccharide (LPS) antibody (kindly provided by Ganjana Lertmemongkolchai) and murine anti-Hcp1 antibody 56-2-2 at the dilution of 500:1, at room temperature for 1 hr. The cells

were washed, and stained with 4,',6-diamino-2-phenylindole (DAPI) at the dilution of 1000:1, goat anti-rabbit Fab conjugated with Alexa Fluor® 488 , and goat anti-mouse rabbit Fab' conjugated with Alexa Fluor® 647 (Life Technologies) at the dilution of 200:1. For colocalization studies with cholera toxin B (CTX), infected cells were costained in addition with CTX conjugated with AF555 (Invitrogen) at the dilution of 1000:1.

The cells were mounted onto clean glass slides using ProLong® Gold Antifade reagent (Life Technologies), and the slides were allowed to cure overnight at 4 ºC. Images were acquired using Carl Zeiss LSM 710 MicroImaging System (Carl Zeiss AG, Oberkochen, Germany) and processed with Adobe® Photoshop® CS4, version 11.0.2 (Adobe Systems Inc., San Jose, CA, USA).

2.4.2 Anti-Hcp1 response in clinical samples

Indirect ELISA was used to detect the anti-Hcp1 response from serum from confirmed *B. pseudomallei* patients. The samples were kindly provided by Dr. Direk Limmathurotsakul from the Department of Tropical Hygiene, Mahidol University, Thailand. Control serum samples were taken with consent from Singaporean healthy donors between ages 21-45.

The ELISA coating buffer was 100 mM bicarbonate/carbonate buffer, pH 9.5. Maxisorp™ plates (Thermo Fisher Scientific Inc.) were coated overnight at 4 ºC with 4 μg of Hcp1 per well, diluted in 1X coating buffer. They were washed 4 times with PBS-T and blocked with 5 % skim milk in PBS at room temperature

for 1 hr. Patients' and controls' serum were diluted 1:100 with the blocking buffer and added to the blocked Maxisorp™ plates at room temperature for 1 hr. The plates were washed 4 times and 100 µL of secondary antibody (goat anti-human antibody conjugated with HRP, Thermo Fisher Scientific Inc.) was added per well at a dilution of 1:5000 in blocking buffer. The wash was repeated and 50 µL of TMB was added per well. 50 µL of the stop solution H_2SO_4 was added upon achieving the desired colour development and the plates were read at 450 nm (415 nm as the reference wavelength).

Human immunoglobulin G (IgG) and immunoglobulin M (IgM) (Sigma-Aldrich) were coated in a 10-fold dilution series of the range 10 pg/ml-100 µg/ml to generate either an IgG or IgM standard curve. Similarly, they were coated overnight at 4 ^{o}C, washed, blocked and assayed with goat anti-human HRP secondary antibody. TMB was added after a final wash for color development, the reaction was stopped with H_2SO_4, and the plates were read at 450 nm (415 nm as the reference wavelength).

Data points from the standard curves and samples were plotted using GraphPad Prism version 5.0a for Mac OS X (Graphpad Software, La Jolla, CA, USA) and linear regression was applied to convert the O.D readings to concentrations in ng/mL.

2.4.3 Hcp1 levels in clinical samples

A microtitre Nunc® MaxiSorp plate (Thermo Fisher Scientific Inc.) was coated

with 1 µg of polyclonal rabbit anti-Hcp1 antibody per well in carbonate buffer, pH 9.5, overnight at 4 °C. Wells were washed with 0.05 % Tween 20 in PBS-T and blocked with 5 % skim milk in PBS-T for 1 hr at room temperature. Patients' and controls' sera were diluted 1:2 with blocking buffer and added to blocked plates at room temperature for 1 hr. Wells were washed and incubated with 2 µg monoclonal mouse anti-Hcp1 antibody (56-1) per well for 1 hr at room temperature. Wells were washed once more and incubated with a goat anti-human secondary antibody conjugated with HRP (Thermo Fisher Scientific Inc.) at a dilution of 1:5000 per well in blocking buffer at room temperature for another hour. The wash was repeated and TMB (BD Biosciences, San Jose, CA USA) served as the substrate. H_2SO_4 was added upon achieving the desired colour development and plates were read at 450 nm (415 nm as the reference wavelength). A standard curve was generated by adding Hcp1 in a 2-fold dilution series of the range coating human IgG or IgM in a 10-fold dilution series of the range 62.5 pg/mL - 4000 pg/mL.

2.4.4 Affinity of Hcp1 for primary immune cells and cell lines

10 mL of blood was drawn from a healthy donor with consent. The blood was diluted 1:1 in PBS + 0.4 % sodium citrate and overlaid upon 10 mL of Ficoll-Paque™ Plus. The overlaid blood was spun at 2400 rpm, at room temperature for 30 min, with the deceleration brakes set to 0. The resulting buffy coat containing peripheral blood mononuclear cells (PBMCs) was harvested, and washed twice, first at 2000 rpm for 5 min, and second at 1500 rpm for 5min,

both times with brakes set to 9.

The PBMCs were incubated either with 160 µg of Hcp1 or bovine serum albumin (BSA). They were incubated in R10 for 1 hr or overnight at 37 ^{o}C. The cells were washed twice in 1X PBS prior to staining. The cells were split into aliquots of 0.5 x 10^6 cells, and first stained with the murine anti-Hcp1 antibody 56-1 at 4 ^{o}C for 1 hr. They were washed once in 1X PBS and stained with the goat anti-mouse antigen binding fragment (Fab') conjugated with Alexa Fluor® 647 for another hour at 4 ^{o}C. They were washed and lastly stained with a combination of antibodies directly conjugated with a fluorophore to distinguish the major PBMCs populations: B cells, T cells, natural killer (NK) cells and monocytes. The antibody cocktail used for staining the cells are as listed below (Table 4). The listed antibodies were mostly from BD Pharmingen® (BD Biosciences, San Jose, CA USA), with the exception of the eFluor® 450 anti CD3 antibody, which was from eBioscience Inc. (San Diego, CA, USA).

The cells were incubated with the cocktail at 4 ^{o}C for 1 hr, washed once in 1X PBS and fixed with 1 % PFA. Cells stained only with the secondary antibodies were the negative control. The fixed cells were analyzed with BD FACSDiva^{TM} Software on a BD LSRFortessa cell analyser (BD Biosciences, San Jose, CA, USA).

Table 4: Antibody cocktail per condition

Cell Type	CD Markers	Fluorophore	Volume (µL)
B cells	CD19	PE[a]	4
	CD20	FITC[b]	4
Monocytes	CD14	PE	4
NK cells	CD16	PE	4
	CD56	APC[c]	4
T cells	CD3	eFluor®450	2
	CD4	PE	4
	CD8	FITC	4

[a]phycoerythrin
[b]fluorescein isothiocynate
[c]allophycocyanin

For Hcp1 affinity assays done with cell lines (RAW 264.7 and U937), 10 µg of Hcp1 was incubated with 0.5 x 10^6 cells per condition overnight at 37 ^oC. The samples were then stained with anti-Hcp1 antibody, fixed in 1% PFA and analysed as aforementioned. For the competition assay with mutant Hcp1s, 0.5 x 10^6 U937 were incubated with or without 100 µg of $Hcp1^{Q46AE47A}$ overnight at 37 ^oC with rotation. Wild type Hcp1 was directly conjugated with AF488 using AF488 Protein Labelling Kit (Invitrogen), according to manufacturer's instructions. The cells were washed, incubated with 10 µg of Hcp1 directly conjugated with AF488 for 1 hr at 37 ^oC with rotation, then washed once more and fixed with 1 % PFA.

2.4.5 Binding of anti- human CD98 antibody to RAW 264.7 cells

Anti-human CD98 antibody (clone MEM108, Biolegend) or an isotype control antibody was incubated with0.5 x 10^6 trypsinized RAW264.7 murine macrophages 4 ^oC for 1 hr. They were washed once in 1X PBS and stained with

the goat anti-mouse antigen binding fragment (Fab') conjugated with Alexa Fluor® 647 for another hour at 4 ºC. They were washed once more in 1X PBS , fixed with 1 % PFA and analyzed with BD FACSDiva™ Software on a BD LSRFortessa cell analyser (BD Biosciences, San Jose, CA, USA).

2.4.6 Generation of an in-frame *Δhcp* mutant

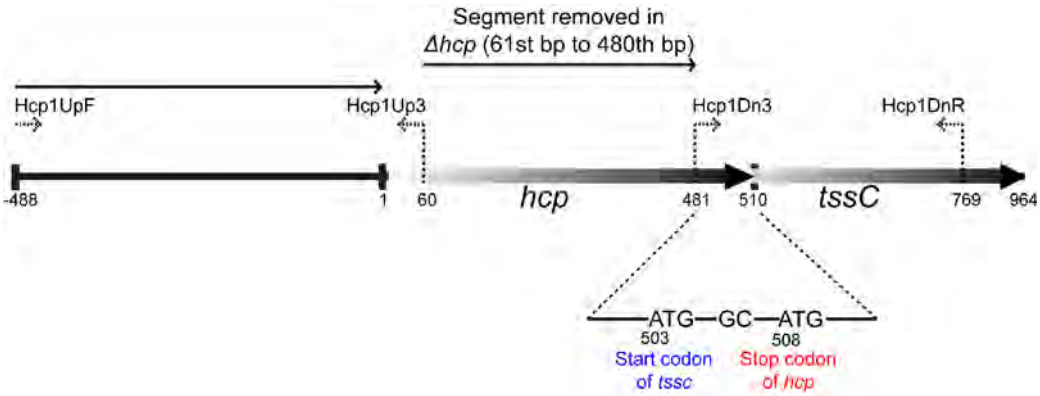

Figure 7: Schematic diagram of the in-frame deletion in the hcp1 gene from B. pseudomallei BPSS 1498.

An in-frame *Δhcp* mutant (*Δhcp1inf*) was generated by removing the region between the 60th and the 481th nucleotide (from the 61st to the 480th nucleotides inclusive). The mutant was generated by Yahua Chen and the thesis author. Two fragments, one upstream and another downstream, of the deletion site were generated. The up fragment consisted of the 1st to 60th bases of *hcp1* and 488 bases upstream of the start codon and the primers used were Hcp1UpF/Hcp1Up3. An EcoRI restriction site was introduced at the 5' end of the forward primer. The down fragment consisted of the 481th to 510th bases of *hcp1* and 335 bases downstream of the stop codon and the primers used were Hcp1Dn3/Hcp1DnR. A 15 bp fragment that is complementary to Hcp1Up3 was

introduced at the 5' end of the forward primer Hcp1Dn3. A PstI restriction site was introduced at the 5' end of the reverse primer. The template DNA was the genomic DNA from *B. pseudomallei,* strain KHW. The PCR reaction mixture contained 2X GoTaq® Green Master Mix (Promega, Madison, WI, USA), 0.2 mM of forward and reverse primers, 100 ng of genomic DNA and 5% dimethyl sulfoxide (DMSO), to a volume of 50 µL. The cycling parameters were 95 °C for 4 min, followed by 30 cycles at 95 °C for 1 min, 56 °C for 1 min, and 72 °C for 2 min and a final extension at 72 °C for 10min. The PCR product was purified with Wizard® SV Gel and PCR Clean-up System (Promega).

The plasmid pK18 (Table 3) was cut with EcoRI and PstI, and the cut plasmid was gel purified. The upstream and downstream fragments were cloned into the cut plasmid by adding 100 ng of the cut plasmid to 50 ng of each fragments, plus 2 µL of 5X In-Fusion® Mix (Clontech Laboratories, Inc, CA, USA). The reaction was incubated at 50 °C for 15 min, followed by 2 min on ice, transformed into chemically competent *Escherichia coli* strain S17 and selected on 25 µg/mL kanamycin LB (LB kanamycin) agar.

Positive clones carrying pK18-*Δhcp1inf* were cultured overnight in LB kanamycin media. They were conjugated with wild type *B. pseudomallei* by incubating 50 µL of S17- pK18-*Δhcp1inf* with 50 µL of overnight *B. pseudomalle*i culture for 6 hr. The exconjugates were restreaked on 50 µg/mL kanamycin, 50 µg/mL gentamycin LB agar and cultured for more than 18 hr. The kanamycin-resistant clones were passaged thrice in salt-free LB media with

10% sucrose (SSF), and streaked on SSF agar. Colonies were picked and screened for kanamycin sensitivity. Kanamycin colonies were further screened by colony PCR, using the primer pair Hcp1 and Hcp1DnR. A desired DNA band of ~500 bp was observed from positive colonies (*Δhcp1inf*).

2.4.7 Complementation of *Δhcp1inf* mutants

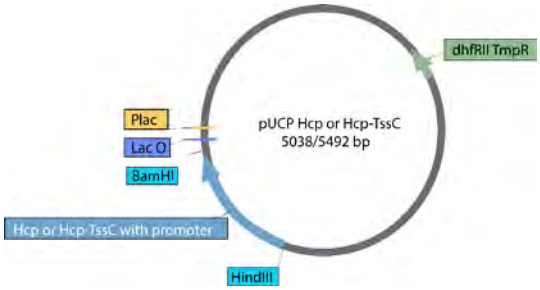

Figure 8: Plasmid map of pUCP-hcp1/ hcp1-tssC1

The complemented mutants were generated by Yahua Chen and the thesis author. The *hcp1* gene or the *hcp1-tssC1* gene, both with the *hcp* promoter, was cloned in the pUCP28T conjugation plasmid (Figure 8). The gene/s were inserted in the reverse orientation relative to the Plac promoter. The *hcp1* gene with its promoter was amplified with the primer pair Hcp1FH/Hcp1RB. The *hcp1-tssC1* gene with the *hcp* promoter was amplified with the primer pair Hcp1FH/TssCB. A HindIII and a BamHI restriction sites were introduced into the 5' of the forward and reverse primers respectively. The template DNA was the genomic DNA from *B. pseudomallei,* strain KHW. The PCR reaction mixture contained 2X GoTaq® Green Master Mix (Promega, Madison, WI, USA), 0.2 mM of forward and reverse primers, 100 ng of genomic DNA and 5% dimethyl sulfoxide (DMSO), to a volume of 50 µL. The cycling parameters

were 95 ºC for 4 min, followed by 30 cycles at 95 ºC for 1 min, 56 ºC for 1 min, and 72 ºC for 2 min and a final extension at 72 ºC for 10min. The PCR product was purified with Wizard® SV Gel and PCR Clean-up System (Promega).

The plasmid pUCP28T (Table 3) was cut with HindIII and BamHI, and the cut plasmid was gel purified. The *hcp1 or hcp1-tssC1* gene fragments were cloned into the cut plasmid by adding 100 ng of the cut plasmid to 100 ng of each fragments, plus 2 μL of 5X In-Fusion® Mix (Clontech Laboratories, Inc, CA, USA). The reaction was incubated at 50 ºC for 15 min, followed by 2 min on ice, transformed into Stellar™ Competent Cells (Clontech), and selected on 30 μg/mL trimethoprim LB (LB trimethoprim) agar. Plasmid DNA from trimethoprim-resistant clones were purified and transformed into chemically competent *Escherichia coli* strain SM10 and selected on 30 μg/mL trimethoprim LB agar. The empty vector pUCP28T was also transformed into SM10.

Positive SM10 clones carrying pUCP-*hcp1* or pUCP-*hcp1tssC1* were cultured overnight in LB trimethoprim media. They were conjugated with *Δhcp1inf* by incubating 50 μL of either SM10-pUCP28T, SM10-pUCP-*hcp1* or SM10-pUCP-*hcp1-tssC1* with 50 μL of overnight *Δhcp1inf* culture for 6 hr. The exconjugates were restreaked on 60 μg/mL trimethoprim, 50 μg/mL gentamycin LB agar and cultured for more than 18 hr. The trimethoprim-resistant clones were restreaked on LB trimethoprim/gentamycin agar, and further restreaked once a week over a period of 1 month to maintain the conjugated plasmid within the bacteria.

2.4.8 *hcp1* expression in infected cells by real-time PCR

0.5 x 10^6 RAW 264.7 cells were seeded and grown overnight in 12 well plates in R10 media. Cells were given fresh media prior to infection and were infected either with *Δhcp1inf* (*Δhcp1inf* conjugated with empty vector), *Δhcp1inf +hcp1*, *Δhcp1inf +hcp1-tssC1* or wild type *B. pseudomallei* at an MOI of 10:1. The cells were infected for 9 hrs, with 250 μg/mL of kanamycin added an hour post-infection. Bacterial and host cell RNA were isolated from infected cells with 1 mL of PureZOL (Bio-Rad Laboratories). 200 μL of chloroform was added per sample, and centrifuged for 15 mins at 12000 rpm at 4 ºC. 350 μL of the top fraction was collected and RNA was purified using illustra RNAspin Mini kit (GE Healthcare Life Sciences). 11 μL of the eluted RNA was used as the template for first strand cDNA synthesis using RevertAid First Strand cDNA Synthesis Kit (Thermo Scientific). 1 μL of cDNA was added to 10 μL of iQSYBR® Green Supermix for iCycler (Bio-Rad Laboratories) in a Bio-Rad iQ5 machine, 8 μL of water and 1 μL of 5mM primers. Real-time PCR primers are listed in Table 2. Relative RNA level of a particular gene in mutant strains was normalized to that of wild type using the $2^{-\Delta\Delta}$Ct method [124] with *rpoB* as reference gene. Results were reported as means of duplicate qPCR reactions.

2.4.9 ^{51}Cr release assay

Target U937 cells were pulsed with chromium-51 (^{51}Cr) (PerkinElmer) for 1 hr at 37 ºC. 1 x 10^6 of target cells were incubated either with 30 μg, 0.1 μg of Hcp1 or no protein, for either 4 hr, 6 hr or overnight at 37 ºC. The supernatants were

centrifuged, harvested and 30 μL of supernatant per condition were added into a LumaPlate (PerkinElmer). The plates were air dried, sealed and counted with TopCount® (PerkinElmer).

2.4.10 NF-κB-SEAP reporter assay

0.5 x 10^6 THP1-Blue™ (InvivoGen, San Diego, CA, USA) cells, which were stably transfected with nuclear factor-kappa-b (NF-κB)-secreted alkaline phosphatase (SEAP) reporter plasmid, were stimulated with either 1 μg of lipoarabinomannan (LAM) from *Mycobacterium tuberculosis*, 4 μg of endotoxin-free Hcp1 or BSA as the negative control protein for 24 hr. The supernatants were harvested, and for each condition, 20 μL of supernatant was added to 20 μL of QUANTI-Blue substrate (InvivoGen). The reaction was incubated for 24 hr at 37 °C, and absorbance was read at 650 nm.

2.4.11 IL-1β assay

2 x 10^6 J774.1 murine macrophages were stimulated with either 10 μg of Hcp1, BSA as the negative control protein or ATP with LPS as the positive control or without LPS. They were stimulated either for 4 hr or overnight at 37 °C. The supernatants were harvested, the cell debris pelleted and removed, and concentrated with a 5,000 MWCO concentrator to 400 μL. Interleukin-1 beta (IL-1β) levels was measured in triplicates with the Human IL-1β ELISA MAX kit according to manufacturer's instructions (BioLegend, San Diego, CA, USA).

2.4.12 MNGC assays

RAW 264.7 cells (2.5 x 10^5 cells per condition) were incubated with 10 μg of recombinant protein at 37 ^oC overnight with rotation. Cells were either unwashed or washed post incubation and plated into 24-well plates in R10 media without antibiotics. They were infected with stationary phase wild type *B. pseudomallei,* the negative control strain *Δhcp1* for MNGC formation, KHW *hcp1*^{L49AT50A} or complemented *Δhcp1inf* mutant strains (Table 3) at a MOI of 10:1. Kanamycin (250 μg/mL per well) was added 1hr post infection and infected cells were stained with Giemsa at specific time points (detailed in the results and their respective captions). For experiments on the effects of the anti-CD98 antibody on MNGC formation, the procedure was as previously described with modifications.[69] The isotype control or anti-CD98 antibody was added 1 hr post-infection as well. The degree of MNGC formation (fusion index) was estimated as previously described[125,126] but with modification. Each well was divided into four distinct quadrants. Cells located in the middle of the well were omitted because they were too dense to enumerate. Images from each quadrant was taken using 10X magnification. The total number of nuclei within MNGCs (> 3 nuclei/cell) and the total number of cells from each quadrant was counted, and summated from all four quadrant. The ratio of the total number of nuclei within MNGCs to the total number of cells multiplied by 100 %. represents the fusion index for each condition.

For MNGCs done with U937 cells, 2.5 x 10^5 of cells per condition were

activated with 20 ng/mL of PMA for 48 hrs to stimulate differentiation to macrophage-like cells. They were infected with stationary phase wild type *B. pseudomallei* at a MOI of 1:2. Kanamycin (250 μg/mL per well) was added 2 hr post infection and infected cells were stained with Giemsa at specific time points.

2.4.13 Radioimmunoprecipitating mammalian ligands of Hcp1

14 x 10^6 U937 cells were harvested and washed once in 1X PBS. They were washed once in R3, which contained 1X methionine and cysteine-free RPMI (Sigma-Aldrich) with 3 % dialysed FBS (Life Technologies Inc.), 1 % L-glutamine and 1 % penicillin/streptomycin. They were incubated with 1 mL of R3 at 37 ^oC for 2 hr, and 100 μL of EasyTag^{TM} Express35S Protein Labelling Mix (PerkinElmer Inc., Waltham, MA, USA) and 40 μg of Hcp1 for another hour.

The cells were washed once in 1X PBS, and lysed with 1 mL of 1 % digitonin (Merck KGaA) in 1X Tris-buffered saline (TBS) for 15min at 4^oC. The lysate was transferred into a screw-cap microcentrifuge tube and was centrifuged at 16,000 rpm for 1 min to pellet the insoluble cell debris. 50 μL of rec-Protein A-Sepharose® 4B (SepA) conjugate (Life Technologies Inc.) was incubated with the supernatant for 30 min at 4 ^oC. The pre-cleared supernatant was split into two aliquots and 10 μg of the murine anti-Hcp1 antibody 56-1 or the negative control antibody (anti-A2-HBV antibody) was incubated overnight at 4 ^oC. 50 μL of SepA was subsequently incubated 4 ^oC for 2 hr.

The aliquots were pelleted and the resulting SepA pellets were washed four times with 0.1 % digitonin in 1X TBS. The pellets were boiled for 15 min with sample loading buffer (0.0625 M Tris, pH 6.8, 10 % glycerol, 2 % SDS, bromophenol blue and 5 % β-mercaptoethanol). The pellets were centrifuged and the resulting supernatant was separated using a 12.5 % polyacrylamide gel via sodium dodecyl sulfate-polyacrylamide gel electrophoresis (SDS-PAGE). The gels were dried using Bio-Rad Model 583 Gel Dryer (Bio-Rad Laboratories) and developed at -80 ^{o}C for 10 days using a CL-XPosure film (Thermo Fisher Scientific).

2.4.14 Identification of candidate ligands by mass spectrometry

The identification of candidate Hcp1 ligands was done in collaboration with Dr Manfred Raida from Singapore Lipidomics Incubator (SLING), NUS. The affinity-immunoprecipitation was done by the thesis author, and the subsequent identification of candidate ligands by mass spectrometry was done by Dr Raida.

2.4.14.1 Immunoprecipitation

Immunoprecipitation was undertaken as previously described with modification. 20 x 10^6 U937 cells were used but they were not radiolabelled. The resulting SepA pellets containing control or Hcp1-specific antibody were washed and bound proteins were solubilized using sample buffer. Solubilized proteins were reduced with *tris*(2-carboxyethyl)phosphine (TCEP) and alkylated with iodoacetamide. The proteins were separated on 4 – 12 % linear gradient

polyacrylamide gels (Life Technologies) and visualized with Coomassie blue staining.

2.4.14.2 Liquid chromatography/tandem mass spectrometry

The entire gel lane per condition (proteins immunoprecipitated with either control or Hcp1-specific antibody) was cut into 48 equal-sized bands and the bands were distributed in pairs into each well of a perforated 96 well plate (Proxeon, Denmark). The gel bands were destained with two incubations with 50 % ethanol in 5 mM triethylammonium bicarbonate (TEAB) buffer pH 8.5 for 60 min at 55 ˚C each, dehydrated with 100 % ethanol for 15 min, rehydrated in TEAB buffer for 15 min and further dehydrated twice for 15 min with 100 % ethanol. Solvents were removed by centrifugation into a non-perforated 96 well plate for 1 min at 1,000 rpm. The dried gel pieces were treated with 20 µl 15 ng /µL trypsin (sequential grade, Life Technologies) in TEAB buffer for 15 min at 0 ˚C. Residual buffer was removed by centrifugation and another 20 µL of TEAB buffer was added. Tryptic digestion was undertaken for 16 hr at 37 ˚C , and stopped by adding 10 µL of 5 % formic acid in water. The solvent was collected by centrifugation into a new 96 well V-shape microtitre plate, which was subsequently used to collect the extracted peptides generated by the tryptic digestion. Peptides were extracted from the gel pieces by two incubations with 1 % formic acid in water at room temperature for 30 min, the first incubation with 50 % acetonitrile in 0.1 % formic acid and followed by another incubation for 15 min with 100 % acetonitrile. The microtitre plate containing the extracted

peptides was frozen for 2 hr at -80 ˚C and freeze dried in a rotary vacuum evaporator. The peptides were dissolved in 10 µL 0.2 % formic acid in water, the plate sealed with a plastic foil and the peptides were analysed by mass spectrometry.

Mass spectrometry was undertaken on an QTOF (AGILENT 6438) equipped with a nano-flow HPLC, a thermostated autosampler, a capillary loading pump (AGILENT 1260) and the chip-system (AGILENT) for separation and electrospray ionisation. Peptides were loaded onto a trap–column and separated in a linear gradient from 8 % acetonitrile with 0.2 % formic acid in water to 35 % acetonitrile with 0.2 % formic acid on a 150 mm x 75 µm C-18 (Reprosil pur, 3 µm, Dr Maisch, Germany, packed by AGILENT) column in the chip format. The peptides were measured in positive ion mode and 4 precursors were recorded per second. The 4 most intense double or triple charged ions above an intensity of 1,000 counts were taken for collision-induced dissociation with nitrogen as collision gas. The fragmented precursor ions were taken for a second fragmentation, then excluded for 15 s. The system was controlled by MassHunter acquisition software version 4.0 (AGILENT).

The raw data files were transformed into mzData.xml format using MassHunter qualitative software (AGILENT). Data base search was undertaken using PEAKS software, which compares the searches using MASCOT[127], X!Tandem and the Peaks/Spider routines (Literature) against the UniProt database. The results were combined within PEAKS and used to select candidate proteins for

further evaluation.

2.4.15 Biochemical validation of candidate ligands

The method used was a combination of aforementioned protocols. 14 x 10^6 U937 cells were harvested and washed once in 1X PBS. They were incubated for 2 hr with Hcp1 or BSA as the negative control protein with rotation at 37 ^oC. They were each lysed with 10 mL of the B-Per®-based buffer, the debris pelleted and incubated with an equilibrated 3 mL HisPur™ Cobalt Resin column for 90 min at room temperature with rotation. Elution was done with 3 resin-bed volumes with elution buffer. The eluate was concentrated with Vivaspin® protein concentrators with MWCO 5000 Da (Sartorius AG) to 200 µL. 40 µg of protein was resolved on a 12 % SDS-PAGE gel, transferred onto a PVDF membrane, blocked, and stained with a rabbit primary antibody against CD98 (Biolegend) or sodium-potasssium (Na,K)-ATPase (Cell Signalling) followed by a goat-anti-rabbit secondary antibody conjugated with HRP. Dilution factor for both primary and secondary antibody was 1:5000.

2.4.16 *In situ* site-directed mutagenesis of Hcp1

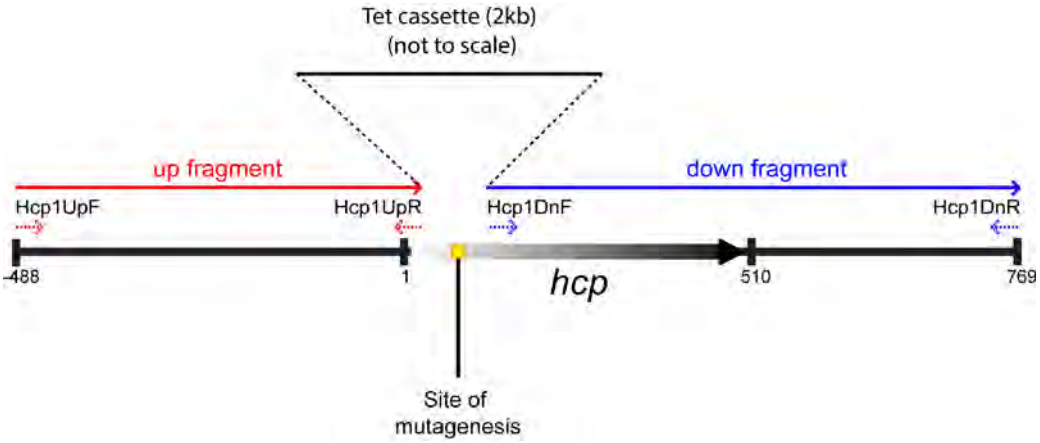

Figure 9: Insertion of tet cassette into hcp1

The first step was to introduce a tetracycline resistance cassette (*tet)* at the *hcp1* site of mutagenesis (Figure 9). Two fragments, one upstream and another downstream, of the mutagenesis site were generated. The up fragment consisted of the 1st to 20th bases of *hcp1* and 488 bases upstream of the start codon and the primers used were Hcp1UpF/Hcp1UpR. A EcoRI and a BamHI restriction sites were introduced at the 5' end of the forward and reverse primer respectively. The down fragment consisted of the 100th to 510th bases of *hcp1* and 335 bases downstream of the stop codon and the primers used were Hcp1DnF/Hcp1DnR. A BamHI and a PstI restriction sites were introduced at the 5' end of the forward and reverse primers respectively. The template DNA was the genomic DNA from *B. pseudomallei,* strain KHW. The PCR reaction mixture contained 2X GoTaq® Green Master Mix (Promega, Madison, WI, USA), 0.2 mM of forward and reverse primers, 100 ng of genomic DNA and 5% dimethyl sulfoxide (DMSO), to a volume of 50 µL. The cycling parameters were 95 °C for 4 min,

followed by 30 cycles at 95 ºC for 1 min, 56 ºC for 1 min, and 72 ºC for 2 min and a final extension at 72 ºC for 10min. The PCR product was purified with Wizard® SV Gel and PCR Clean-up System (Promega).

The plasmid pK18 (Table 3) was cut with EcoRI and PstI, and the cut plasmid was gel purified. The *hcp1* up and down fragments were cloned into the cut plasmid by adding 100 ng of the cut plasmid to 50 ng of *hcp1* up fragment (up) and 50 ng of *hcp1* down fragment (dn), plus 2 μL of 5X In-Fusion® Mix (Clontech Laboratories, Inc, CA, USA). The reaction was incubated at 50 ºC for 15 min, followed by 2 min on ice, transformed into Stellar™ Competent Cells (Clontech), and selected on 25 μg/mL kanamycin LB plate. Positive clones carrying the pK18-up-dn-*hcp1* plasmid were harvested and purified, and digested with 10 units of BamHI and incubated with 1 μL TSAP overnight at 37 ºC. 2 mg of *tet* cassette containing-PFRTT1 plasmid was also digested with BamHI overnight at 37 ºC. The digest was resolved on 1 % agarose and the desired *tet* cassette band (2 kb) was excised and gel purified. 100 ng of the cut pK18 vector was ligated with 96.7 ng of *tet* cassette fragment (3:1 molar ratio) by incubating the mixture overnight with 1 unit of T4 ligase in 1X ligation buffer (to a reaction volume of 10 μL) at 4 ºC. The ligation mixture was transformed in the chemically competent *Escherichia coli* strain S17 and selected on LB kanamycin agar.

Positive clones carrying pK18-up-*tet*-dn-*hcp1* were cultured overnight in LB kanamycin media. They were conjugated with wild type *B. pseudomallei* by

incubating 50 μL of S17-pK18-up-*tet*-dn-*hcp1* with 50 μL of overnight *B. pseudomalle*i culture for 6 hr. The exconjugates were restreaked on 50 μg/mL tetracycline, 50 μg/mL gentamycin LB agar and cultured for more than 18 hr. The tetracycline-resistant clones were passaged thrice in salt-free LB media with 10% sucrose (SSF), and streaked on SSF agar. Colonies were picked and screened for tetracycline/gentamycin sensitivity. Tetracycline/gentamycin-sensitive colonies were further screened by colony PCR, using the primer pair Hcp1F and Hcp1R. A desired DNA band of ~2.3 kb was observed from positive colonies (KHW up-*tet*-dn-*hcp1*).

The next step was to generate pK18 plasmids carrying *hcp1* with the desired mutations and conjugate them into KHW up-*tet*-dn-*hcp1*. The plasmid carrying double alanine substitutions at amino acids positions 46 and 47 was termed pK18-*hcp1*^{Q46AE47A} and the plasmid carrying double alanine substitutions at amino acids positions 49 and 50 was termed pK18-*hcp1*$^{L49AT50A.}$ The cloning and conjugation protocols were similar to the procedure described for generating KHW up-*tet*-dn-*hcp1*.

To generate pK18-*hcp1*^{Q46AE47A}, the genomic DNA from *B. pseudomallei* was amplified with two primer sets: Hcp1F/Hcp1Q46AE47AR and Hcp1Q46AE47AF/Hcp1R (Table 2). The PCR products were purified and cloned into pK18 using the In-Fusion® kit. The In-Fusion® reaction consisted of 50 ng of both fragments and 100 ng of EcoRI/PstI-restricted pK18 plasmid. The reaction was transformed into S17 and positive clones were selected with

kanamycin. pK18-*hcp1*^{L49AT50A} was generated using the same approach, but the primer sets were Hcp1F/Hcp1L49AT50AR and Hcp1L49AT50AF/Hcp1R.

Positive S17 clones carrying the double mutations were cultured overnight in LB kanamycin media and conjugated to KHW up-*tet*-dn-*hcp1*. The exconjugates were restreaked onto 250 μg/mL kanamycin, 50 μg/mL gentamycin LB agar, and passaged thrice in SSF media. They were streaked onto SSF agar, and selected for tetracycline/gentamycin sensitivity. Antibiotic-sensitive clones were verified for the double substitutions *hcp1*^{Q46AE47A} or *hcp1*^{L49AT50A} by sequencing.

Chapter 3.

Generation and Characterization of Biochemical Tools and Reagents for *B. pseudomallei* Hcp1

3.1 Introduction

The first stage in dissecting the biology of Hcp1 is to generate antibody-based tools that can be used to enable a study of its biochemistry and cell biology *in* vitro. There are no antibodies for Hcp1 that are commercially available. Hence generating an in-house monoclonal antibodies against *B. pseudomallei* Hcp1 represents one of the vital tools required for a thorough biochemical and cellular analysis *in vitro.*

To make a new anti-Hcp1 monoclonal antibody we employed the classical methodology developed by Köhler and Milstein,[116] which was to fuse splenocytes derived from mice hyper-immunized with recombinant Hcp1 with myeloma fusion partners to generate a large panel of immortalized B-cell hybridomas that were subsequently screened for anti-Hcp1 antibody production. The antibodies from the culture supernatants of candidate hybridomas were screened using indirect enzyme-linked immuno sorbent assay (ELISA), fluorescence-activated cell sorting (FACS)-based assay and protein immunoblot,

which ensured that the selected monoclonal antibody would have the required functional versatility for a broad range of biochemical assays.

3.2 Results

3.2.1 Recombinant expression and purification of Hcp1 antigen

The genetic and protein sequences are presented in Figure 10. The translated protein sequence of *hcp1* predicted it as a 17-18 kDa protein. However, studies on Hcp from *P. aeruginosa* show that the monomers are able to self-organize spontaneously as hexamers and higher-ordered structures under physiological conditions.[76,100] It does not contain a canonical N-terminal signal peptide, suggesting that it is secreted via a novel pathway independent of both the Sec system and twin-arginine translocation (Tat) pathway.[128]

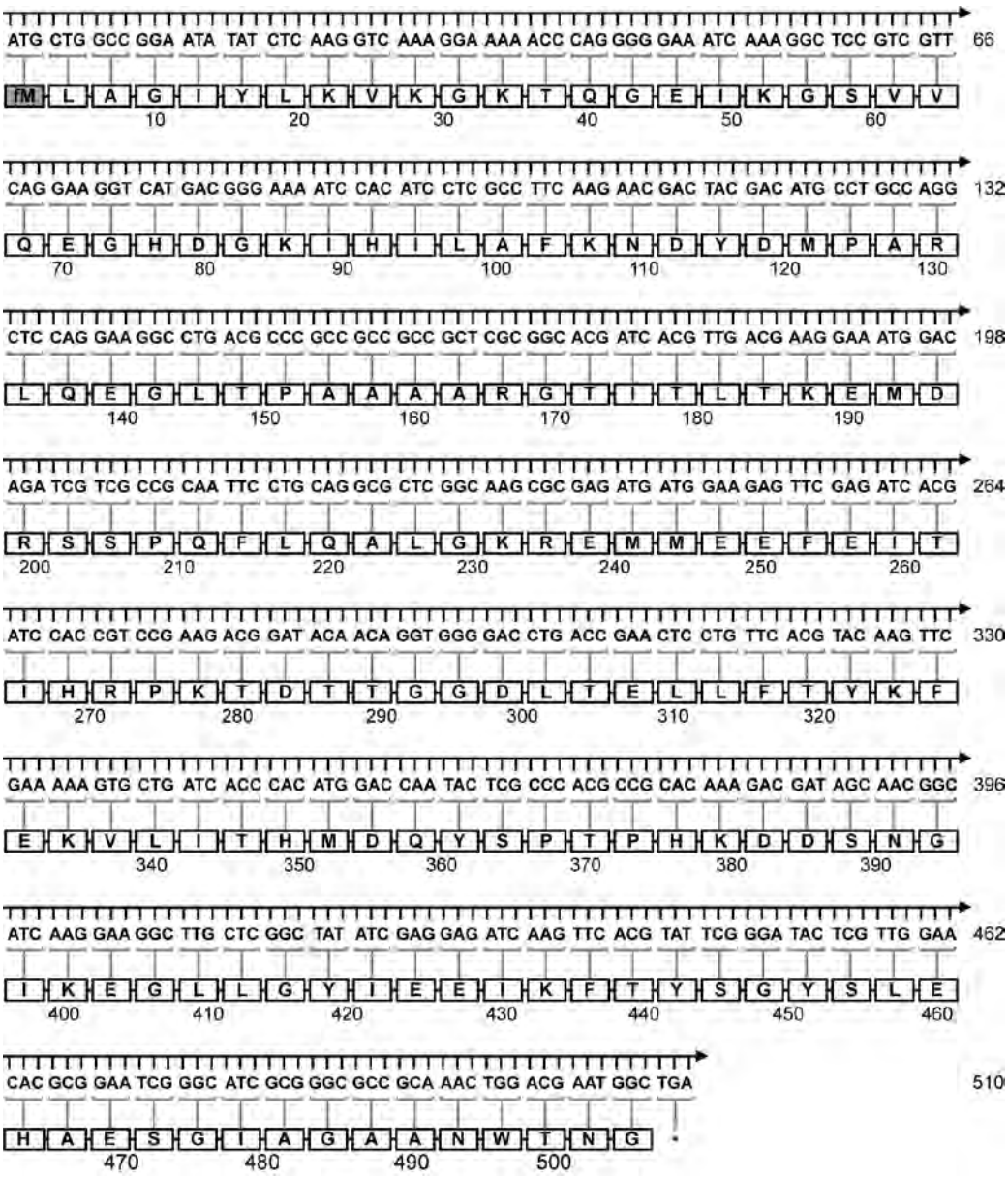

Figure 10: Genetic and protein sequences of Hcp1 from B. pseudomallei strain K96243. The numerals represent the nucleotide position on the DNA coding strand and the starting amino acid residue N-formylmethionine (fM)) is highlighted in black.

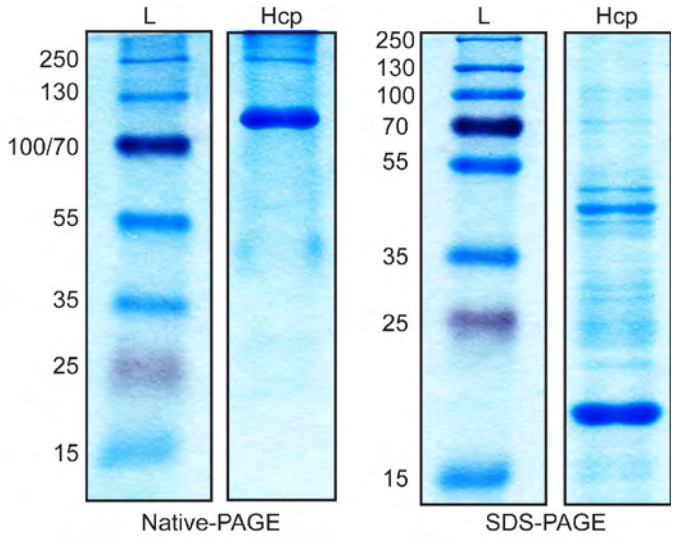

Figure 11: Native and denatured Hcp1. 10 µg of protein was ran per lane. The numerals indicate the size of the prestained marker proteins L, protein ladder, Hcp1, recombinant Hcp1 protein.

We cloned the *hcp1* gene into a pET-28a(+) vector and expressed it as a N-terminal polyhistidine-tag protein in BL21(DE3) *Escherichia coli.* The induced recombinant protein Hcp1 was purified and evaluated on both native (Native-PAGE) and sodium dodecyl sulfate polyacrylamide gel (SDS-PAGE) (Figure 11). The native hexamers ran as expected higher than the 100 kDa marker on the Native-PAGE, and denatured monomers ran higher than the 15 kDa marker on SDS-PAGE.

3.2.2 Generation of murine monoclonal antibody against Hcp1

3.2.2.1 ELISA-based screening for polyclonal antibodies specific for Hcp1

We immunized 4 to 8-weeks old Balb/c female mice with Hcp1 over the course of 45 days and took cheek bleeds on the 21st day to measure the anti-Hcp1 IgG

response in the immunized mice. The mice were sacrificed on the 45th day and their splenocytes fused with the myeloma cell line NS1 to generate immortalized hybridomas that would produce anti-Hcp1 IgGs.

The resulting hybridomas were screened by ELISA for anti-Hcp1 polyclonal antibodies. As a check for antigen specificity, they were assayed with both Hcp1 and recombinant TssM, the latter being another *B. pseudomallei*-derived antigen serving as the control antigen (Figure 12).

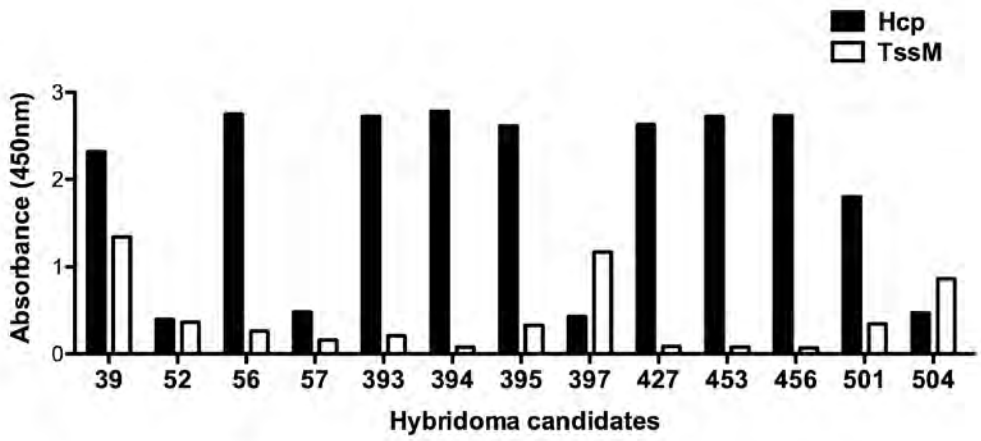

Figure 12: Representative murine hybridoma producing polyclonal antibodies against Hcp1. The figure presents a representative subset of hybridoma candidates producing polyclonal antibodies, which were given numeric designation (i.e 39, 52 etc.) 4µg of antigen were coated per well. Optical density (O.D) was taken at 450nm.

There were 960 successful fusions that had to be rapidly screened for anti-Hcp1 positivity. Only those that showed unambiguous anti-Hcp1 responses (O.D > 1) were considered anti-Hcp1 positive. In addition, the chosen hybridoma would be subjected to several subsequent rounds of ELISA screen. As the hybridoma were cultured in 96-well plates and required rapid transfer into larger well for subculture and maintenance, a single reading was taken so that the anti-Hcp1

hybridomas could be quickly identified. Of the 960 candidate hybridoma screened by ELISA, 18% were positive for anti-Hcp1 IgG (Figure 13).

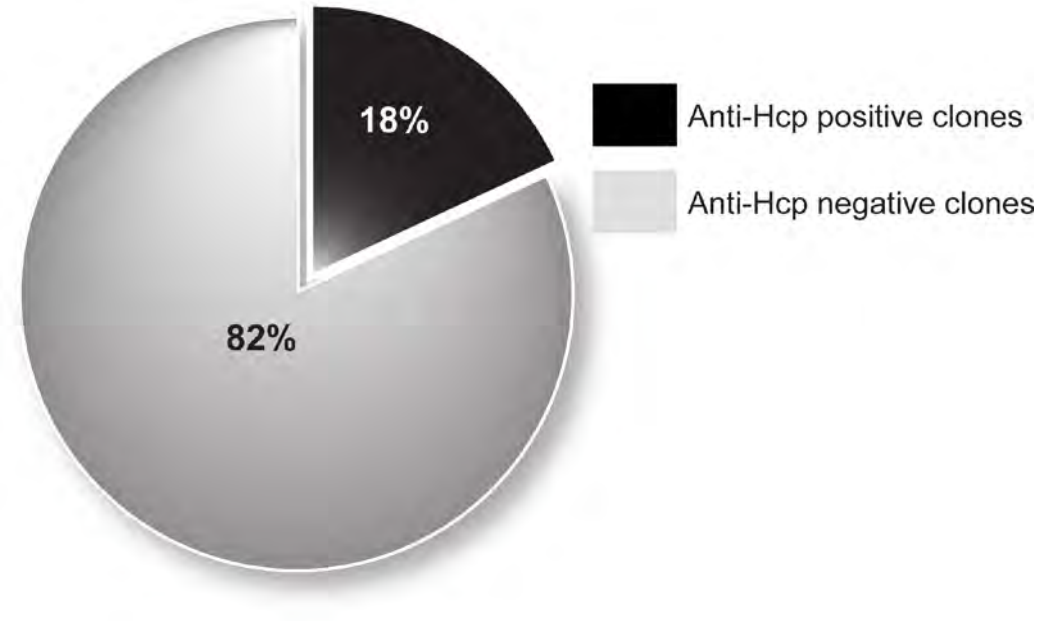

Figure 13: Overall percentage of hybridomas positive for anti-Hcp1 IgG response. Hybridomas giving optical density (O.D) readings of 0.5 or above are considered positive hybridoma cell lines producing anti-Hcp1 antibodies. A total of 960 hybridomas were screened.

3.2.2.2 FACS-based screening for polyclonal antibody

Previous studies have intimated that the Hcp1 protein is able to bind to the surface of mammalian cells.[106] Hence, we applied a second fluorescent-activated cell sorting (FACS)-based screening approach to the candidates that showed anti-Hcp1 positivity by ELISA. This was to select for hybridomas that produced IgG with the ability to detect surface-bound Hcp1 on a myelomonocytic cell line U937 (Figure 14).

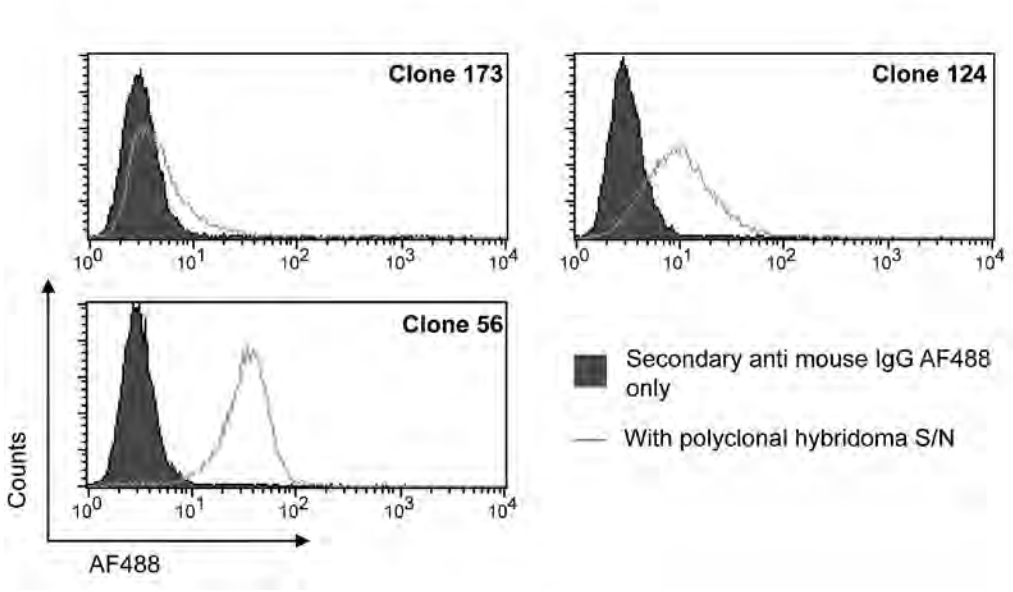

Figure 14: Representative murine hybridoma clones producing antibodies against surface-bound Hcp1 to U937. The figure presents data from clone 56, 124 and 173 (3 out of 192 clones), which showed anti-Hcp1 positivity by ELISA. 3 ng/mL of protein per 0.5 million cells were used to screen the selected clones. A goat anti-mouse Alexa Fluor® 488 (AF488) antibody was used to detect IgG that were bound to the coated Hcp1. Filled histograms represent secondary antibody controls and unfilled histograms represent the addition of anti-Hcp1 polyclonal supernatant (S/N).

Several candidate hybridoma clones showed anti-Hcp1 positivity in the FACS-based screen (Figure 14). Of the representative subset presented in Figure 14, only clone 56 showed a clear single log-shift relative to the secondary control. We selected clone 56 for several rounds of limiting dilution and screens (ELISA- and FACS-based) to generate a hybridoma cell line that produced monoclonal antibodies against Hcp1.

3.2.2.3 Sequence of the monoclonal anti-Hcp1 antibody 56-1

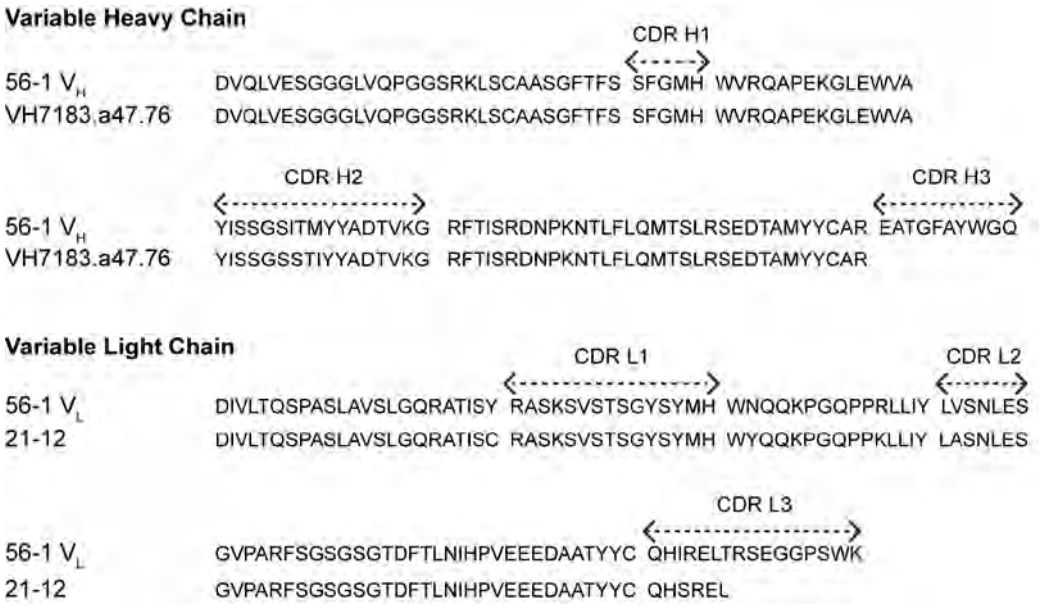

Figure 15: Sequences of variable regions of monoclonal anti-Hcp1 murine antibody 56-1. The complementarity determining regions (CDRs) for the variable heavy (V_H) and light (V_L) chains are demarcated.

Of the several anti-Hcp1 monoclonals generated, 56-1 was chosen to be sent for genetic sequencing. The resulting sequences for the variable heavy (V_H) and light chain (V_L) were scanned against the Kabat sequence database (Figure 15).[129] The closest germline sequence match to V_H was VH7183.a47.76 and to V_L was 21-12 (98.3% identity for both V_H and V_L) .

3.2.2.4 Specificity of 56-1

The Hcp1 protein is not constitutively expressed in the wild type *B. pseudomallei* strain KHW. It is under the control of a novel regulatory cascade that directs the expression of the type 3 (T3SS) and type 6 secretion systems, of

which the two-component transcriptional regulatory system VirAG is a component.[71,111] The overexpression of VirAG induces the expression of Hcp1 in Luria Broth (LB) medium.[70,84] We verified the specificity of the anti-Hcp1 antibody 56-1 using a protein immunoblot approach. The antibody was assayed using the lysate from the wild type *B. pseudomallei* strain, a *Δhcp1* deletion strain (*Δhcp1::tmp),* and a *virAG* deletion strain with constitutive tetracycline promoter cassette insertion (*ΔvirAG::tet).* Wild type *B. pseudomallei* and *Δhcp1::tmp* were the negative controls for Hcp1 expression. The *ΔvirAG::tet* expresses *t6ss1* because it is driven by the promoter of the tetracycline resistance cassette, hence it will also express the Hcp1 protein.

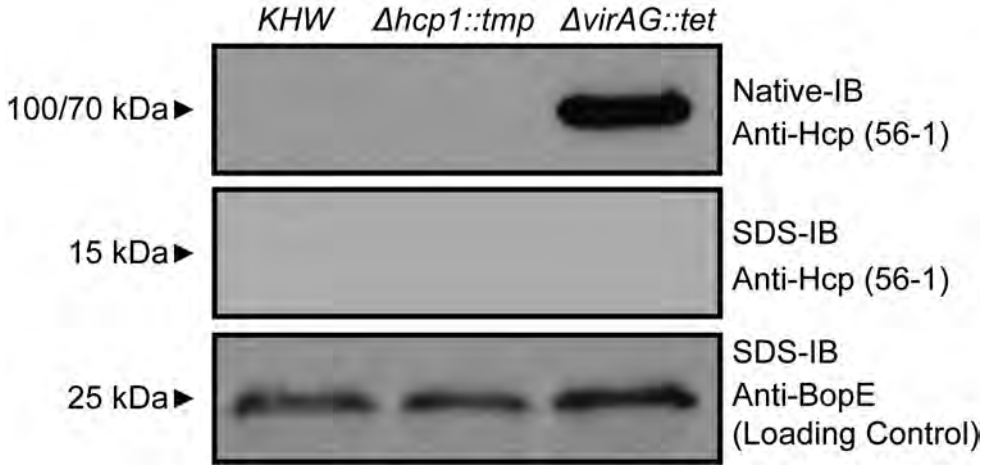

Figure 16: Specificity of 56-1 for native Hcp1. Lysates from wild type B. pseudomallei (KHW), Δhcp1::tmp and ΔvirAG::tet were resolved and immunoblotted in their native (Native-IB) or denatured forms (SDS-IB). The expected size of native hexameric Hcp1 is approximately 108 kDa, and the denatured monomer 17 kDa. The loading control was BopE, a 25 kDa protein belonging to the T3SS.

The anti-Hcp1 antibody 56-1 was only able to detect native hexameric Hcp1, but not the denatured monomers (Figure 16). The staining of endogenous Hcp1 by 56-1 was highly specific because a single band was detected in the lysate

from *ΔvirAG::tet,* but not from wild type *B. pseudomallei* and *Δhcp1::tmp.*

3.3 Discussion

The monoclonal anti-Hcp1 antibody 56-1 was generated with the objective of making it as versatile a tool as possible that could be applied to various assays. Hence the polyclonal hybridomas were subjected to both ELISA- and FACS-based screens prior to performing the limiting dilution. However, 56-1 is only able to recognize hexameric Hcp1 and not its monomer. Therefore, the immunodominant epitopes in native Hcp1 might be conformational epitopes. To generate antibodies that recognize monomeric Hcp1, the antigen used in the selection process might require denaturation or heat-treatment to disrupt its spontaneous oligomerization *in vitro*.

In addition, 56-1 is unable to recognize fixed endogenous Hcp1 that is produced during an infection of U937 cells with wild type *B. pseudomallei* (Figure 17). The infected cells were fixed in 1% paraformaldehyde (PFA) prior to staining with the antibody, hence the conformational epitope of 56-1 might have been disrupted by the fixation process. Hence the mother polyclonal stock of 56-1, named 56, was subjected to a second round of limiting dilution. The resulting clones were screening using fixed activated-U937 cells infected with *B. pseudomallei*, and fixed cells infected with *Δhcp1* were the negative control. The resulting sister clone 56-2-2 was able to specifically recognize fixed endogenous Hcp1 (Figure 17) and will be further described in Section 5.2.1.

Hence 56-1 was used for all anti-Hcp1 antibody-based assays, except for the *in vitro* imaging of fixed endogenous Hcp1.

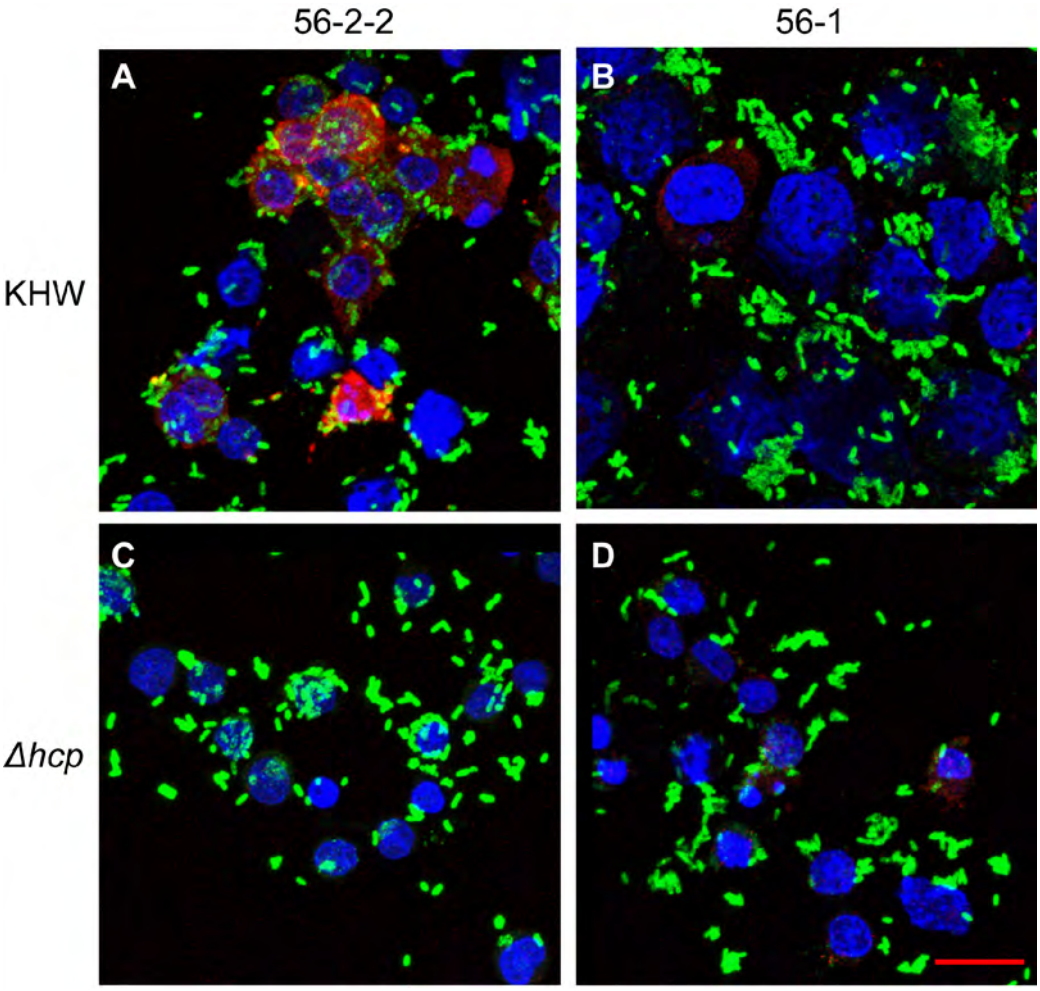

Figure 17: Screening for Hcp antibodies specific for fixed endogenous Hcp1. PMA-activated U937 infected with either log phase wild type bacteria B. pseudomallei (KHW) (Figure 17A and B) or Δhcp1 mutant (negative control) (Figure 17C and D). The cells were stained with anti-Hcp1 antibodies 56-2-2 (Figure 17A and C) or 56-1 (Figure 17B and D), followed by a secondary anti-mouse IgG antibody conjugated to Alexa Fluor® 647 (red). Bacteria were stained for LPS (green). Mammalian cell nuclei were stained using DAPI (blue). Results shown are representative of two independent experiments. PMA (phorbol 12-myristate 13-acetate), LPS (lipopolysaccharide), DAPI (4',6-diamidino-2-phenylindole). Scale bar: 20 µm.

Chapter 4.

Structure of *B. pseudomallei* Hcp1

4.1 Introduction

The crystal structures of Hcp1 and Hcp3 from *P. aeruginosa* (Hcp1^{PA} and Hcp3^{PA} respectively) and their homolog EvpC from E. *tarda* have been resolved.[76,101,102] They share significant structural homology, but several loops of Hcp3 differed in length and conformation with the other two proteins (Figure 18).[102]

Figure 18: Cα superposition of Hcp1^{PA} (green), Hcp3^{PA} (magenta) and EvpC (cyan).[102]

As Hcp assembles into a tubular structure that is essential for T6SS function, the elucidation of its structure could offer unique insights into the function of *B. pseudomallei* Hcp1. For the convenience of distinguishing between

B. pseudomallei Hcp1 and Hcps of other bacteria, the former is abbreviated as $Hcp1^{BP}$ in this chapter. The structural determination studies were done in collaboration with Dr Chacko Jobichen in the laboratory of Professor J. Sivaraman in the Department of Biological Sciences at NUS.

4.2 Results

4.2.1 Overview of the structure of *B. pseudomallei* Hcp1

Initially, we attempted to solve the structure of $Hcp1^{BP}$ by crystallizing native Hcp1 and solving its phase problem via molecular replacement. For the initial crystallization attempts, native Hcp1 with a N-terminal 6x-polyhistidine-tag (His-tag) was used, but the crystals were either too small, or were not of a high enough diffraction quality. The His-tag was switched to the C-terminus and L-selenomethionine (L-SeMet) was incorporated into the recombinant protein, which gave good diffraction quality crystals. Diffraction data was obtained at the resolution of 2.6 Å (Table 5). The electron density map, which is the representation of the crystal structure based on the diffraction data, was constructed by the summation of the experimentally determined parameters (phase, amplitude and frequency) of the diffraction waves by Fourier transformation.[130] The electron density map was iteratively refined and fitted with a three-dimensional protein model of $Hcp1^{BP}$ (Figure 19).

Table 5: Data collection, phasing and refinement statistics

Data collection	
Unit cell (Å):	a=b=82.74, c= 64.79
Space group:	P6
Resolution range (Å):	25-2.62 (2.71-2.62)
Wavelength(Å):	0.97857
Observed reflections:	225713
Unique reflections:	7654
Completeness (%):	100 (100)
Overall (I/σI):	15.4
Redundancy:	29.5 (29.2)
R Sym:	0.115 (0.274)
Refinement and quality	
Resolution range:	15-2.62
R work:	0.24
R free:	0.285
RMSD bond length (Å)	0.01
RMSD bond angles (Degree)	1.479
Average B factors	
Main Chain:	29.7
Side Chain and waters:	30.3
Ramachandran Plot	
Most Favoured regions (%)	75.53
Allowed regions (%)	23.37
Disallowed regions (%)	1.1

Statistics from the current model. [a] $R_{sym} = \Sigma|I_i - \langle I \rangle|/\Sigma|I_i|$ *where* I_i *is the intensity of the* i^{th} *measurement, and* $\langle I \rangle$ *is the mean intensity for that reflection.*

[b] $R_{work} = \Sigma|F_{obs} - F_{calc}|/\Sigma|F_{obs}|$ *where* F_{calc} *and* F_{obs} *are the calculated and observed structure factor amplitudes, respectively.*

[c] R_{free} *= as for* R_{work}*, but for 10.0% of the total reflections chosen at random and omitted from refinement.*

**Values in the parenthesis are the highest resolution bin values.*

Hcp1 molecule consists of residues from Gly15 to Gly169.
Table was generated in collaboration with Dr Chacko Jobichen.

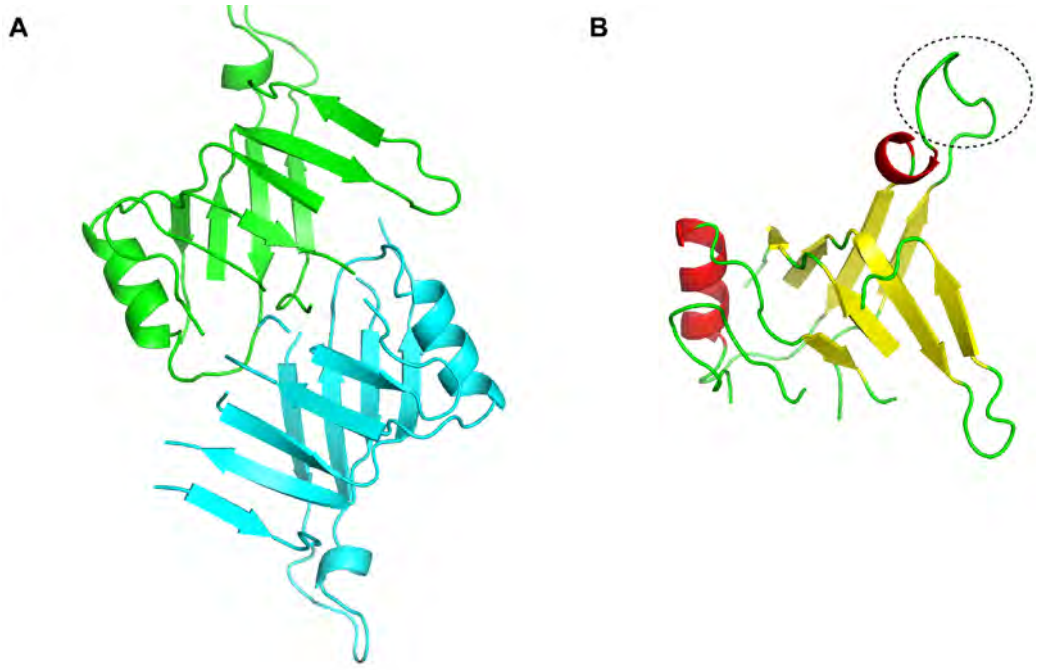

Figure 19: Ribbon diagram of the two Hcp1^{BP} molecules in an asymmetric unit. The model of one Hcp1^{BP} molecule consists of residues Gly15 to Gly169, with omissions between residues His90 and Phe106, and between residues Thr124 and Tyr140. The two monomers of Hcp^{BP} are shown in green (monomer A) and cyan (monomer B) (Figure 19A). Hcp1 monomer. The β-barrel domain is shown in yellow, the α-helix in red and and the extended loop in green (circled). Structural figures were prepared using PyMol.[156] *Figure was generated in collaboration with Dr Chacko Jobichen.*

The structure was solved using single-wavelength anomalous dispersion with 2 Hcp1^{BP} molecules in an asymmetrical unit (Figure 19A). The regions between residues His90 and Phe106, and between residues Thr124 and Tyr140 were omitted from the model as they were not defined in the electron density map.

The Ramachandran plot shows the distribution of torsion angles (φ for N-Cα bonds and ψ for C-Cα) of a protein structure and provides an overview of the favoured (red and shades of yellow) and unfavoured regions (white) of torsion angle values.[131] It is used to indicate the quality of the predicted three-

dimensional model. Most of the residues (99 %) in the model predicted for Hcp1^{BP} laid within the favoured region of the Ramachandran plot (Figure 20), hence the model had good stereo-chemical parameters.

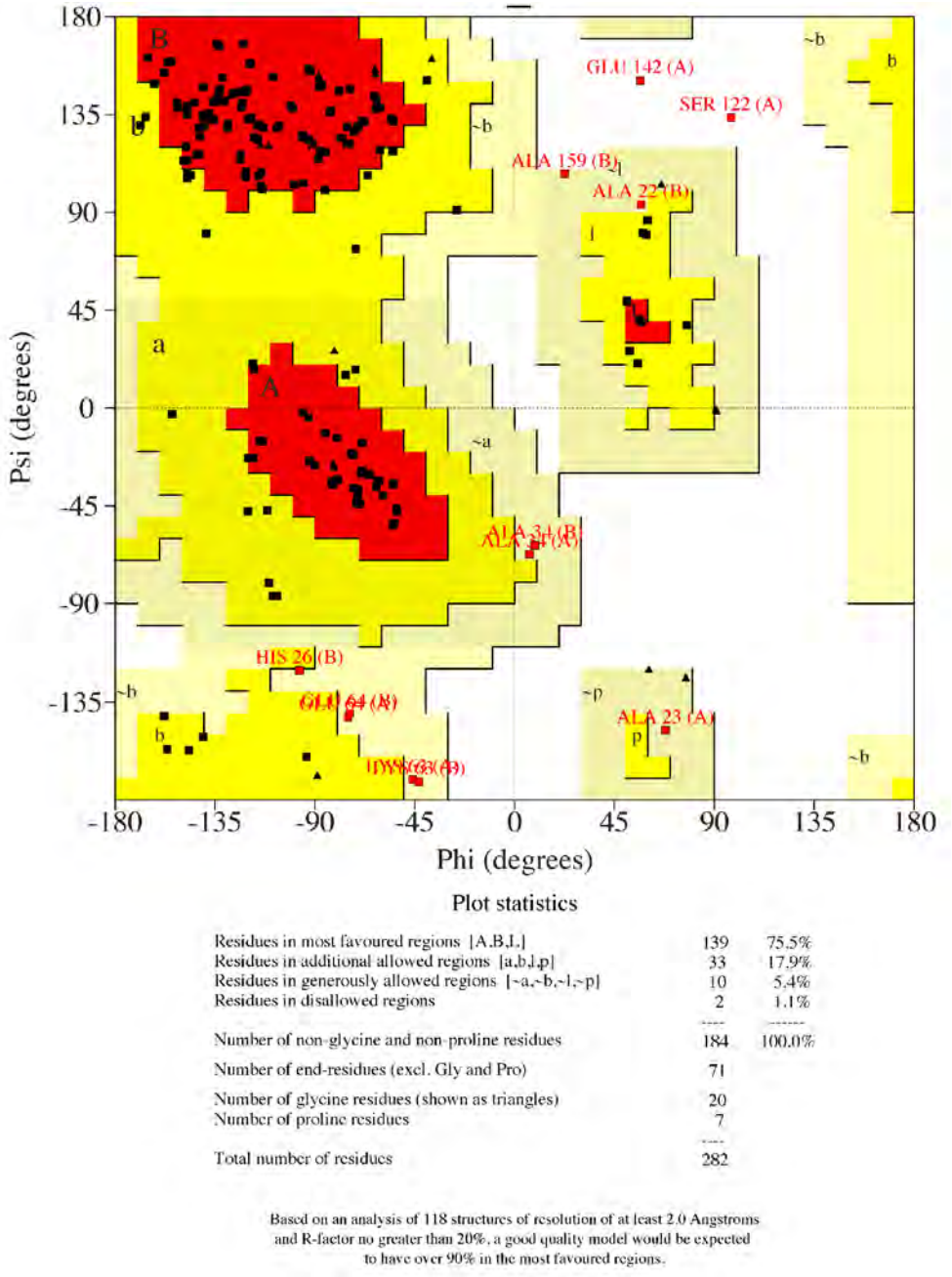

Figure 20: Ramachandran plot of the phi-psi torsion angles of all residues in the Hcp1 structure. Plot was generated using PROCHECK.[131,154]

Each molecule of $Hcp1^{BP}$ mainly consists of a β-barrel domain, with several loops mostly on one end of the β-barrel (Figure 19B). The diameter of the monomeric β-barrel is approximately 9-10 Å, consisting of 9 anti-parallel β-strands. Located on one side of the β-barrel is an α-helix (Ser69 – Lys78). The residues Asp40 to Arg56 form an extended loop that protrudes away from the β-barrel (Figure 19B, dotted circle) and this loop region is well defined in the electron density map.

4.2.2 Structural and Sequential Comparison of $Hcp1^{BP}$ and its Homologs

We performed a search for topologically similar proteins within the Protein Data Bank (www.pdb.org) with the program DALI.[132] Significant structural homology was observed between EvpC (PDB code 3EAA; rmsd = 3.3Å for 105 Cα atoms; 23% sequence identity), $Hcp1^{PA}$ (PDB code 1Y12; rmsd = 3.3Å for 105 Cα atoms; 18% sequence identity), $Hcp3^{PA}$ (PDB code 3HE1; rmsd = 1.7Å for 99 Cα atoms; 24% sequence identity), and $Hcp1^{BP}$.

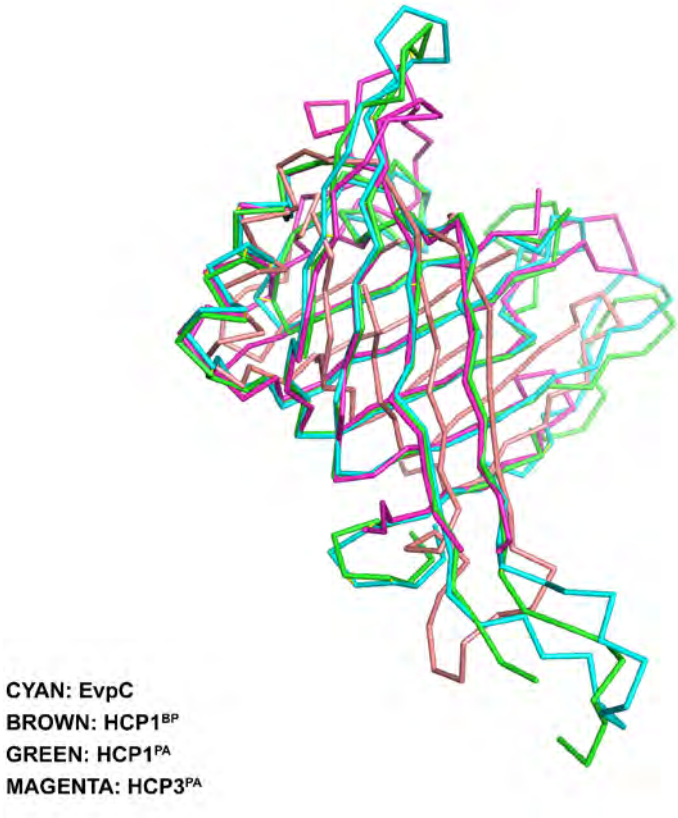

Figure 21: Cα superposition of Hcp1^{BP} (brown) with its structural homologs (EvpC (cyan), Hcp1^{PA} (green) and Hcp3^{PA} (magenta)). Figure was generated in collaboration with Dr Chacko Jobichen.

The main common feature shared between these Hcp molecules is the overall β-barrel architecture (Figure 21). However, significant differences was also observed through a superposition of Hcp1^{BP} Cα atoms with those belonging these homologs (EvpC, Hcp1^{PA} and Hcp3^{PA}). The major extended loop of Hcp1^{BP} (Figure 21, brown) between Asp40 and Arg56 is shifted by 15.6 Å relative to Hcp1^{PA} (Figure 21, green) and EvpC (Figure 21, cyan). In addition, several loops of Hcp3^{PA} (Figure 21, magenta) are different in length and conformation, when compared to Hcp1^{BP}.

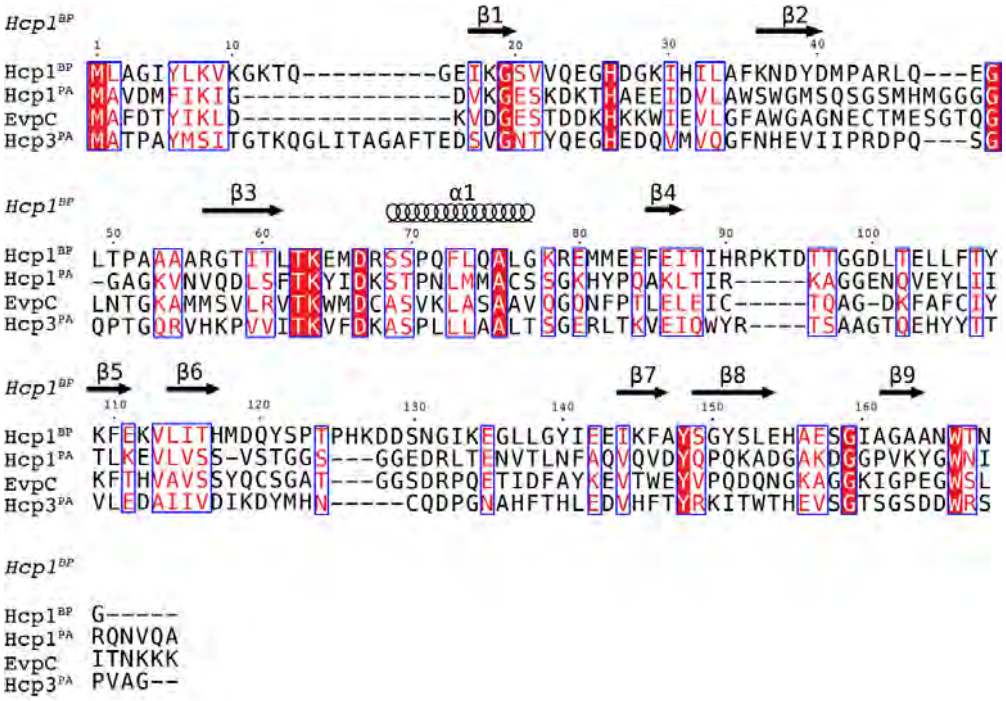

Figure 22: Protein sequence alignment of Hcp1^{BP} with other known structural homologs Hcp1^{PA}, EvpC and Hcp3^{PA}. Key: Single letters: amino acids. Red letters in unfilled boxes: similar amino acid residues. White letters in filled boxes: conserved amino acid residues. Arrow: beta sheet. Spiral: alpha helix. Sequence alignment was done by Clustal W[133] and the figure was prepared using ESPript.[152]

A protein sequence alignment was also performed using Clustal W.[133] Sequence identity between these proteins was low, approximately 25% as previously mentioned. There are 10 conserved amino acids in the β-barrel domain (Figure 22), but with the exception to Gly48, there is no invariant residue in the extended loop region (Asp40-Arg56). The absence of a side chain in glycine allows flexibility in the polypeptide chain, which possibly is the reason why Gly48 is conserved in the loop region. The codon 46 is occupied by residues with charged side chains for Hcp1^{PA}(His46), Hcp3^{PA}(Gln46) and Hcp1^{BP}(Gln46), while Leu49 is identical in both Hcp1^{BP} and EvpC.

4.2.3 Oligomerization of Hcp1^{BP}

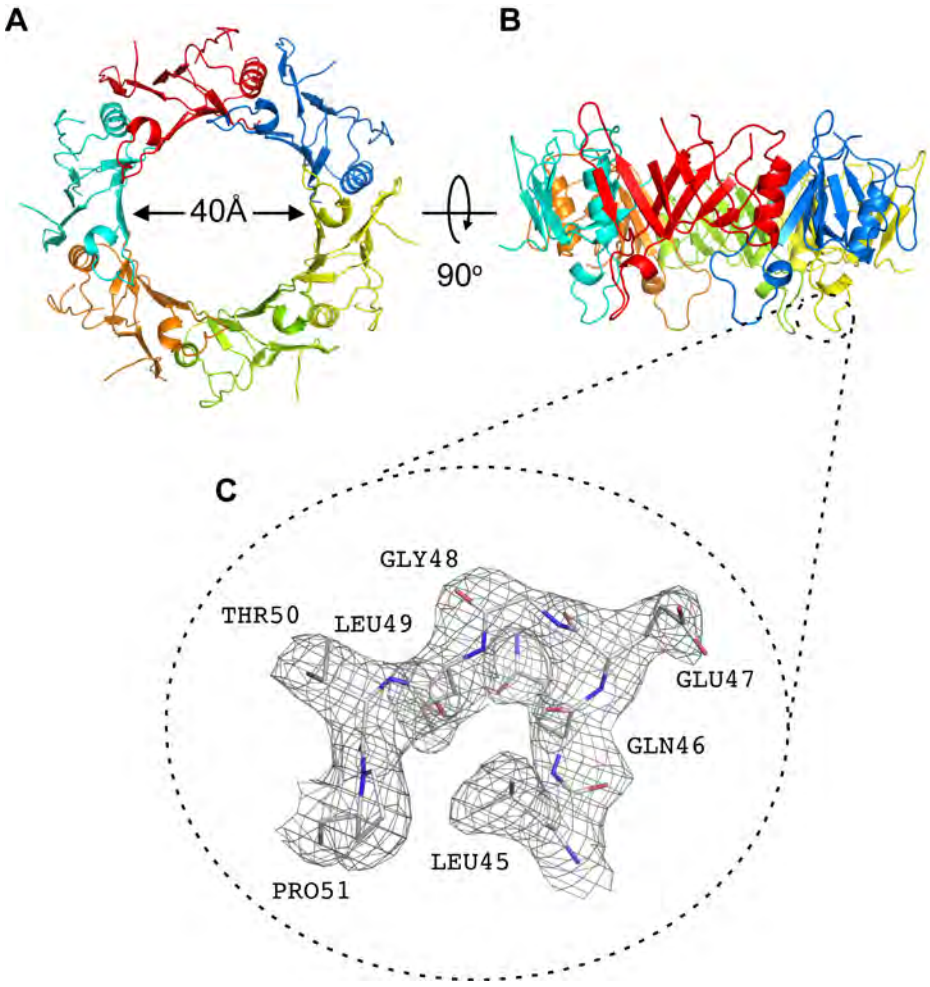

Figure 23: Hexameric ring of Hcp1^{BP}. This ring has an outer diameter of 80 Å and an inner diameter of 40 Å. Top view of the hexameric ring (Figure 23A). Side view of hexameric ring (Figure 23B). Magnified view of the extended loop, showing critical amino acid residues (Figure 23C). Figure was generated in collaboration with Dr Chacko Jobichen.

From an asymmetric unit with two Hcp1^{BP} molecule, hexameric rings could be generated by a 6-fold symmetry with 12 molecules, forming an assembly of two rings (Figure 23A). The rings have an outer diameter of 80 Å and an inner diameter of 40 Å, which may stack to form a continuous tubule. An orientation of the hexamer molecules sideways showed an array of 6 extended loops

(Asp40 to Arg56) (Figure 23B). A magnification of the modeled interface between the extended loops of interacting monomers revealed several contacts with less than 3.5 Å in distance (Figure 23C). Most of them are hydrogen bonding contacts involving the residues Gln46 to Thr50 from interacting monomers of adjacent hexameric ring (Figure 24).

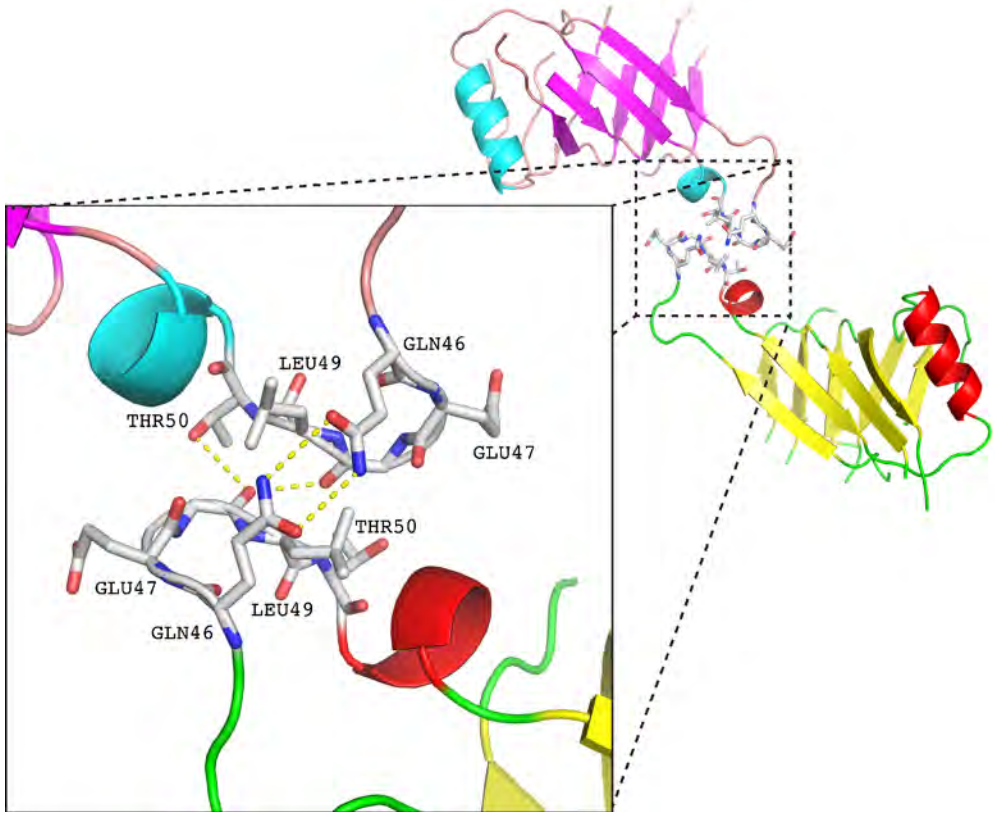

Figure 24: Putative critical inter-hexameric residues. The interface between monomer A (pink and blue) and monomer B (yellow and red) are magnified in the insert. Residues with less than 3.5 Å are labelled (Glu47, Gln46, Leu49 and Thr50) and representative inter-residue hydrogen bonds are illustrated (yellow dotted lines). Figure was generated in collaboration with Dr Chacko Jobichen.

4.3 Discussion

The resolution of $Hcp1^{BP}$'s structure supports several properties of Hcp that have been previously reported.[76,100–102] It has an overall β-barrel structure, is able to form hexamers, and these hexamers stack to form a continuous pore with an outer diameter of 80 Å and an inner diameter of 40 Å.

However, our studies also highlighted a significant difference between $Hcp1^{BP}$ and other reported structures of related Hcps' which is its extended loop region. We first show through amino acid sequence alignment that the residue Gln46 or Leu49 located in this region are conserved between $Hcp1^{BP}$ and its structural homologues. Apart from Gly48,[101] this conservation was not reported in previous studies, possibly due to the low sequence identity of Hcp between difference bacterial species.[76,101,102] Nevertheless it was suggested in one of these studies that the most highly conserved residues are found on the top and bottom faces of the hexamer,[76] which corresponds to the orientation of the extended loops in the $Hcp1^{BP}$ hexamers. More importantly, the inter-ring interactions of these extended loops highlight a region unique to the structure of $Hcp1^{BP}$ that could potentially be important for its biological activity. Thus, we mutated the key residues in this extended loop to verify their effect on the function of $Hcp1^{BP}$ that will be described in Chapter 5.

Chapter 5.

Properties and Function of *B. pseudomallei* Hcp1

5.1 Introduction

Several groups have identified candidate lists of immunoreactive *B. pseudomallei* proteins that are either predicted to be surface proteins or located in the bacterium's secretome.[134] However, Hcp1 is not listed as a possible candidate, even though the Hcp1 from *P. aeruginosa* and *A. hydrophila* have been shown to be immunogenic. Hence, the immunogenicity of *B. pseudomallei* Hcp1 remains to be verified.

It is also not known whether *B. pseudomallei* Hcp1 has any function beyond its structural role in the assembly of the T6SS needle for secretion of T6SS substrates. However as mentioned in Chapter 1, the function of Hcp was more extensively explored in *A. hydrophila* and *E. coli*. Hence the direct effect of *B. pseudomallei* Hcp1 on host cells was investigated. Based on the structural information of Hcp1, we also examined how the extended loop region contributed to Hcp1 function.

5.2 Results

5.2.1 Endogenous Hcp1 during *in vitro* infection

We infected PMA-activated U937 cells with *B. pseudomallei* to visualize the localization of endogenous Hcp1 during infection (Figure 25A), with the *Δhcp1* mutant as the background control (Figure 25B). The cells were infected for 7 hr at the multiplicity of infection (MOI) of 10:1. The staining for Hcp1 was not uniformly distributed (red) and did not readily colocalize with the wild type bacteria (green). It was concentrated mostly around host cell clusters (blue) and only colocalized with bacteria associated with host cells (yellow). In a separate experiment, the cell membrane was stained using cholera toxin B conjugated with AF588 (CTX, orange) (Figure 25C and D). The cells were infected with either the wild type bacteria (Figure 25C) or the *Δhcp1* mutant as a negative control since the gene was disrupted and no Hcp1 protein will be produced (Figure 25D). For cells infected with the wild type bacteria, the strong staining for Hcp1 (red) colocalized with CTX. This indicated that Hcp1 could be found on the surface of the host cells during infection *in vitro.*

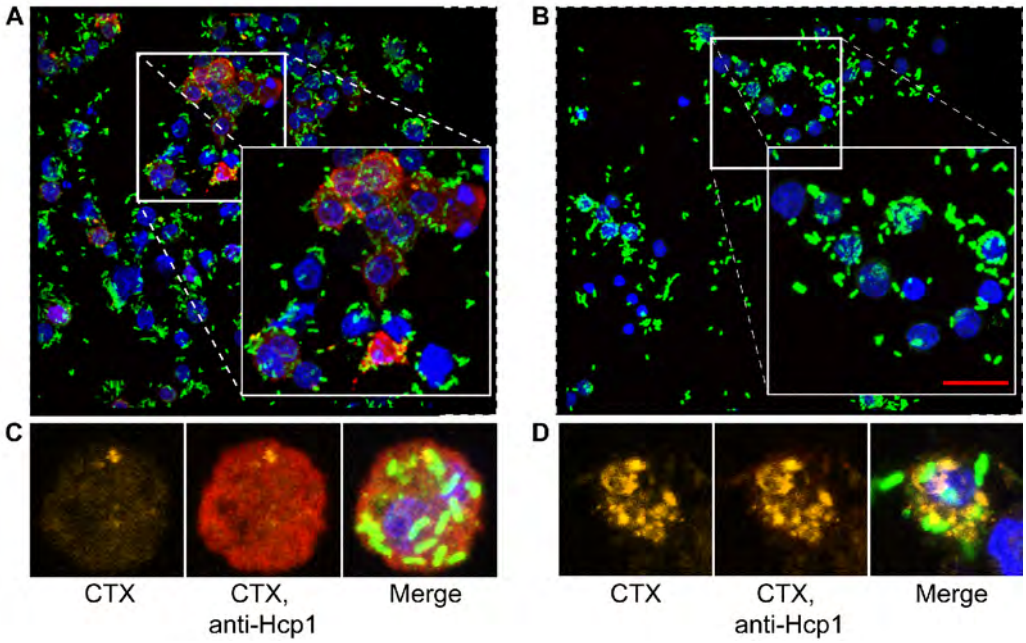

Figure 25: Imaging endogenous Hcp during infection in vitro. PMA-activated U937 infected with log phase wild type bacteria B. pseudomallei were stained for Hcp1 (red) (Figure 25A). Control image was captured using cells infected with log phase Δhcp1 mutant (Figure 25B). Bacteria were stained for LPS (green). Mammalian cell nuclei were stained using DAPI (blue). Results shown are representative of two independent experiments. PMA (phorbol 12-myristate 13-acetate), LPS (lipopolysaccharide), DAPI (4',6-diamidino-2-phenylindole). Infected U937 were also costained for cholera toxin B-AF555 (CTX). Colocalization of Hcp1 with CTX was observed with cells infected with the wild type bacteria (Figure 25C), but not with the Δhcp1 mutant (Figure 25D). Scale bar: 20 μm.

5.2.2 Anti-Hcp1 IgG and IgM response in melioidosis patients

To address whether Hcp1 could be detected during infection in humans, we examined the presence of the Hcp1 protein in sera from melioidosis patients but were unable to detect it (Figure 26A). We further examined the anti-Hcp1 IgG and IgM response in melioidosis patients versus healthy controls by ELISA. The titers of anti-Hcp IgG and IgM in patients' sera were significantly higher relative to healthy controls' ($p < 0.0001$ and $p = 0.006$, respectively) (Figure 26B and 26C, respectively).

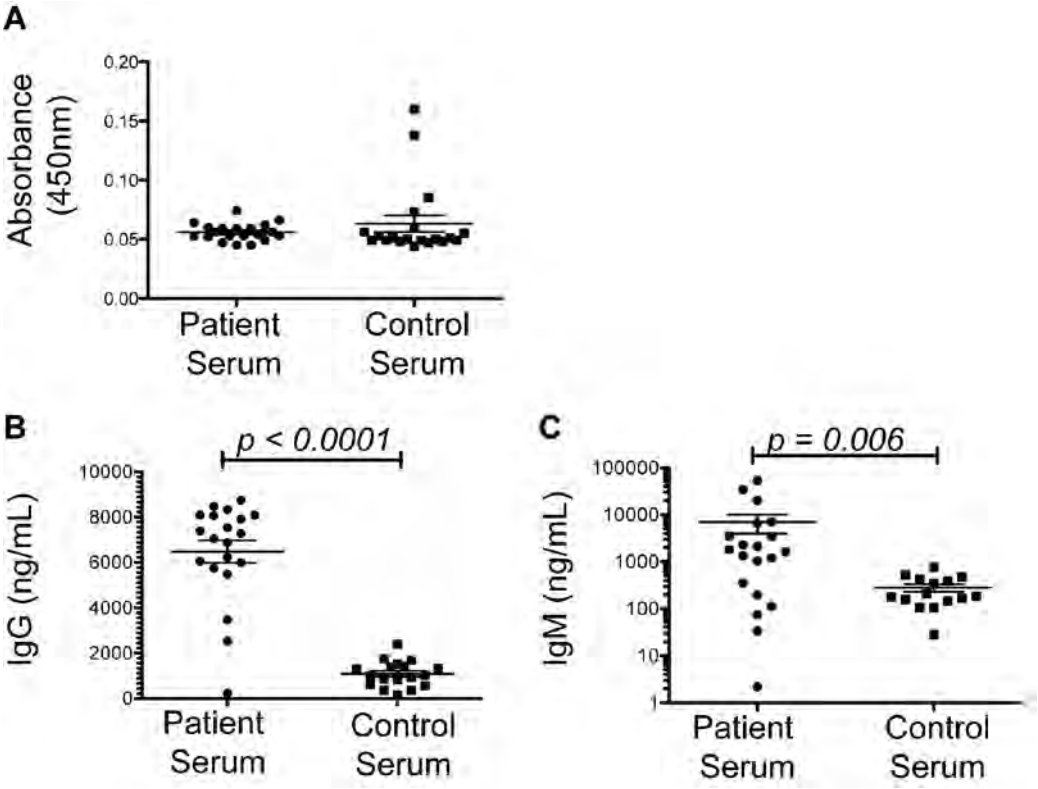

Figure 26: Hcp1 levels and anti-Hcp1 antibody responses in patients' versus controls' sera. Hcp1 serum levels were assayed with sandwich ELISA (Figure 26A). Results were expressed by absorbance measured at 450nm. IgG (Figure 26B) and IgM (Figure 26C) responses against native Hcp1 were assessed by ELISA in the serum of melioidosis patients or healthy individuals. Results are expressed as ng/mL of IgG and IgM. Statistics were calculated using the non-parametric, two-tailed Mann-Whitney test. IgG (Immunoglobulin G), IgM (Immunoglobulin M).

5.2.3 Affinity of Hcp1 for antigen-presenting cells

We incubated Hcp1 with peripheral blood mononuclear cells and found that it preferentially bound to the antigen presenting cells, namely B cells and monocytes (Figure 27). Surface-bound Hcp1 was detectable after one hour of incubation, with maximal binding observed after 24 hours.

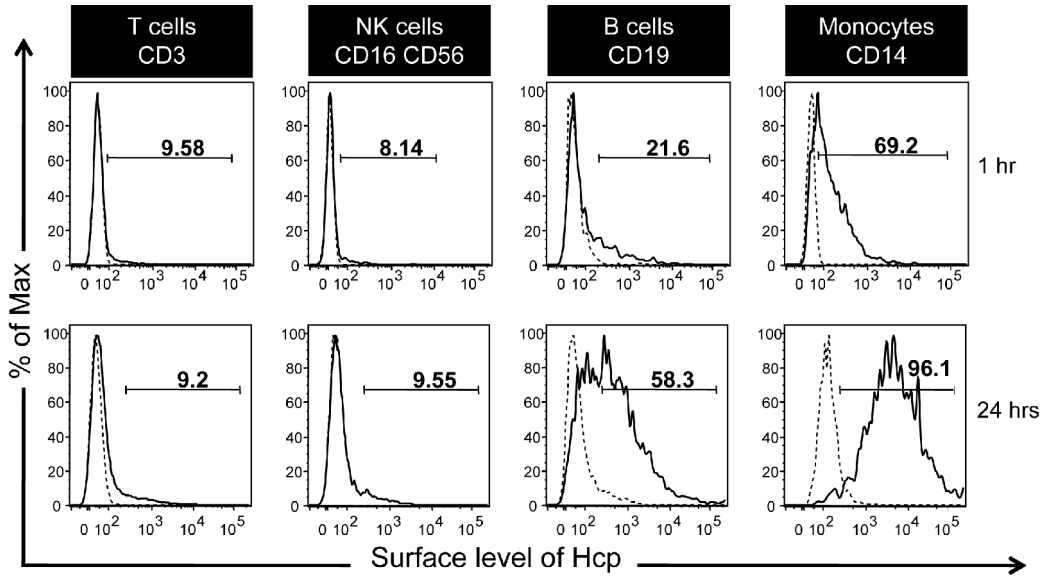

Figure 27: Affinity of Hcp1 for antigen presenting cells. 10 µg of Hcp1 was incubated with peripheral mononuclear cells at indicated time points. They were stained either with (solid line) or without (dotted line) anti-Hcp1 antibody, followed by anti-mouse AF4647 secondary antibody.

5.2.4 Exogenous addition of Hcp1 enhances MNGC formation in infected cells

We also incubated Hcp1 with RAW 264.7 macrophage cell line and similar to a previous study,[106] it was able to adhere to the surface of these cells (Figure 28).

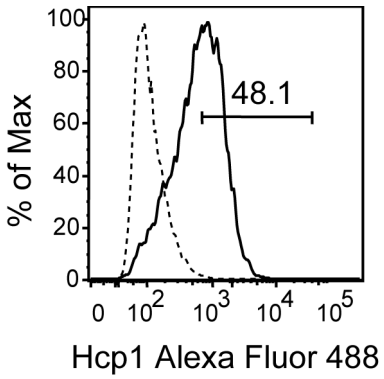

Figure 28: The surface binding of Hcp1 to RAW 264.7 macrophage cell line. The murine macrophage cells were incubated with either Hcp1-His (solid line) or BSA (dotted line) and cells were stained for Hcp1. Results shown are representative of two independent experiments.

To examine what other effects Hcp could exert on host cells, we determine whether addition of Hcp could induce host cell cytotoxicity as measured by ^{51}Cr release and found none (Figure 29A). Hcp1 also did not activate NF-κB as measured in THP-1 Blue cells whereas positive control LAM did (Figure 29B). It was unable to induce caspase-1 activation and the release of IL-1ß, as it did not induce IL-1ß above that of the negative control (LPS + BSA). LPS + ATP served as the positive control (Figure 29C).

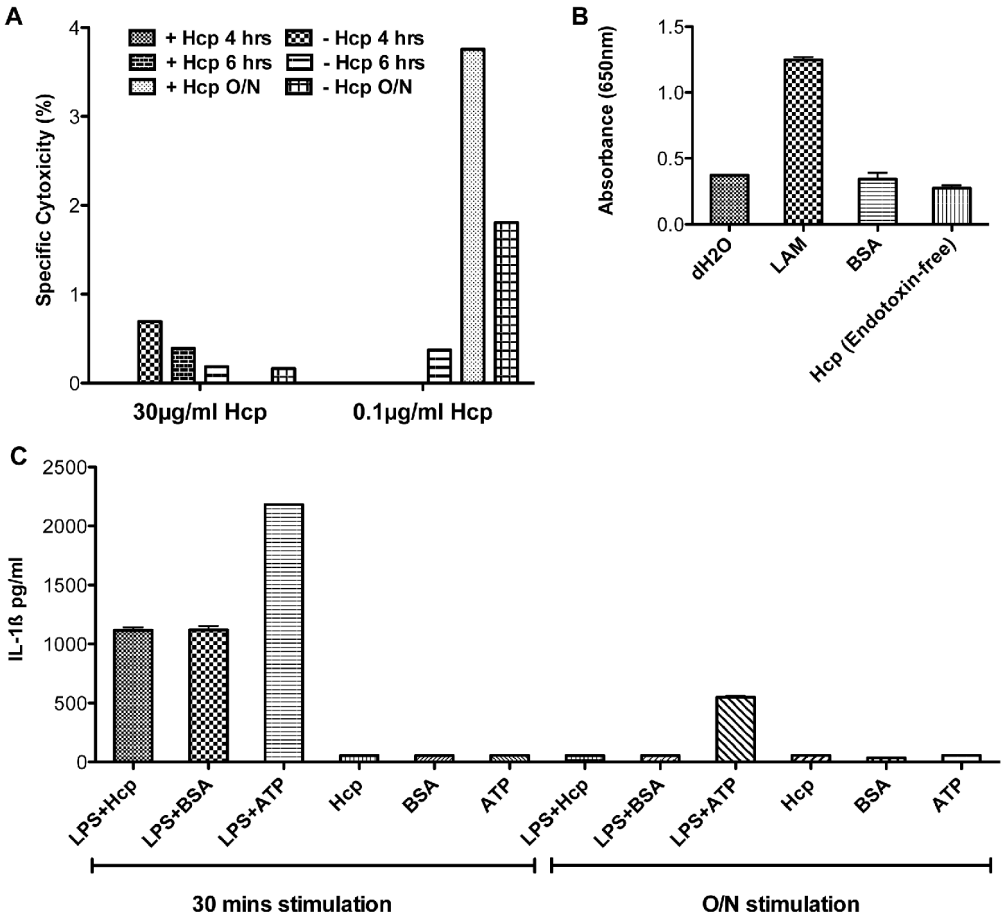

Figure 29: Functional assays on Hcp1. Hcp1 was not cytotoxic (Figure 29A). U937 cells pulsed with chromium-51 were incubated with Hcp1 at indicated time points. Cell lysis was expressed as percentage specific cytotoxicity (%). Hcp1 did not activate NF-κB (Figure 29B). THP1-Blue cells were treated with either LAM, BSA or endotoxin-free Hcp1. The cells were assayed for secreted alkaline phosphatase (absorbance 650 nm), which was the reporter protein for NF-κB activation, Results were expressed as relative light units (R.L.U). Hcp1 did not induce IL-1ß expression (Figure 29C). J774.1 mouse macrophages were stimulated with combinations of Hcp, BSA, ATP and LPS, for 30 mins or overnight. Levels of IL-1ß in the supernatant were measured and expressed as pg/mL. BSA, bovine serum albumin; dH2O, water control; LAM, lipoarabinomannan; LPS, lipopolysaccharide from M. tuberculosis; O/N, overnight.

B. pseudomallei T6SS1 is necessary for the formation of MNGC during bacterial infection.[70,71] The criteria for MNGC formation was the presence of polykaryocytes, as opposed to cell aggregates. In support of the observation that a functional T6SS is required for MNGC formation, we observed that the *Δhcp1* deletion mutant lost its ability to induce MNGC (Figure 30A). MNGC formation induced by wild type *B. pseudomallei* could be detected from approximately 9 hr post-infection (Figure 30B).

We subsequently preincubated RAW246.7 macrophages with Hcp1 prior to infection with *B. pseudomallei*, and found an observable change in the rate of MNGC formation in treated cells. At the same time point of 9 hr after infection, the Hcp1-treated cells formed much more extensive MNGC compared to the untreated controls (Figure 30B versus Figure 30A). Bovine serum albumin (BSA)-treated cells formed cellular aggregates with no or few discernible multinuclei rather than MNGC (Figure 30C). This indicates that the enhancing effect Hcp1 had on MNGC formation is unique to Hcp1 and not due to non-specific cellular aggregation. The fusion index for infected cells pretreated with Hcp1 was significantly higher compared to the other conditions (Figure 30D and E).

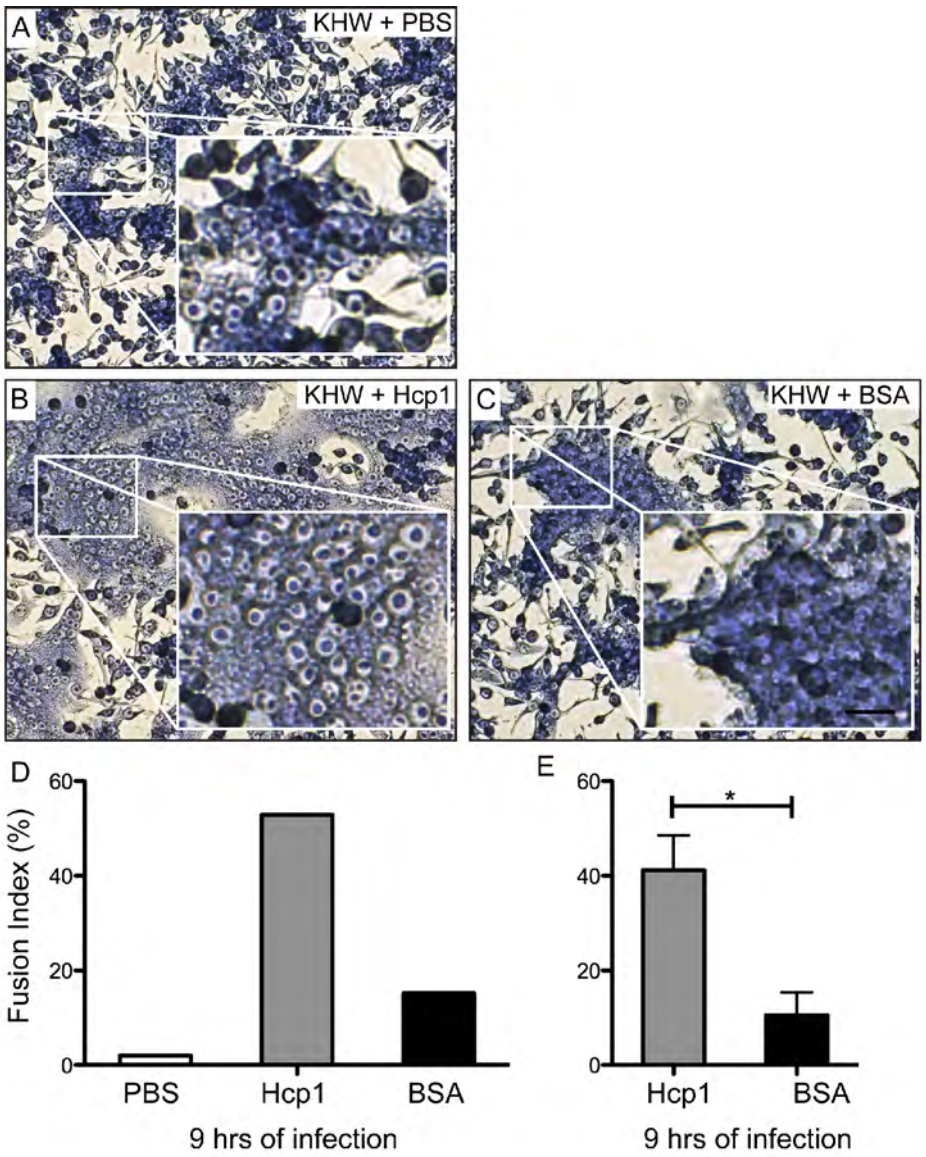

Figure 30: The effect of Hcp1 on MNGC formation. RAW 264.7 macrophages were treated with either PBS (Figure 30A), Hcp1 (Figure 30B) or BSA (Figure 30C). They were infected with overnight culture of wild type bacteria B. pseudomallei (KHW) (Figure 30A-C) at MOI 10:1 for 9 hours. Fusion indices were calculated for each treatment from a single experiment (Figure 30D). Fusion indices on cells treated with Hcp1 or BSA were calculated from three independent experiments and represented as means with standard deviation (Figure 30E). Scale bar: 40 µm.

5.2.5 Candidate mammalian ligands of Hcp1

5.2.5.1 Candidate ligands of Hcp1

This MNGC-enhancement effect might be mediated through interactions with specific proteins found on the mammalian cell's surface. Hence, we determined possible candidate ligands of Hcp1 using radioimmunoprecipitation. We found several potential cell surface binding partners of Hcp1 (Figure 31). U937 cells pulsed with ^{35}S-methionine in methionine/cysteine free medium were incubated with Hcp1 and lysed in detergent buffer. The lysate was immunoprecipitated with Hcp1-specific antibody and analyzed by SDS-PAGE. From the dried SDS-PAGE gel, several radioactive bands were detected in samples treated with Hcp1-specific antibody but not in those treated with an isotype control monoclonal antibody.

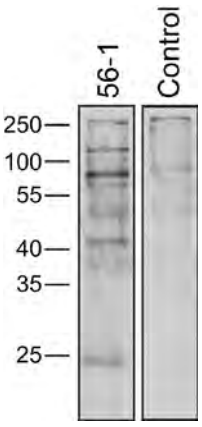

Figure 31: Pulse-labeling experiments to discover candidate ligands of Hcp1. ^{35}S-methionine pulsed U937 lysate were incubated with anti-Hcp1 antibody 56-1 or isotype control. Immunoprecipitated proteins were electrophoresed with SDS-PAGE, the gel was vacuum dried and autoradiography was done. Equal amount of protein (40 ng) of protein was loaded for each lane. Results shown are representative of two independent experiments.

5.2.5.2 Analysis of immunoprecipitated protein by mass spectrometry

Non-radioactive lysates were generated and immunoprecipitated with anti-Hcp1 antibody or an isotype control. The immunoprecipitated proteins were submitted for liquid chromatography-tandem mass spectrometry (LC-MS/MS) analysis.

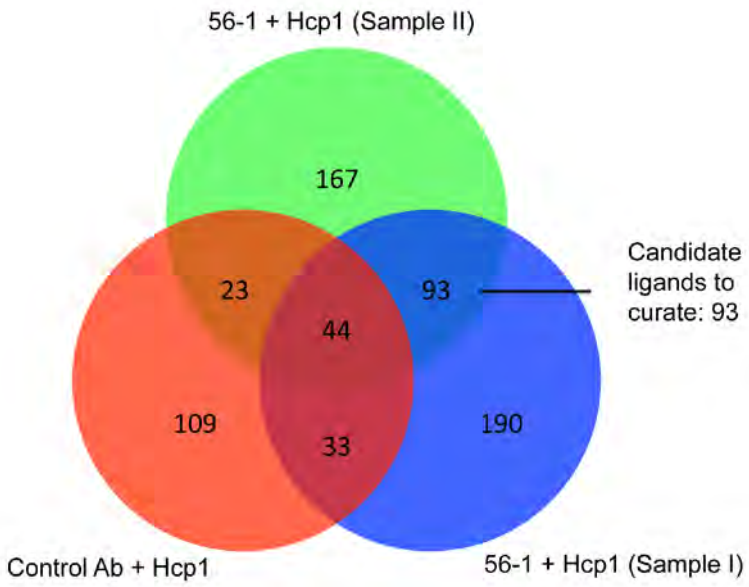

Figure 32: Comparison of protein hits from control sample and samples immunoprecipitated with 56-1 (anti-Hcp1 antibody). Samples were lysates generated from Hcp1-coated U937 cells. Comparison was made using PEAKS. 56-1 + Hcp1 (Sample I) and (Sample II), two replicate samples immunoprecipitated with 56-1. Control Ab + Hcp1, sample immunoprecipitated with isotype control antibody (Ab).

360 proteins in the sample treated with Hcp1-specific antibody (56-1 + Hcp1 (Sample I)) and 327 proteins for its duplicate (Sample II), and 209 proteins were identified for the control sample (Control Ab + Hcp1) (Figure 32). 93 proteins were found unique to the two samples treated with 56-1 and but not the control sample. Heat shock and cytoskeletal proteins were omitted from the list of 93, leaving four proteins as potential candidates (Table 6).

Table 6: Protein identification using PEAKS

Protein ID[a]	**Description**	**Unique peptides**[b]	**Protein score**[c]
IPI00182757	Isoform 1 of protein KIAA1967	29	99.2
IPI00646182	ATPase, Na+/K+ transporting, alpha 1 polypeptide	5	99.1
IPI00027493	4F2 cell-surface antigen heavy chain (CD98)	3	98.9
IPI00027430	Leukosialin (CD43)	2	84.0

[a]*Protein ID – identification number corresponding to International Protein Index (IPI) database human version 3.87;* [b]*Unique peptides – number of unique and significant spectra contributing to identification;* [c]*Protein score – the percentage confidence score reflecting the weighted sum of peptide probability scores from the protein.*

5.2.5.3 Biochemical validation of candidate ligands

CD98, a fusion regulatory protein, is one of the candidate ligands. Activating antibodies against CD98 were able to induce homotypic cell aggregation and MNGC formation of monocytes without any fusogen,[135] whereas inhibitory anti-CD98 antibodies were able to block *B. pseudomallei*-induced MNGC formation.[125] Hence, to further verify the identification of CD98 as a ligand for Hcp1, whole cells bound with either Hcp1 or BSA were lysed, affinity-purified, analyzed by SDS-PAGE and immunoblotted with a specific anti-CD98 antibody. Equal amount of proteins were loaded for both conditions (Figure 33A). CD98 was detected in the samples treated with Hcp1, confirming that this is a target receptor (Figure 33B). The experiment was repeated for the candidate Na+/K+ ATPase, one of the three other aforementioned candidate ligands, but it were both detected in samples treated with or without Hcp1, hence it was not verified as a specific target ligand for Hcp1 ((Figure 33C).

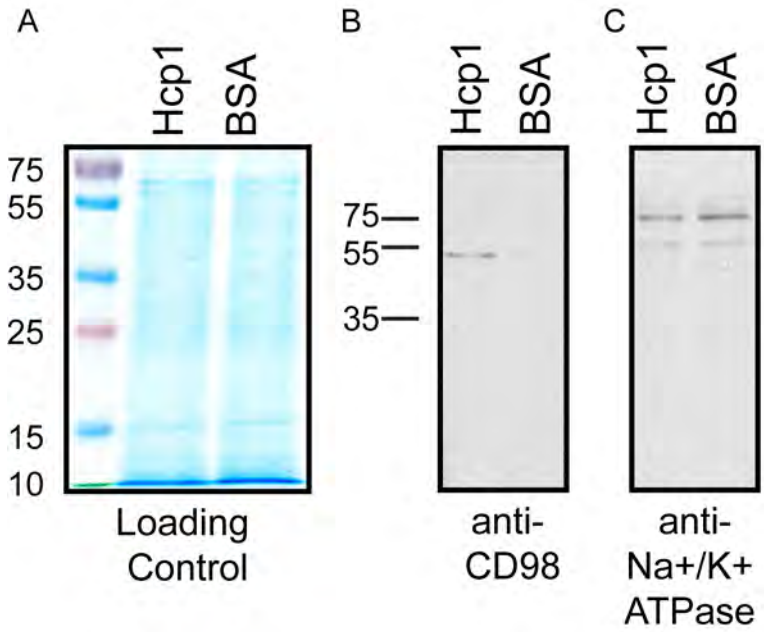

Figure 33: Biochemical validation of candidate mammalian ligands. U937 cells were incubated with either Hcp1 or BSA overnight at 37 °C. After lysis, the proteins were precipitated with cobalt resin and the purified eluate was concentrated. The eluate was subjected to Coomassie staining or immunoblot analysis for both conditions. Coomasie staining showed equal protein loading for both lanes (Figure 33A). Immunoblot analysis using a rabbit polyclonal anti-CD98 antibody (Figure 33B) or rabbit polyclonal anti-Na+/K+ ATPase antibody (Figure 33C).

KIAA1967 (deleted in breast cancer, DBC1) is a nucleus-localized transcription factor[136–138] and CD43 is ubiquitously expressed on both myeloid and non-myeloid lineage immune cells.[139] They are unlikely to be relevant based on the differential Hcp1 binding to monocytes and B cells versus T and NK cells.

5.2.6 Anti-CD98 antibody blocks MNGC formation

A previous study on the role of host cell surface molecules on MNGC formation showed that antibodies against CD98, CD47 (an integrin-associated protein), E-selectin (CD62E) and E-cadherin (CD324) could inhibit cell fusion.[69] Human U937 cells were used in the aforementioned study. Despite using the experimental conditions as previously described,[69] we were unable to replicate

MNGC formation in U937 cells successfully (Figure 34).

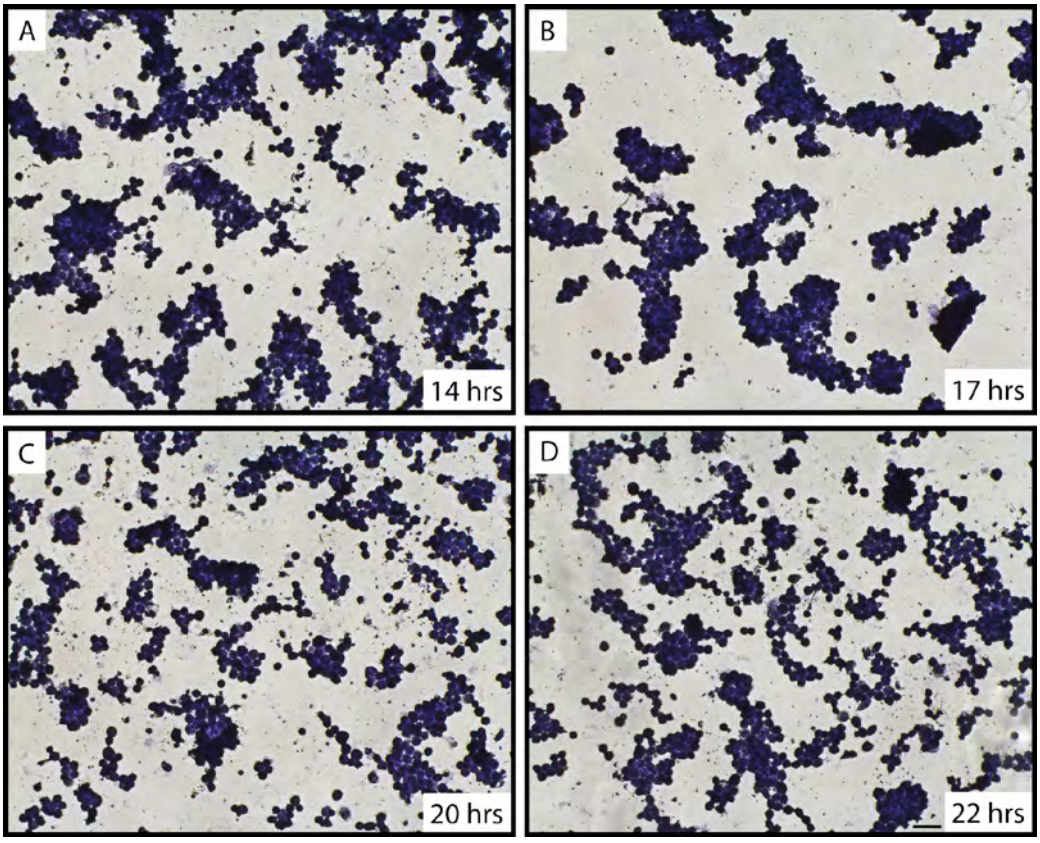

Figure 34: Effect of wild type B. pseudomallei infection on PMA-activated U937 cells. Cells were infected for 14 – 22 hrs (Figure 34A-D) and visualized with Giemsa stain. Results shown are from a single experiment. Scale bar: 50µm.

We thus sought to replicate the experiment in murine RAW264.7 cells, but using the same anti-CD98 antibody used in the previous work, which is against human CD98 (clone MEM-108).[69] Sequence alignment of the heavy chain from *homo sapiens* (Accession No: NP_001012680) and *mus musculus* (Accession no: AAB03769.1) show 75 % sequence identity (Figure 35) between the two proteins. The anti-human CD98 antibody bound to RAW 264.7 cells while its isotype control antibody did not (Figure 36). Given that there is high sequence identity between the human and murine CD98s, we made the assumption that

the anti-human CD98 antibody was cross-reacting with murine CD98.

```
CD98 Homo sapiens  103  MSQDTEVDMKEVELNELEPEKQPMNAASGAAMSLAGAEKNGLVKIKVAEDEAEAAAAAKF  162
                        MSQDTEVDMK+VELNELEPEKQPMNAA GAAMSLAGAEKNGLVKIKVAEDE EA  AAKF
CD98 Mus musculus  1    MSQDTEVDMKDVELNELEPEKQPMNAADGAAMSLAGAEKNGLVKIKVAEDETEAGVAAKF  60

CD98 Homo sapiens  163  TGLSKEELLKVAGSPGWVRTRWALLLLFWLGWLGMLAGAVVIIVRAPRCRELPAQKWWHT  222
                        TGLSKEELLKVAGSPGWVRTRWALLLLFWLGWLGMLAGAVVIIVRAPRCRELP Q+WWH
CD98 Mus musculus  61   TGLSKEELLKVAGSPGWVRTRWALLLLFWLGWLGMLAGAVVIIVRAPRCRELPVQRWWHK  120

CD98 Homo sapiens  223  GALYRIGDLQAFQGHGAGNLAGLKGRLDYLSSLKVKGLVLGPIHKNQKDDVAQTDLLQID  282
                        GALYRIGDLQAF G  AG +AGLK  L+YLS+LKVKGLVLGPIHKNQKD++ +TDL QI+
CD98 Mus musculus  121  GALYRIGDLQAFVGRDAGGIAGLKSHLEYLSTLKVKGLVLGPIHKNQKDEINETDLKQIN  180

CD98 Homo sapiens  283  PNFGSKEDFDSLLQSAKKKSIRVILDLTPNYRGENSWF-STQVDTVATKVKDALEFWLQA  341
                        P  GS+EDF  LLQSAKKKSI +ILDLTPNY+G+N+WF   Q D VATK+K+AL  WLQ
CD98 Mus musculus  181  PTLGSQEDFKDLLQSAKKKSIHIILDLTPNYQGQNAWFLPAQADIVATKMKEALSSWLQD  240

CD98 Homo sapiens  342  GVDGFQVRDIENLKDASSFLAEWQNITKGFSEDRLLIAGTNSSDLQQILSLLESNKDLLL  401
                        GVDGFQ RD+  L +A  +LAEWQNITK  SEDRL+IAGT SSDLQQI+++L+S  DLLL
CD98 Mus musculus  241  GVDGFQFRDVGKLMNAPLYLAEWQNITKNLSEDRLVIAGTESSDLQQIVNILDSTSDLLL  300

CD98 Homo sapiens  402  TSSYLSDSGSTGEHTKSLVTQYLNATGNRWCSWSLSQARLLTSFLPAQLLRLYQLMLFTL  461
                        TSSYLS+S  TGE T+SL T+ ++ATG+ WCSWS+SQA LL  F+P  LLRLYQL+LFTL
CD98 Mus musculus  301  TSSYLSNSTHTGERTESLDTRLVSATGSHWCSWSVSQAALLADFIPDHLLRLYQLLLFTL  360

CD98 Homo sapiens  462  PGTPVFSYGDEIGLDAAALPGQPMEAPVMLWDESSFPDIPGAVSANMTVKGQSEDPGSLL  521
                        PGTPVFSYGDE+GL   ALPGQP +AP+M W+ESS   IP  VS NMTVKGQ+EDPGSLL
CD98 Mus musculus  361  PGTPVFSYGDELGLQ-GALPGQPAKAPLMPWNESSIFHIPRPVSLNMTVKGQNEDPGSLL  419

CD98 Homo sapiens  522  SLFRRLSDQRSKERSLLHGDFHAFSAGPGLFSYIRHWDQNERFLVVLNFGDVGLSAGLQA  581
                        + FRRLSD R KERSLLHGDFHA S+ P LFSYIRHWDQNER+LVVLNF D G SA L A
CD98 Mus musculus  420  TQFRRLSDLRGKERSLLHGDFHALSSTPDLFSYIRHWDQNERYLVVLNFRDSGRSARLGA  479

CD98 Homo sapiens  582  SDLPASASLPAKADLLLST---QPGREEGSPLELERLKLEPHEGLLLRFPYAA  631
                        S+LPA  SLPA A LLLST   +  REE + L+LE L L P+EGLLL+FP+ A
CD98 Mus musculus  480  SNLPAGISLPASAKLLLSTDSARQSREEDTSLKLENLSLNPYEGLLLQFPFVA  532
```

Figure 35: Protein sequence alignment of the heavy chain from CD98 (4F2) from homo sapiens and mus musculus. Key: Single letters: amino acids. +: similar amino acid residues. Single letters between sequences: conserved amino acid residues.

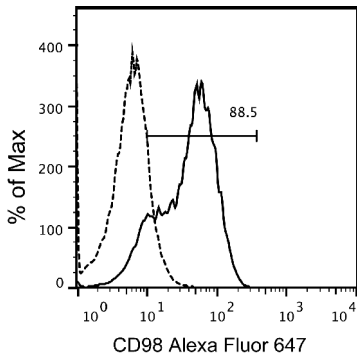

Figure 36: Affinity of anti-human CD98 (clone MEM-108) antibody for RAW 264.7 macrophage cell line. The murine macrophage cells were stained with either anti-CD98 (solid line) or an isotype control antibody (dotted line), followed by an Alexa Fluor® 647-conjugated anti-mouse secondary antibody. Results shown are from a single experiment.

RAW 264.7 cells treated with wild type Hcp1 was infected with wild type *B. pseudomallei* for 9 and 11 hours. The infected cells were treated with either isotype control antibody or the anti-CD98 antibody an hour post-infection. At 9 hours post-infection, small MNGCs could be observed in the cells treated with the control antibody (Figure 37A) but not in the anti-CD98 antibody treated cells (Figure 37B). Extensive MNGC formation was observed in the cells treated with the control antibody at 11 hours post-infection (Figure 37C), but the cells treated with anti-CD98 antibody remained unfused (Figure 37D).

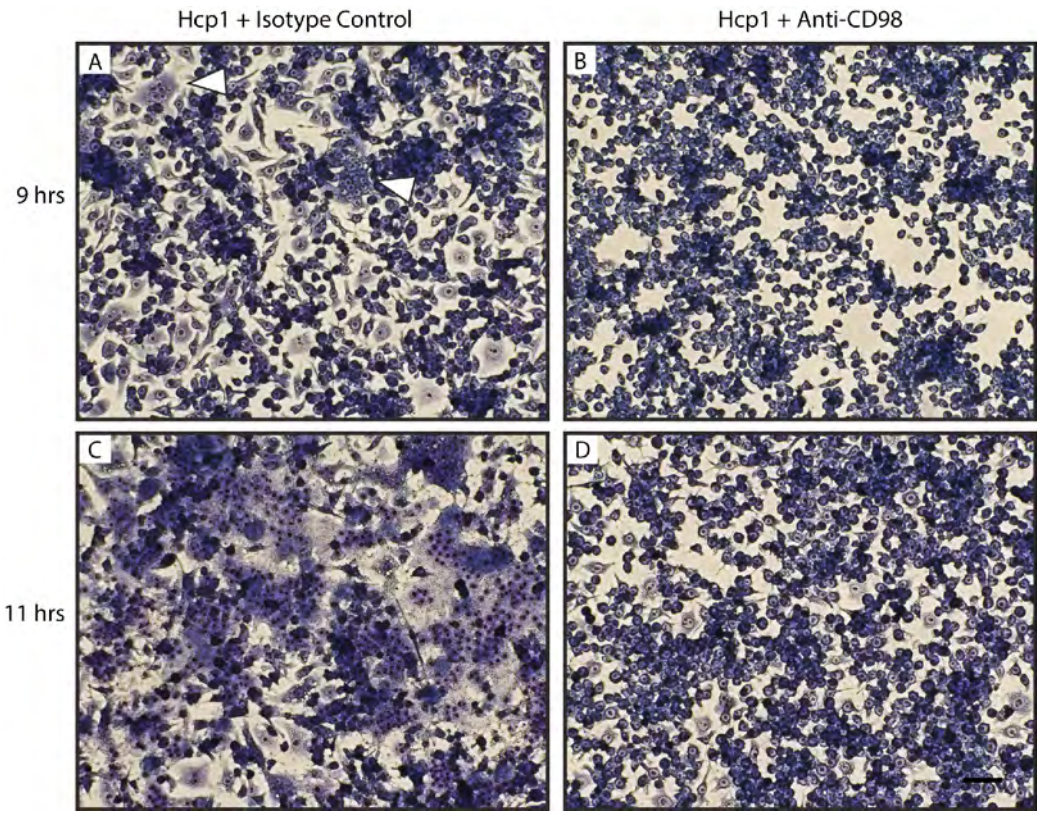

Figure 37: Effect of anti-CD98 antibody on MNGC formation. RAW 264.7 cells treated with wild type Hcp1 were infected with wild type B. pseudomallei for 9 hours (Figure 37A and B) and 11 hours (Figure 37C and D). The cells were also treated with either isotype control antibody (Hcp1 + Isotype Control) (Figure 37A and C) or anti-CD98 antibody (Hcp1 + Anti-CD98) (37B and D) and visualized with Giemsa stain. Results shown are from a single experiment. White arrows highlight the small MNGCs.

5.2.7 Generation of an in-frame *Δhcp1* mutant to determine how the structure of Hcp1 impact on T6SS function.

The expression of the T6SS1 is controlled by VirAG and BprC. Within the gene cluster, *hcp1* has its own upstream promoter and its stop codon overlaps with the start codon of the next downstream gene *tssC* (Figure 7 in Materials and Methods).

In the previous experiments (Section 3.2.2.4, Figure 16, and Section 5.2.1, Figure 25), the mutants *Δhcp1:tmp* and *Δhcp1* were used a negative control for anti-Hcp1 antibody specificity where no Hcp1 was expressed. These mutant carried an out-of-frame mutation (Table 3). The bacterial numbers in the infected cells between mutant and wild type were equivalent at the point of these experiments. It is also certain that the antibody is specific for Hcp1 and not other *B. pseudomallei* proteins, because the antibody does not bind to another *B. pseudomallei*-derived protein TssM (Figure 12), and is binding to a single protein of the expected molecular weight (Figure 16). Hence in these instances, the question of whether the downstream T6SS genes were affected or was inconsequential.

Given that addition of exogenous Hcp enhances MNGC formation in infected cells and infection of cells results in surface localization of endogenous Hcp, it may be possible that these surface-localized Hcp found in infected host cells serves to enhance MNGC formation during a natural infection. However the

generation of a *Δhcp1* would compromise the whole T6SS apparatus. This results in our inability to ascribe the functional defect such as MNGC formation to *hcp1* or to any other T6SS genes as a *Δhcp1* mutant has no secretion function and therefore no effector function due to the structural role that Hcp1 has. Nevertheless, as the previous *Δhcp1* mutants was out of frame, we recreated an in-frame *Δhcp1* mutant to demonstrate the importance of T6SS function to MNGC formation.

An in-frame *Δhcp1* mutant (*Δhcp1inf*) (Table 3 and Figure 7) was generated and complemented with the *hcp1* gene (pUCP-*hcp1)* or *hcp1-tssC1* genes *(*pUCP-*hcp1-tssC1),* because a deletion of *hcp1* could also be a polar deletion that affects the expression of *tssC.* The genes *hcp1 and hcp1-tssC1* were each ligated into the pUCP28T vector in the reverse orientation to the pLacZ promoter, so that the expression of the *hcp1* would be controlled by its endogenous promoter.

However, in an infection assay with RAW 264.7 cells, the expression of *hcp1* in the complemented mutants were less than 10% of the wild type *B. pseudomallei* (Figure 38A). Hence unlike the wild type *B. pseudomallei* (Figure 38B), the negative control (*Δhcp1inf* + pUCP28T, Figure 38C) and the complemented mutants were unable to induce MNGC in RAW 264.7 cells (Figure 38D-E).

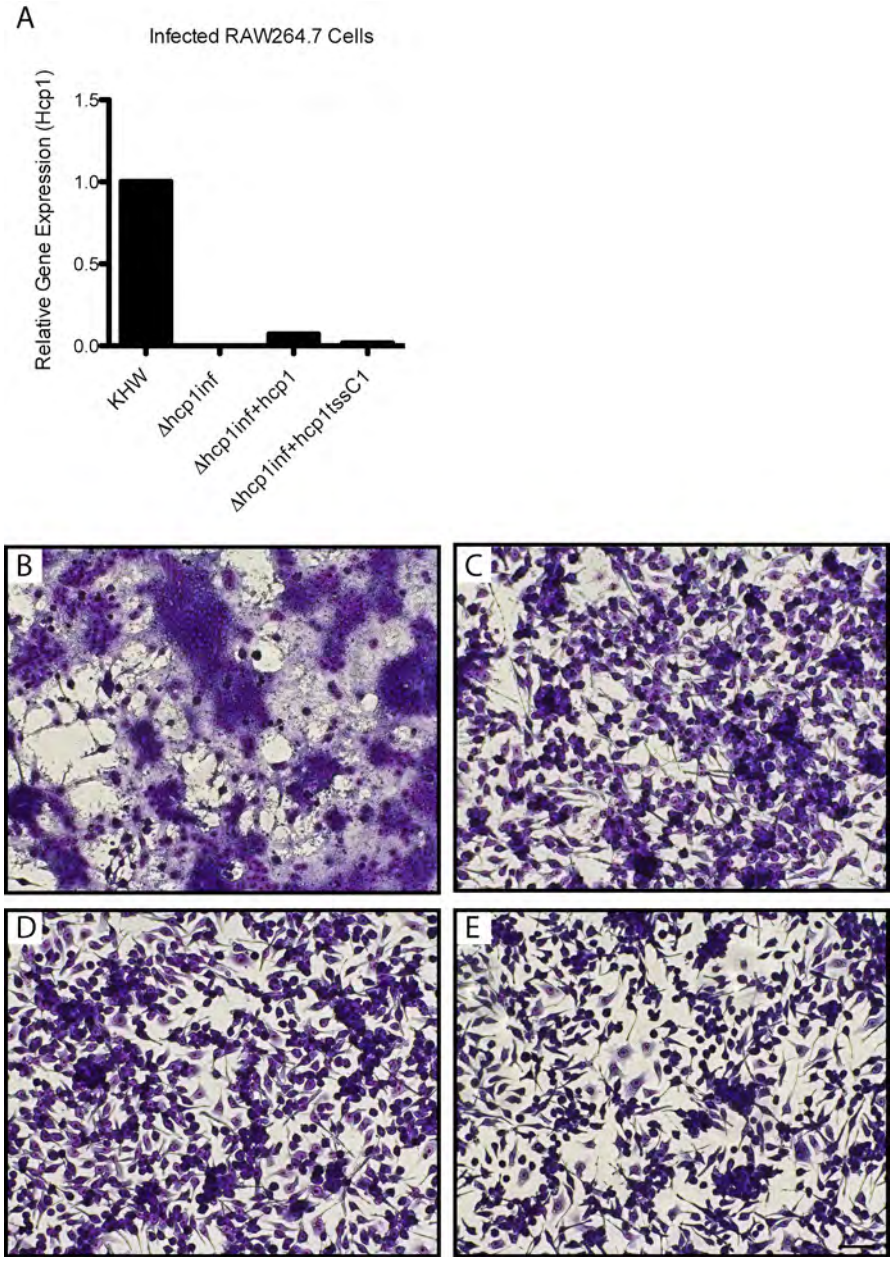

Figure 38: The phenotype of the complemented Δhcp1inf mutant. RAW 264.7 cells were infected with wild type B. pseudomallei (KHW), Δhcp1inf + pUCP28T (Δhcp1inf), Δhcp1inf + pUCP-hcp1 (Δhcp1inf + hcp1) and Δhcp1inf+pUCP-hcp1-tssC1 (Δhcp1inf+hcp1-tssC1) for 9 hrs and assayed for relative expression of hcp1 (Figure 38A). RAW 264.7 cells infected with KHW (Figure 38B), Δhcp1inf (Figure 38C), Δhcp1inf+hcp1 (Figure 38D) and Δhcp1inf+hcp1-tssC1 (Figure 38E) for 9 hrs were assayed for MNGC formation. Scale bar: 50 µm

Our inability to complement the function of the *Δhcp1inf* might be due to the need of a stronger promoter other than the endogenous *hcp1* promoter to drive

hcp1 expression. Placing the *hcp1 gene* under a strong constitutive promoter such as Plac may resolve the issue of low mRNA expression in the complemented mutants and lead to a sucessful complementation.

5.2.8 Recombinant Hcp1 double mutant proteins suppress MNGC formation

We generated two Hcp1 mutants $Hcp1^{Q46AE47A}$ and $Hcp1^{L49AT50A}$, where the former had alanine substitutions at positions 46 (glutamine, Q) and 47 (glutamic acid, E) and the latter at positions 49 (leucine, L) and 50 (threonine, T). These mutations reside within the extended loop region (Figure 23) of Hcp1.

We examined whether the mutant proteins retain the same cell adhesive property as the wild type Hcp1 by incubating them with RAW 264.7 macrophages. The mutant and wild type Hcp1 showed comparable binding to the cells (Figure 39A), with $Hcp1^{Q46AE47A}$ showing slightly lower binding (yellow histogram) but this difference was not significant. Preincubation of 10-fold more mutant $Hcp1^{Q46AE47A}$ protein relative to wild type Hcp1 to host cells did not prevent the binding of wild type Hcp1 to cells (Figure 39B). Hence the mutant protein did not competitively inhibit the binding of wild type Hcp1 to host cells.

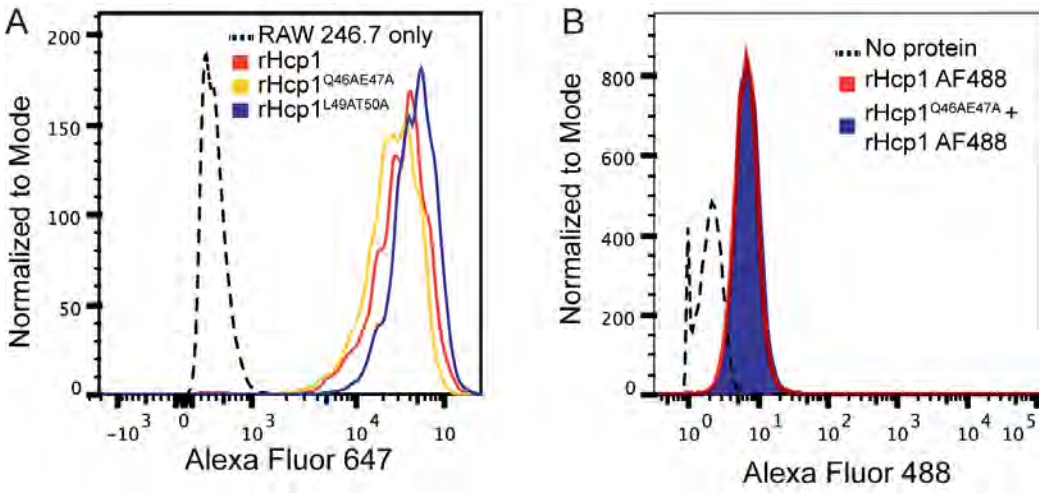

Figure 39: Binding properties of wild type and mutant Hcp1s. The mutants show comparable binding to RAW 264.7 relative to wild type Hcp1 (Figure 39A). Cells were either untreated (red histogram), or treated with 100 µg of Hcp1^{Q46AE47A} (blue solid histogram) overnight, and subsequently incubated with 10 µg of wild type Hcp1 conjugated to AF488 (Hcp1 AF488). The negative control was unlabelled cells (black dotted histogram).

The oligomerization states of wild type Hcp1 and mutant proteins Hcp1^{Q46AE47A} and Hcp1^{L49AT50A} in solution were compared using dynamic light scattering (DLS) (Figure 40 and Table 7). We were only able to obtain data for wild type Hcp1 and Hcp1^{Q46AE47A}. DLS of concentrated wild type Hcp1 (8 mg/mL) showed an apparent molecular weight of 270 kDa corresponding to two hexamers of Hcp1 (Figure 40B and Table 7). However, the mutant Hcp1^{Q46AE47A} at 8 mg/mL only showed 142 kDa, which corresponds to a hexamer (Figure 40D and Table 7). These observations suggest that the mutated residues might be important for the stacking assembly of Hcp1.

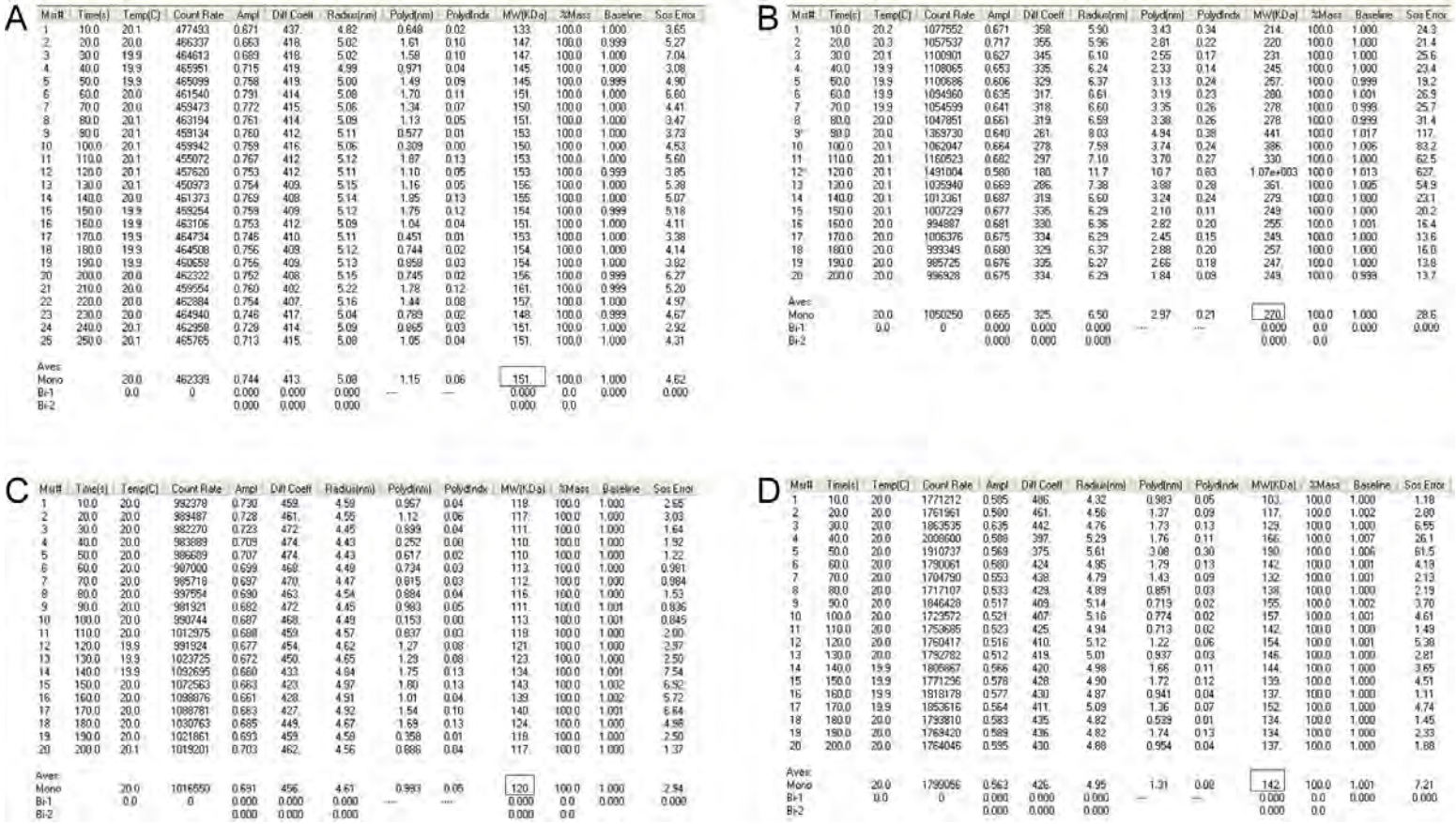

A

Mst#	Time(s)	Temp(C)	Count Rate	Ampl	Diff Coeff	Radius(nm)	Polyd(nm)	Polydindx	MW(KDa)	%Mass	Baseline	Sos Error
1	10.0	20.1	477493	0.671	437.	4.82	0.648	0.02	133.	100.0	1.000	3.65
2	20.0	20.0	466337	0.663	418.	5.02	1.61	0.10	147.	100.0	0.999	5.27
3	30.0	19.9	464613	0.689	418.	5.02	1.58	0.10	147.	100.0	1.000	7.04
4	40.0	19.9	465951	0.715	419.	4.99	0.971	0.04	145.	100.0	1.000	3.08
5	50.0	19.9	465099	0.758	419.	5.00	1.49	0.09	145.	100.0	0.999	4.90
6	60.0	20.0	461540	0.791	414.	5.08	1.70	0.11	151.	100.0	1.000	6.60
7	70.0	20.0	459473	0.772	415.	5.06	1.34	0.07	150.	100.0	1.000	4.41
8	80.0	20.1	463194	0.761	414.	5.09	1.13	0.05	151.	100.0	1.000	3.47
9	90.0	20.1	459134	0.760	412.	5.11	0.577	0.01	153.	100.0	1.000	3.73
10	100.0	20.1	459942	0.758	416.	5.06	0.309	0.00	150.	100.0	1.000	4.53
11	110.0	20.1	455072	0.767	412.	5.12	1.87	0.13	153.	100.0	1.000	5.60
12	120.0	20.1	457620	0.753	412.	5.11	1.10	0.05	153.	100.0	0.999	3.85
13	130.0	20.1	459373	0.754	409.	5.15	1.16	0.05	156.	100.0	1.000	5.38
14	140.0	20.0	461373	0.769	408.	5.14	1.95	0.13	155.	100.0	1.000	5.07
15	150.0	19.9	459254	0.758	409.	5.12	1.75	0.12	154.	100.0	0.999	5.18
16	160.0	19.9	463106	0.753	412.	5.09	1.04	0.04	151.	100.0	1.000	4.11
17	170.0	19.9	464734	0.746	410.	5.11	0.451	0.01	153.	100.0	1.000	3.38
18	180.0	19.9	464508	0.756	409.	5.12	0.744	0.02	154.	100.0	1.000	4.14
19	190.0	19.9	460658	0.756	409.	5.13	0.958	0.03	154.	100.0	1.000	3.82
20	200.0	20.0	462322	0.752	408.	5.15	0.745	0.02	156.	100.0	0.999	6.27
21	210.0	20.0	459554	0.760	402.	5.22	1.78	0.12	161.	100.0	0.999	5.20
22	220.0	20.0	462884	0.754	407.	5.16	1.44	0.08	157.	100.0	1.000	4.97
23	230.0	20.0	464940	0.746	417.	5.04	0.788	0.02	148.	100.0	0.999	4.67
24	240.0	20.1	462958	0.729	414.	5.09	0.965	0.03	151.	100.0	1.000	2.92
25	250.0	20.1	465765	0.713	415.	5.08	1.05	0.04	151.	100.0	1.000	4.31
Aves:												
Mono		20.0	462339.	0.744	413.	5.08	1.15	0.06	151.	100.0	1.000	4.62
Bi-1		0.0	0	0.000	0.000	0.000	---	---	0.000	0.0	0.000	0.000
Bi-2				0.000	0.000	0.000			0.000	0.0		

B

Mst#	Time(s)	Temp(C)	Count Rate	Ampl	Diff Coeff	Radius(nm)	Polyd(nm)	Polydindx	MW(KDa)	%Mass	Baseline	Sos Error
1	10.0	20.2	1077552	0.671	358.	5.90	3.43	0.34	214.	100.0	1.000	24.3
2	20.0	20.3	1057537	0.717	355.	5.96	2.81	0.22	220.	100.0	1.000	21.4
3	30.0	20.1	1100901	0.627	345.	6.10	2.55	0.17	231.	100.0	1.000	25.6
4	40.0	19.9	1108065	0.653	335.	6.24	2.33	0.14	245.	100.0	1.000	23.4
5	50.0	19.9	1100686	0.606	329.	6.37	3.13	0.24	257.	100.0	0.999	19.2
6	60.0	19.9	1094960	0.635	317.	6.61	3.19	0.23	280.	100.0	1.001	26.9
7	70.0	19.9	1054599	0.641	318.	6.60	3.35	0.26	278.	100.0	0.999	25.7
8	80.0	20.0	1047851	0.661	319.	6.59	3.38	0.26	278.	100.0	0.999	31.4
9	90.0	20.0	1359730	0.640	261.	8.03	4.94	0.38	441.	100.0	1.017	117.
10	100.0	20.1	1062047	0.664	278.	7.58	3.74	0.24	386.	100.0	1.006	83.2
11	110.0	20.1	1160523	0.682	297.	7.10	3.70	0.27	330.	100.0	1.000	62.5
12	120.0	20.1	1491004	0.580	180.	11.7	10.7	0.83	1.07e+003	100.0	1.013	627.
13	130.0	20.1	1025940	0.669	286.	7.38	3.88	0.28	361.	100.0	1.005	54.9
14	140.0	20.1	1013361	0.687	319.	6.60	3.24	0.24	279.	100.0	1.000	23.1
15	150.0	20.1	1007229	0.677	335.	6.29	2.10	0.11	249.	100.0	1.000	20.2
16	160.0	20.0	994887	0.681	330.	6.36	2.82	0.20	255.	100.0	1.001	16.4
17	170.0	20.0	1006376	0.675	334.	6.29	2.45	0.15	249.	100.0	1.000	13.6
18	180.0	20.0	999349	0.680	329.	6.37	2.88	0.20	257.	100.0	1.000	16.0
19	190.0	20.0	985725	0.676	335.	6.27	2.65	0.18	247.	100.0	1.000	13.8
20	200.0	20.0	996828	0.675	334.	6.29	1.84	0.09	249.	100.0	0.999	13.7
Aves:												
Mono		20.0	1050250	0.665	325.	6.50	2.97	0.21	270.	100.0	1.000	28.6
Bi-1		0.0	0	0.000	0.000	0.000	---	---	0.000	0.0	0.000	0.000
Bi-2				0.000	0.000	0.000			0.000	0.0		

C

Mst#	Time(s)	Temp(C)	Count Rate	Ampl	Diff Coeff	Radius(nm)	Polyd(nm)	Polydindx	MW(KDa)	%Mass	Baseline	Sos Error
1	10.0	20.0	992378	0.730	459.	4.59	0.957	0.04	119.	100.0	1.000	2.65
2	20.0	20.0	989487	0.728	461.	4.55	1.12	0.06	117.	100.0	1.000	3.03
3	30.0	20.0	982270	0.723	472.	4.45	0.899	0.04	111.	100.0	1.000	1.64
4	40.0	20.0	983889	0.709	474.	4.43	0.252	0.00	110.	100.0	1.000	1.92
5	50.0	20.0	986689	0.707	474.	4.43	0.617	0.02	110.	100.0	1.000	1.22
6	60.0	20.0	987000	0.699	468.	4.49	0.734	0.03	113.	100.0	1.000	0.981
7	70.0	20.0	985718	0.697	470.	4.47	0.815	0.03	112.	100.0	1.000	0.984
8	80.0	20.0	997554	0.690	463.	4.54	0.884	0.04	116.	100.0	1.000	1.53
9	90.0	20.0	981921	0.682	472.	4.45	0.993	0.05	111.	100.0	1.001	0.836
10	100.0	20.0	990744	0.687	468.	4.49	0.153	0.00	113.	100.0	1.001	0.845
11	110.0	20.0	1012975	0.698	459.	4.57	0.837	0.03	119.	100.0	1.000	2.00
12	120.0	19.9	991924	0.677	454.	4.62	1.27	0.08	121.	100.0	1.000	2.97
13	130.0	19.9	1023725	0.672	450.	4.65	1.29	0.08	123.	100.0	1.000	2.50
14	140.0	19.9	1092695	0.680	433.	4.84	1.75	0.13	134.	100.0	1.001	7.54
15	150.0	20.0	1072563	0.663	423.	4.97	1.80	0.13	143.	100.0	1.002	6.92
16	160.0	20.0	1098876	0.661	428.	4.91	1.01	0.04	139.	100.0	1.002	5.72
17	170.0	20.0	1088781	0.683	427.	4.92	1.54	0.10	140.	100.0	1.001	6.64
18	180.0	20.0	1030763	0.685	449.	4.67	1.69	0.13	124.	100.0	1.000	4.98
19	190.0	20.0	1021861	0.693	459.	4.59	0.358	0.01	119.	100.0	1.000	2.50
20	200.0	20.1	1019201	0.703	462.	4.56	0.686	0.04	117.	100.0	1.000	1.37
Aves:												
Mono		20.0	1016550	0.691	456.	4.61	0.993	0.05	120.	100.0	1.000	2.54
Bi-1		0.0	0	0.000	0.000	0.000	---	---	0.000	0.0	0.000	0.000
Bi-2				0.000	0.000	0.000			0.000	0.0		

D

Mst#	Time(s)	Temp(C)	Count Rate	Ampl	Diff Coeff	Radius(nm)	Polyd(nm)	Polydindx	MW(KDa)	%Mass	Baseline	Sos Error
1	10.0	20.0	1771212	0.585	486.	4.32	0.993	0.05	103.	100.0	1.000	1.18
2	20.0	20.0	1761961	0.560	461.	4.56	1.37	0.09	117.	100.0	1.002	2.80
3	30.0	20.0	1863535	0.635	442.	4.76	1.73	0.13	129.	100.0	1.000	6.55
4	40.0	20.0	2008600	0.588	397.	5.29	1.76	0.11	166.	100.0	1.007	26.1
5	50.0	20.0	1910737	0.569	375.	5.61	3.08	0.30	190.	100.0	1.006	61.5
6	60.0	20.0	1790061	0.580	424.	4.95	1.79	0.13	142.	100.0	1.001	4.19
7	70.0	20.0	1704790	0.553	438.	4.79	1.43	0.09	132.	100.0	1.001	2.13
8	80.0	20.0	1717107	0.533	429.	4.89	0.851	0.03	138.	100.0	1.000	2.19
9	90.0	20.0	1646428	0.517	409.	5.14	0.719	0.02	155.	100.0	1.002	3.70
10	100.0	20.0	1723572	0.521	407.	5.16	0.774	0.02	157.	100.0	1.001	4.61
11	110.0	20.0	1758685	0.523	425.	4.94	0.713	0.02	142.	100.0	1.000	1.49
12	120.0	20.0	1760417	0.516	410.	5.12	1.22	0.06	154.	100.0	1.001	5.38
13	130.0	20.0	1782082	0.512	419.	5.01	0.937	0.03	146.	100.0	1.000	2.81
14	140.0	19.9	1806867	0.566	420.	4.98	1.66	0.11	144.	100.0	1.000	3.65
15	150.0	19.9	1771236	0.578	428.	4.90	1.72	0.12	139.	100.0	1.000	4.51
16	160.0	19.9	1818179	0.577	430.	4.87	0.941	0.04	137.	100.0	1.000	1.11
17	170.0	19.9	1853616	0.564	411.	5.09	1.36	0.07	152.	100.0	1.000	4.74
18	180.0	20.0	1793810	0.583	435.	4.82	0.539	0.01	134.	100.0	1.000	1.45
19	190.0	20.0	1769420	0.589	436.	4.82	1.74	0.13	134.	100.0	1.000	2.33
20	200.0	20.0	1764046	0.595	430.	4.88	0.954	0.04	137.	100.0	1.000	1.88
Aves:												
Mono		20.0	1799056	0.563	426.	4.95	1.31	0.09	142.	100.0	1.001	7.21
Bi-1		0.0	0	0.000	0.000	0.000	---	---	0.000	0.0	0.000	0.000
Bi-2				0.000	0.000	0.000			0.000	0.0		

Figure 40: Dynamic light scattering profile for wild type Hcp1 and Hcp1^{Q46AE47A} at 2 mg/mL (Panel A) and 8 mg/mL (Panel B). Molecular weights for Hcp1 were 151 kDa and 270 kDA respectively. The mutated protein Hcp1^{Q46AE47A} at 2 mg/mL (Panel C) and 8 mg/mL (Panel D). Molecular weights for Hcp1^{Q46AE47A} were 120 kDa and 142 kDA respectively. Figure was generated in collaboration with Dr Chacko Jobichen.

Table 7: Summary of DLS results on wild type Hcp1 and Hcp1^{Q46AE47A}

Sample	**Radius[a] (nm)**	**Polyd (nm)[b]**	**MW[c]**	**Sos Error[d]**
A (Hcp1 2mg/mL)	5.08	1.15	151	4.62
B (Hcp1 8mg/mL)	6.50	2.97	270	28.6
C (Hcp1^{Q46AE47A} 2mg/mL)	4.61	0.993	120	2.94
D (Hcp1^{Q46AE47A} 8mg/mL)	4.95	1.31	142	7.21

[a]Radius - hydrodynamic radius of the molecule. [b]Polyd - polydispersity parameter. [c]MW – estimated molecular weight. [d]Sos error – value lesser than 50 indicates a good fit.

We assessed the effects of surface-bound mutant Hcp1 proteins on MNGC formation of infected RAW 264.7 macrophages. Untreated infected cells showed much more extensive MNGC (Figure 41A) relative to the cells treated with the mutant proteins, which developed small MNGC (Figure 41B and C). The fusion indices were significantly lower in those treated with mutant Hcp1 (Figure 41G). This shows that the mutant proteins do not enhance MNGC formation and also interfere with the natural development of MNGC.

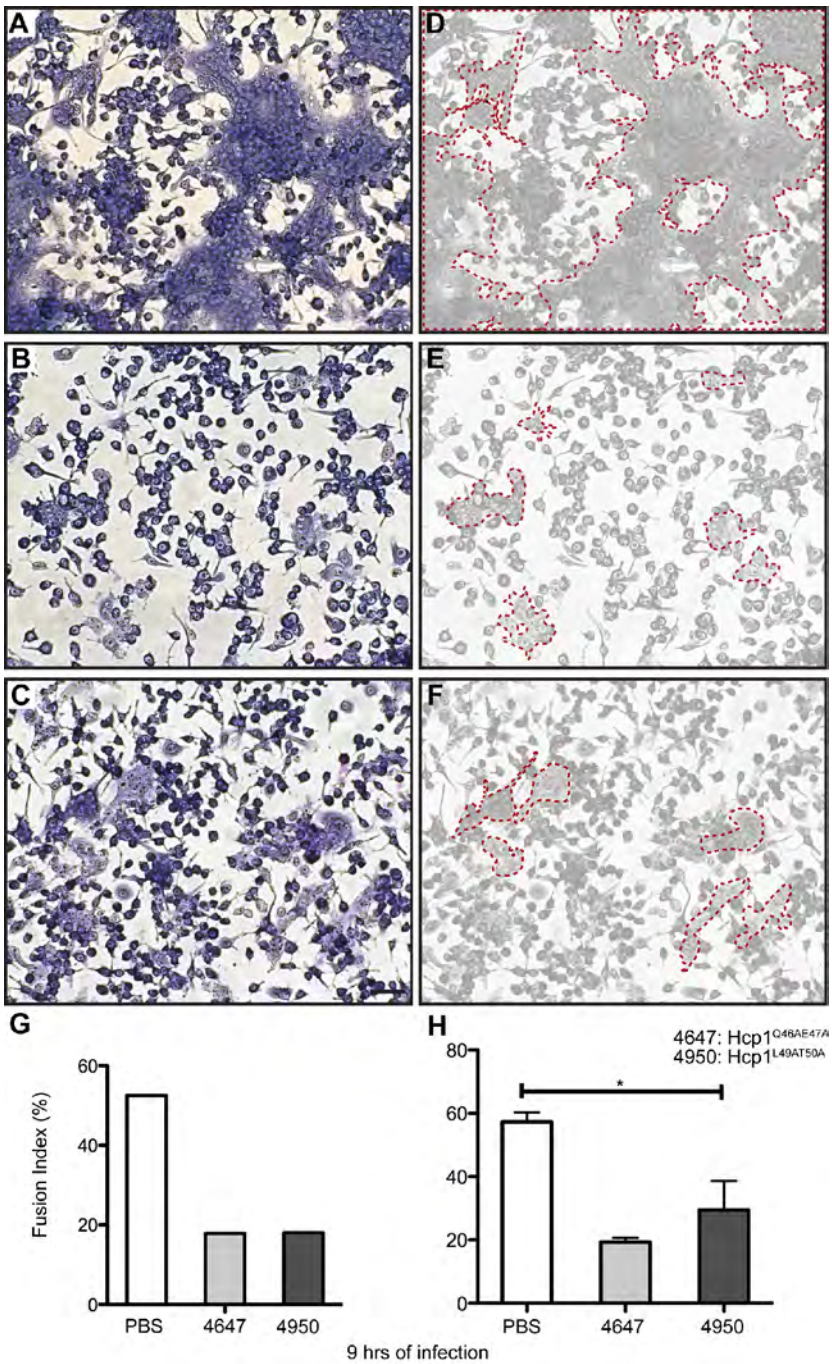

Figure 41: Effect of surface-bound mutant Hcp1 (Hcp1^{Q46AE47A} and Hcp1^{L49AT50A}) on MNGC formation. The treated cells were subsequently infected with wild type B. pseudomallei for 9 hrs and visualized with Giemsa stain (Figure 41A-C). The double mutants appear to suppress MNGC formation in infected cells (Figure 41B and C) relative to untreated infected cells (Figure 41A). The MNGC formed for each condition are outlined (dotted red lines) correspondingly against faded black-and-white rendering of the original colour image (Figure 41D-F). Fusion indices for each treatment were calculated for the experiment shown in Figure 41A-F (Figure 41G). Fusion indices on untreated or treated cells were calculated from three independent experiments and represented as means with standard deviation (Figure 41H). Scale bar: 40 µm.

To determine whether the same point mutations present in the endogenous Hcp of the bacteria compromise MNGC formation, we first generated a deletion knockout of *hcp1* in wild type *B. pseudomallei*, followed by knocking in a copy of *hcp1* with alanines substituted at either positions 46Q and 47E (KHW *hcp1*^{Q46AE47A}) or 49L and 50T (KHW *hcp1*^{L49AT50A}) at the original chromosomal site via homologous recombination. These double substitutions are the same as that found in Hcp1^{Q46AE47A} and Hcp1^{L49AT50A} respectively. However, we only managed to generate KHW *hcp1*^{L49AT50A}.

The double substitution mutant was unable to form MNGC at the time-points examined (Figure 42B and D), whereas MNGC formation was observed for the wild type bacteria (KHW) at both time points (Figure 42A and C). It was also unable to secrete Hcp1 as no Hcp1 (red) was detected on host cells (Figure 42F) in contrast to the wild type bacteria (Figure 42E). However, we also have to consider two possibilities that could have occurred due to the genetic manipulation. 1) The allelic complementation could have introduced off-target mutations that affected the bacteria's ability to form MNGCs. 2) The mutated Hcp might also not be expressed or not to the same levels as the wild type protein, therefore affecting detection of the secreted protein and subsequently MNGC formation. To control for the first possibility, the wild type copy of *hcp* should be reintroduced into KHW *hcp1*^{L49AT50A} by homologous recombination or complemented on a plasmid and assayed for the ability to form MNGC. A restoration to the wild type phenotype would be indicative for the absence of

off-target mutations. For the second possibility, the expression of Hcp should be assayed at the protein level for both wild type bacteria and KHW *hcp1*^{L49AT50A}.

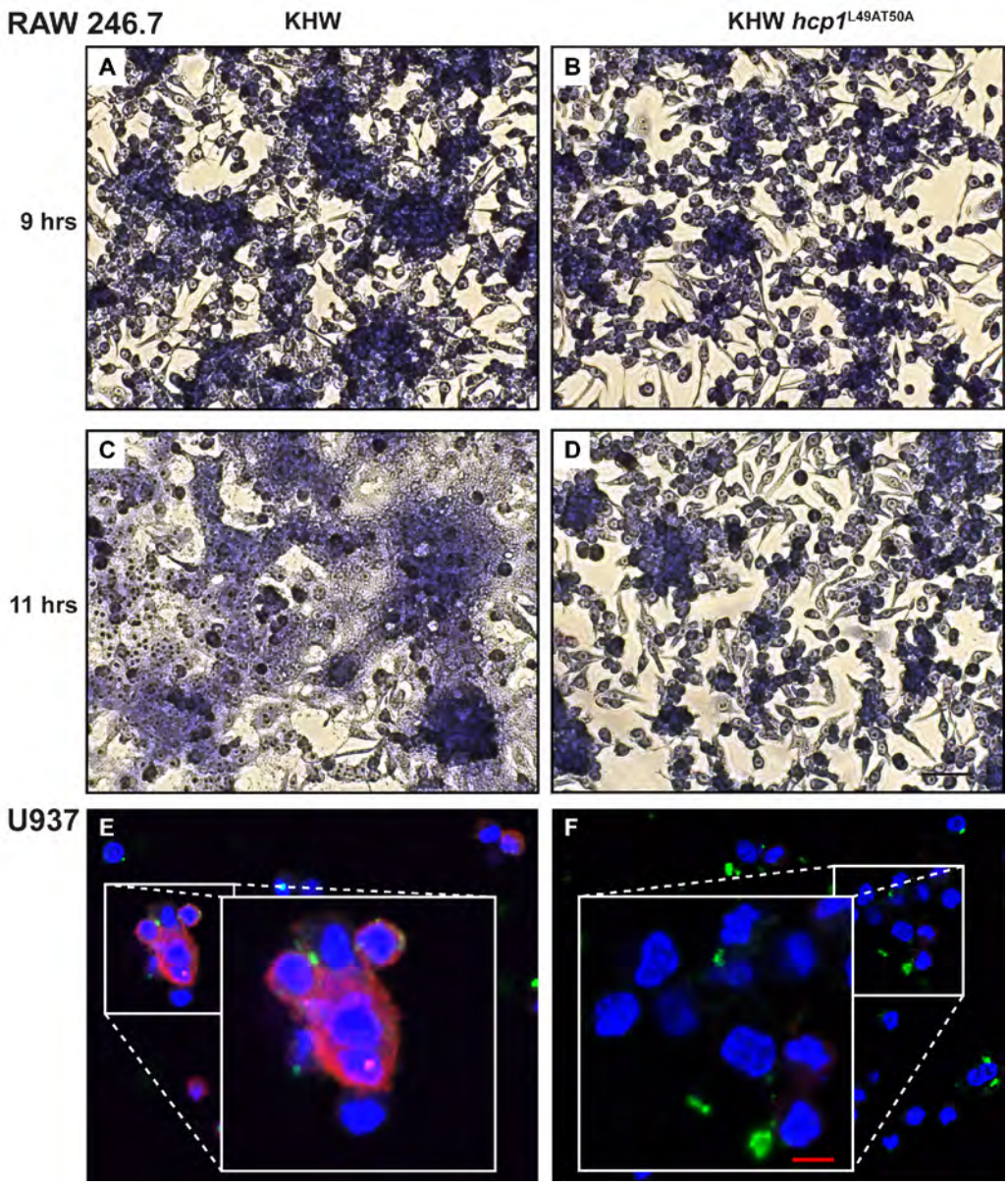

Figure 42: Effect of in situ L49AT50T substitution on the function of Hcp1. RAW 264.7 macrophages were infected with either overnight culture of wild type B. pseudomallei (KHW) or KHW hcp1^{L49AT50A} mutant for the indicated time points and were stained for MNGC formation (Figure 42A-D). Results shown are representative of two independent experiments. Activated U937 were infected with log phase wild type B. pseudomallei or KHW hcp1^{L49AT50A} mutant for 8 hr and stained for Hcp1 (red) (Figure 42E and F). The bacteria were stained by LPS (green). Mammalian cell nuclei were stained using DAPI (blue). Scale bar: 40µm (black) and 10 µm (red).

5.3 Discussion

Hcp1 from *B. pseudomallei* had previously been shown to be secreted by T6SS1 and could be recognized on an immunoblot by pooled sera of melioidosis patients.[70] We found that melioidosis patients have a high titer of anti-Hcp1 immunoglobulins, suggesting that Hcp1 from *B. pseudomallei* is a significant target of the host humoral response. Since Hcp1 could be detected on the surface of host cells early during *in vitro* infection before cell death occurs, it is possible that the protein is actively being secreted during infection rather than being released due to a passive process of host cell lysis. Recombinant Hcp1 from *B. pseudomallei* also binds to the surface of host cells. Its surface localization and preferential binding for antigen-presenting cells could contribute to its immunogenicity. A high anti-Hcp response was also previously reported in cystic fibrosis patients with chronic *P. aeruginosa* infections, but weak or negligible responses from patients infected with a shorter duration.[76] This means that Hcp protein is available for immune processing during bacterial infection.

To our knowledge, this is the first instance the detection and localization of endogenous Hcp has been imaged during an infection. The localization of endogenous Hcp within bacterial compartments had been studied by several groups,[102,140,141] and they reported that Hcp can be detected in all bacterial cellular compartments (membrane, periplasmic space and cytosol) and culture medium. However, we did not find much colocalization between Hcp1 and the

bacteria during infection. The anti-Hcp1 signal colocalized with the host cell membrane, hence the endogenous Hcp1 detected could be bound to the membrane. In *B. pseudomallei*, the overexpression of the two component regulatory system VirAG *in trans* is necessary for the detection of T6SS1 secreted substrates Hcp1 and VgrG in bacterial cultures.[142] This is because the expression of T6SS1 in free-living bacteria is very low.[71] Upon bacterial entry into host cytosol, intracellular cytosolic signals activate T6SS1 expression (Figure 43, point 1),[71] but these endogenous signals regulating its expression have not been reported. However, our assay circumvents this problem and allows the tracking of T6SS1 secretion and function during an infection when T6SS1 is highly upregulated.[71]

Cell-to-cell fusion is one of the basic biological capabilities of macrophages, as exemplified by the physiological example of osteoclast formation. The molecular mechanism of macrophage fusion is a multistage process, which firstly requires the macrophages to become fusion-competent, move towards each other, attach and bring their membranes within close proximity by the means of cell adhesion molecules, finally culminating into a merging of the cellular membranes and reorganization of intracellular components.[143,144] With respect to *B. pseudomallei*-induced MNGC of macrophages, primary or established cell lines, it has been shown that this process requires cell fusion factors such as integrin-associated protein (CD47), E-selectin (CD62E), E-cadherin, and fusion regulatory protein 1 (CD98) (Figure 43, point 3).[69] We identified four candidate mammalian ligands of Hcp1 by mass spectrometry and

SLC3A2 (4F2), the heavy chain of CD98, was biochemically validated as one of the ligands of Hcp1. Antibodies against CD98 have been shown to either suppress or enhance MNGC formation,[126,145] and it is possible that Hcp1's MNGC-enhancing effect mimics the MNGC-inducing anti-CD98 antibodies.

Although Hcp1 binds to host cells, we were unable to detect any Hcp1-induced cellular activation, unlike that reported in *A. hydrophila* and *E. coli.*[106,107] Surface-bound Hcp1 also does not induce more cell death or bacterial entry upon infection. However, it hastens the formation of MNGC although it does not cause MNGC formation on its own. Although MNGC formation has not been proven to contribute to disease during an *in vivo* infection, the presence of granulomas and giant cells in mouse models[67] and in melioidosis patients[68] suggest the relevance of MNGC in disease pathogenesis. Studies have shown that bacterial entry into host cytosol,[79,146] and the expression of T6SS1[64,71] are critical to MNGC formation by *B. pseudomallei.* The pre-incubation of cells with Hcp1 reduced the time required for MNGC formation, and we speculate that the coated Hcp1 acts as a seed for the oligomerization of endogenous Hcp1 (Figure 43, point 4). We speculate that this possible "seeding" effect could occur during an actual infection, whereby Hcp1 released by intracellular cytosolic bacteria binds the neighbouring uninfected host cells to prime these cells for subsequent cell-to-cell fusion and spread. However, Hcp1 is not the fusogenic factor, for addition of Hcp1 alone is insufficient to induce fusion (data not shown). Thus, the bacterial fusogenic factor remains to be identified and it is

likely that a T6SS1 secreted effector is responsible.

The mutations in the unique extended loop region of Hcp1 disrupt the stacking of the hexameric rings in the cell-free model, and thus likely compromise the formation of the tube-like structure (Figure 43, point 2). The double substitution bacterial mutant also did not secrete Hcp1 that was detectable on the surface of infected cells. We hypothesize that this could be an indication of defective tube assembly, with an associated impairment in the induction of MNGC. However, in order to support the hypothesis, additional controls have to be done to rule out the possibilities of off-target mutations that affect MNGC formation and reduced Hcp protein expression as a result of the allelic complementation. If the controls affirm that the substitutions were as intended and the protein expression remains unaffected, we may conclude that the inability of the mutant Hcp1 to self-assemble as stacks led to the dramatic suppression of MNGC formation during bacterial infection. This leads us to propose a model to explain the action of surface-bound Hcp1 in influencing MNGC formation (Figure 43). As T6SS1 expression occurs intracellularly[71,79] and MNGC is formed when the bacteria are in the cytosol[64,71], some bacteria in the cytosol could have their T6SS1 orientated towards the host cell surface. During an infection, Hcp1 secreted and bound on the cell surface could help in tube formation or increase interaction with host cell surface fusion factors such as CD98. On the other hand, the mutant Hcp1 with an altered structural configuration from the wild type protein may interact differently or impede interaction with host cell fusion factors to prevent cell

fusion. Our ability to change the structural and functional properties of Hcp with two amino acid changes in the loop region opens up the possibility that the recombinant mutant Hcp can be used as a tool to abrogate bacterial induced MNGC formation. This represents a novel strategy of limiting bacterial spread to neighbouring cells.

Thus, the way Hcp1 is stacked into assembly units depends critically on the residues in the extended loop region, and directly affects its function and the pathogenesis of the pathogen. We have shown that Hcp1 is not simply a structural component of T6SS1 but also functions like a T6SS effector. Hcp may have evolved additional roles in facilitating bacterial pathogenesis, such as improving its cell-to-cell spread through increased MNGC formation in this particular pathogen because of its unique ability to be secreted onto the surface of host cells and to promote cell fusion.

Structural analysis of the Hcp1 protein revealed an extended loop region that may be unique to *B. pseudomallei* Hcp1. This led us to select mutations in Hcp1 to determine how structural changes could affect its function. Pre-incubation of mutant Hcp1 suppressed MNGC formation during infection with *B. pseudomallei,* suggesting that it must actively interfere with the function of T6SS1. We show that substitution of Gln46 and Glu47 affects the stacking of Hcp1 hexamers, prevents the secretion of endogenous Hcp, and that CD98 is one of the ligands of Hcp1. Hence we speculate that $Hcp1^{Q46AE47A}$ interferes with

Hcp1 may hinder the formation of tube, and prevent the secretion of effector molecules (Figure 43, point 6). The exogenous Hcp mutant may also fail to interact with the cell fusion factors (Figure 43, point 7.)

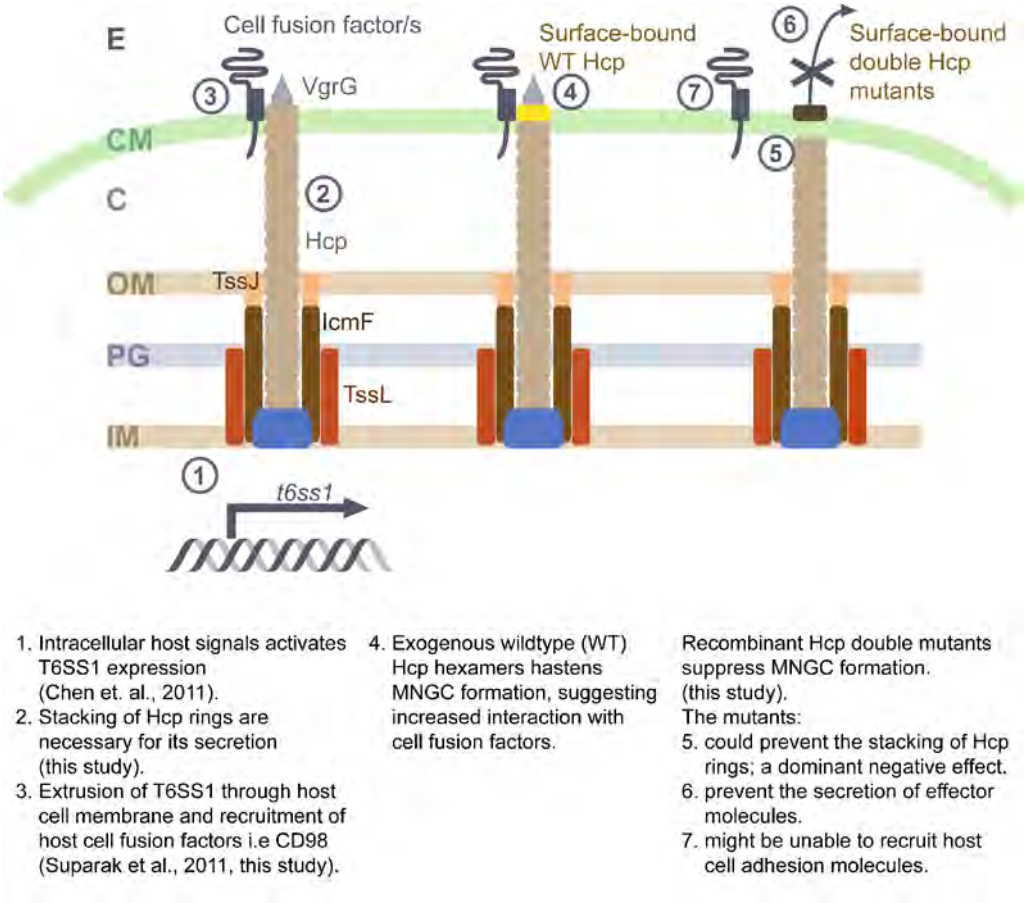

Figure 43: A hypothetical model proposing the mechanism of surface-bound Hcp1's (yellow) enhancement and Hcp1 mutants' (dark brown) suppression of MNGC formation. E, extracellular space; CM, host cell membrane; C, host cytosol; OM, bacterial outer membrane; PG, peptidoglycan; IM, bacterial inner membrane.

Chapter 6.

Final Discussion and Future Directions

Melioidosis is a potentially fatal disease caused by the Gram-negative bacterium *Burkholderia pseudomallei*. It is predominantly endemic in tropical climates and is a public health concern.[27] Its causative agent, *B. pseudomallei,* has been classified as category B bioterrorism agent by the US Centers for Disease Control and Prevention. It is a facultative intracellular bacterium that invades a range of phagocytic and non phagocytic cells, and resists killing by polymorphonuclear cells.[147–149] Internalized *B. pseudomallei* are capable of vacuolar escape into the host cytoplasm, inducing actin-based motility and actin-reorganization to form membrane protrusions.[64,150] What further defines the unique pathogenesis of *B. pseudomallei,* is the direct cell-to-cell fusion that contributes to the formation of MNGC.[65] MNGC formation has been identified as a function of the Type VI Secretion System cluster 1 (T6SS1), one of the six T6SSs *B. pseudomallei* possesses.[70,71] T6SS serves a range of function in other Gram-negative proteobacteria, such as mediating competitive inter-bacterial interactions or cooperative inter-bacterial behaviours,[80,87] but in the case of *B. pseudomallei*, T6SS1 is critical for bacterial pathogenesis *in vivo*.[70]

The specific role of MNGC formation in the pathogenesis of melioidosis remains to be defined. Nevertheless, granulomas in patients and chronic mouse infection models have been observed.[67,68] Granuloma formation *in vivo* following *B. pseudomallei* infection may represent either a host response to attempt to contain the organism, or a bacterial strategy to facilitate cell-to-cell spread, evade host immune responses, and persist within an infected host.

Studies on *B. pseudomallei*-induced MNGC showed that T6SS1 mutants i.e *ΔtssA*, *ΔtssB*, *Δhcp1*, *ΔbprC* and *ΔvirAG* were unable to cause MNGC formation.[70,71] These mutants affect T6SS1 expression, assembly and function, and thus highlight the critical role that T6SS1 plays in this process.

However, very little is known about the direct interactions between the host and the specific T6SS1 bacterial factors that regulate the process of MNGC formation. Our studies show for the first time that Hcp1, a hallmark protein of T6SS1 function, is also an effector protein that has the ability to hasten *B. pseudomallei*-induced MNGC formation. Its immunogenic properties may be due in part to its ability to be secreted and to bind to the surface of antigen-presenting cells. However, its ability to hasten MNGC formation could offset the disadvantage conferred by its immunogenic nature through reducing the surface-area of Hcp1's exposure to the host humoral defenses, thus shielding the innermost cells within the MNGC in which the bacteria are able to thrive. A vaccine study on Hcp1 showed that despite its immunogenic nature, *B. pseudomallei* Hcp1 is not a suitable vaccine candidate because of the poor

protection engendered against morbidity and mortality and its inability to prevent chronic colonization after challenge.[70] However, it was suggested that Hcp1 is a good candidate for use as a serodiagnostic reagent for melioidosis[70] and in support of this view, we have also found significant a anti-Hcp1 immunoglobulin response in melioidosis patients.

A recent study demonstrated that *B. pseudomallei*-induced fusion of human macrophages *in vitro* requires cell surface receptors which are namely CD47, CD62E, CD98 and CD324.[69] The authors proposed that *B. pseudomallei* may favour this process by modulating the surface expression of those receptors.[69] We discovered that Hcp1 binds to several host ligands, and supports their finding of CD98 as a binding partner of Hcp1. In lieu of these findings, it is possible that the bacterium promotes cell fusion by the combined effect of Hcp1's direct interaction with CD98, as well as through the upregulation of CD98 to promote greater interaction between secreted Hcp1. A biochemical validation of the two other candidate Hcp1 ligands, KIAA1967 (DBC1) and leukosialin (CD43), could also be done to verify if they too are involved in specific interactions with Hcp1.

We sought to understand the mechanism of Hcp1's role in *B. pseudomallei*-induced MNGC formation by solving the protein structure of *B. pseudomallei* Hcp1. Structure-guided mutagenesis of the Hcp1 protein led us to discover the region and the precise amino acids residues that are critical for tube formation. The very same mutations generated mutant proteins that were

able to suppress *B. pseudomallei*-induced MNGC formation, and *in situ* mutations in the bacteria prevented the secretion of endogenous Hcp1.

These findings were unexpected as the mutant proteins were capable of binding to the surface of cells. The mechanism of suppression by these surface-bound mutant proteins is currently under investigation in our laboratory. Our preliminary finding showed that the mutant Hcp1 did not competitively inhibit the binding of the wild type Hcp1, hence it would be interesting to find out if both mutant and wild type Hcp1 interact with the same panel of host cellular factors. In addition, imaging Hcp1 during an infection *in vitro* using cryo-electron microscopy would inform whether Hcp1 exists as tubes or as hexameric rings at the cell surface. A subsequent introduction of the Hcp1 mutant proteins into this experiment could show whether the mutant proteins perturb Hcp1's higher-ordered structure.

Hcp1's effects of MNGC formation could also be further dissected using a bacteria-free model of cell-fusion, namely the fusion of primary monocytes by activating anti-CD98 antibodies.[98] It would elucidate whether Hcp1 on its own is sufficient to affect MNGC formation, or that it requires other bacterial factors such as the other components of T6SS1.

The *in vivo* effect of the surface-bound mutant proteins during *B. pseudomallei* infection also warrants further investigation. It would be useful to examine if these mutant proteins could alter the pathology of the disease or limit bacterial

spread. A similar experiment could also be done with antibodies against the aforementioned cell surface molecules CD47 and CD98. A comparison of the resulting data would inform if the Hcp1 mutant proteins and the anti-cell surface molecule antibodies exert their suppressive effects on *B. pseudomallei*-induced MNGC formation in distinctive or similar ways.

In conclusion, our study uncovers a novel role for Hcp in *B. pseudomallei* infection that is disparate from its function as a component of the secretion apparatus in T6SS, and how critical amino acids in its unique extended loop contributes towards elucidating the mechanism of *B. pseudomallei*-induced MNGC formation.

Bibilography

1. White, N. J. Melioidosis. *The Lancet* **361,** 1715–1722 (2003).
2. Cheng, A. C. & Currie, B. J. Melioidosis: epidemiology, pathophysiology, and management. *Clin. Microbiol. Rev.* **18,** 383–416 (2005).
3. Whitmore, A. & Krishnaswami, C. S. An account of the discovery of a hitherto undescribed infective disease occuring among the population of Rangoon. *Indian Med. Gaz.* **47,** 262–267 (1912).
4. Stanton, A. T. & Fletcher, W. Melioidosis: a new disease of tropics. *Trans. 4th Congr. Far East. Assoc. Trop. Med.* **2,** 196–198 (1921).
5. Dance, D. A. Melioidosis: the tip of the iceberg? *Clin. Microbiol. Rev.* **4,** 52–60 (1991).
6. Howe, C., Sampath, A. & Sponitz, M. The *pseudomallei* group: a review. *J. Infect. Dis.* **124,** 598–606 (1971).
7. Ngauy, V., Lemeshev, Y., Sadkowski, L. & Crawford, G. Cutaneous melioidosis in a man who was taken as a prisoner of war by the Japanese during World War II. *J. Clin. Microbiol.* **43,** 970–972 (2005).
8. Currie, B. J., Dance, D. A. & Cheng, A. C. The global distribution of *Burkholderia pseudomallei* and melioidosis: an update. *Trans. R. Soc. Trop. Med. Hyg.* **102,** S1–S4 (2008).
9. Currie, B. J. *et al.* Melioidosis epidemiology and risk factors from a prospective whole-population study in northern Australia. *Trop. Med. Int.*

Health **9,** 1167–1174 (2004).

10. Suputtamongkol, Y. *et al.* The epidemiology of melioidosis in Ubon Ratchatani, northeast Thailand. *Int. J. Epidemiol.* **23,** 1082–1090 (1994).
11. Limmathurotsakul, D. *et al.* Increasing incidence of human melioidosis in northeast thailand. *Am. J. Trop. Med. Hyg.* **82,** 1113–1117 (2010).
12. Lo, T. J., Ang, L. W., James, L. & Goh, K. T. Melioidosis in a Tropical City State, Singapore. *Emerg. Infect. Dis.* **15,** 1645–1647 (2009).
13. How, S.H., Ng, K.H, Jamalludin, A.R, Shah, A. & Rathor, Y. Melioidosis in Pahang, Malaysia. *Med. J. Malaysia* **60,** 606–613 (2005).
14. Hassan, M. *et al.* Incidence, risk factors and clinical epidemiology of melioidosis: a complex socio-ecological emerging infectious disease in the Alor Setar region of Kedah, Malaysia. *Bmc Infect. Dis.* **10,** 302 (2010).
15. Heng, B. H., Goh, K. T., Yap, E. H. & Yeo, M. Epidemiological surveillance of melioidosis in Singapore. *Ann.-Acad. Med. Singap.* **27,** 478–484 (1998).
16. Currie, B. J. Advances and remaining uncertainties in the epidemiology of *Burkholderia pseudomallei* and melioidosis. *Trans. R. Soc. Trop. Med. Hyg.* **102,** 225–227 (2008).
17. Limmathurotsakul, D. *et al.* Systematic review and consensus guidelines for environmental sampling of *Burkholderia pseudomallei*. *PLoS Negl. Trop. Dis.* **7,** e2105 (2013).
18. Shih, H.-I. *et al.* Sporadic and outbreak cases of melioidosis in southern

taiwan: clinical features and antimicrobial susceptibility. *Infection* **37,** 9-15 (2008).

19. Yang, S. Melioidosis research in China. *Acta Trop.* **77,** 157–165 (2000).
20. John, T.J. *et al.* Melioidosis in India: the tip of the iceberg? *Indian J. Med. Res.* **103,** 62–65 (1996).
21. Rolim, D. B. *et al.* Melioidosis, northeastern Brazil. *Emerg. Infect. Dis.* **11,** 1458 (2005).
22. Kronmann, K., Truett, A., Hale, B. & Crum-Cianflone, N. Melioidosis after brief exposure: a serologic survey in US marines. *Am. J. Trop. Med. Hyg.* **80,** 182–184 (2009).
23. Ezzedine, K., Heenen, M. & Malvy, D. Melioidosis in traveler, Belgium. **13,** 946–947 (2007).
24. Yazdanpanah, Y. *et al.* Melioidotic osteomyelitis of the femur occuring in a traveler. *J. Travel Med.* **9,** 53–54 (2002).
25. Visca, P., Cazzola, G., Petrucca, A. & Braggion, C. Travel-associated *Burkholderia pseudomallei* infection (melioidosis) in a patient with cystic fibrosis: a case report. *Clin. Infect. Dis.* **32,** E15–E16 (2001).
26. Schwarzmaier, A., Riezinger-Geppert, G., Schober, G., Karnik, R. & Valentin, A. Fulminant septic melioidosis after a vacation in Thailand. *Wien Klin. Wochenschr.* **112,** 892–895 (2000).
27. Dance, D. A. Melioidosis as an emerging global problem. *Acta Trop.* **74,** 115–119 (2000).
28. Wiersinga, W. J., van der Poll, T., White, N. J., Day, N. P. & Peacock, S. J.

Melioidosis: insights into the pathogenicity of *Burkholderia pseudomallei*. *Nat. Rev. Microbiol.* **4,** 272–282 (2006).

29. Wiersinga, W. J., Currie, B. J. & Peacock, S. J. Melioidosis. *N. Engl. J. Med.* **367,** 1035–1044 (2012).
30. Currie, B. J., Ward, L. & Cheng, A. C. The epidemiology and clinical spectrum of melioidosis: 540 cases from the 20 Year Darwin prospective study. *PLoS Negl. Trop. Dis.* **4,** e900 (2010).
31. Chaowagul, W. *et al.* Melioidosis: a major cause of community-acquired septicemia in northeastern Thailand. *J. Infect. Dis.* **159,** 890–899 (1989).
32. Currie, B. J. & Jacups, S. P. Intensity of rainfall and severity of melioidosis, Australia. *Emerg. Infect. Dis.* **9,** 1538 (2003).
33. Ketterer, P.J *et al.* Melioidosis in intensive piggeries in South-Eastern Queensland. *Aust. Vet. J.* **63,** 146–149
34. Limmathurotsakul, D. *et al.* Activities of daily living associated with acquisition of melioidosis in Northeast Thailand: a matched case-control study. *PLoS Negl. Trop. Dis.* **7,** e2072 (2013).
35. Holland, D. J, Wesley, A, Drinkovic, D & Currie, B.J. Cystic fibrosis and *Burkholderia pseudomallei*: an emerging problem. *Clin. Infect. Dis.* **35,** e138–e140 (2002).
36. McCormick, J. *et al.* Human-to-human transmission of *Pseudomonas pseudomallei*. *Ann. Intern. Med.* **83,** 512–513 (1975).
37. Halder, D, Zainal, N, Wah, C.M & Haq, J.A. Neonatal meningitis and septicaemia caused by *Burkholderia pseudomallei. Ann. Trop. Paediatr.*

18, 161–164 (1998).

38. Lumbiganon, P., Chotechuangnirun, N & Kosalaraksa, P. Neonatal melioidosis: a report of 5 cases.

39. Punyagupta, S., Sirisanthana, T. & Stapatayavong, B. in *Melioidosis* 217–229 (Bangkok Medical Publisher, 1989).

40. Ralph, A., McBride, J. & Currie, B. Transmission of *Burkholderia pseudomallei* via breast milk in northern Australia. *Pediatr. Infect. Dis. J.* **23,** 1169–1171 (2004).

41. Low, Choy, Mayo, J.M, Janmaat, A & Currie, B.J, B. J. Animal melioidosis in Australia. *Acta Trop.* **74,** (2000).

42. Leelarasamee, A. & Bovornkitti, S. Melioidosis: a review and update. *Rev. Infect. Dis.* **11,** 413–425 (1989).

43. Chaowagul, W. *et al.* Relapse in melioidosis: incidence and risk factors. *J. Infect. Dis.* **168,** 1181–1185 (1993).

44. Mathew, S. *et al.* Surgical presentation of melioidosis in India. *Natl. Med. J. India* **12,** 59–61 (1999).

45. Puthucheary, S., Parasakthi, N. & Lee, M. Septicaemic melioidosis: a review of 50 cases from Malaysia. *Trans. R. Soc. Trop. Med. Hyg.* **86,** 683–685 (1992).

46. Wibulpolprasert, B. & Dhiensiri, T. Visceral organ abscesses in melioidosis: sonographic findings. *J. Clin. Ultrasound* **27,** 29–34 (1999).

47. Kandasamy, Y. & Norton, R. Paediatric melioidosis in North Queensland, Australia. *J. Paediatr. Child Health* **44,** 706–708 (2008).

48. Edmond, K., Bauert, P. & Currie, B. Paediatric melioidosis in the Northern Territory of Australia: an expanding clinical spectrum. *J. Paediatr. Child Health* **37,** 337–341 (2001).

49. Edmond, K., Currie, B., Brewster, D. & Kilburn, C. Paediatric melioidosis in tropical Australia. *Pediatr. Infect. Dis. J.* **17,** 77–80 (1998).

50. Woods, M. *et al.* Neurological melioidosis: seven cases from the Northern Territory of Australia. *Clin. Infect. Dis.* **15,** 163–169 (1992).

51. Lumbiganon, P. & Viengnondha, S. Clinical manifestations of melioidosis in children. *Pediatr. Infect. Dis. J.* **14,** 136–140 (1995).

52. Saipan, P. Neurological manifestations of melioidosis in children. *Southeast Asian J. Trop. Med. Public Health* **29,** 856–859 (1998).

53. Simpson, A. J. H, Howe, P. A, Wuthiekanun, V & White, N. J. A comparison of lysis centrifugation, pour plate, and conventional blood culture methods in the diagnosis of septicaemic melioidosis. *J. Clin. Pathol.* **52,** 616–619 (1999).

54. Dance, D.A.B, Wuthiekanun, V, Naigowit, P & White, N. J. Identification of *Pseudomonas pseudomallei* in clinical practice: use of simple screening tests and API 20NE. *J. Clin. Pathol.* **42,** 645–648 (1989).

55. Anuntagool, N *et al.* Monoclonal antibody-based rapid identification of *Burkholderia pseudomallei* in blood culture fluid from patients with community-acquired septicaemia. *J. Med. Microbiol.* **49,** 1075–1078

56. Ashdown, L.R. Indirect haemagglutination test for melioidosis. *Med. J. Aust.* **147,** 364–365

57. Naigowit, P *et al.* Application of indirect immunofluorescence microscopy to colony identification of *Pseudomonas pseudomallei. Asia Pac. J. Allergy Immunol.* **11,** 149–154

58. Walsh, A. L *et al.* Immunofluorescence microscopy for the rapid diagnosis of melioidosis. *J. Clin. Pathol.* **47,** 377–379

59. Yap, E. H. *et al.* Serodiagnosis of melioidosis in Singapore by the indirect haemagglutination test. *Singapore Med. J.* **32,**

60. Lipsitz, R. *et al.* Workshop on treatment of and postexposure prophylaxis for *Burkholderia pseudomallei* and *B. mallei* infection, 2010. *Emerg. Infect. Dis.* **18,** e2 (2010).

61. Chetchotisakd, P. *et al.* Trimethoprim-sulfamethoxazole versus trimethoprim-sulfamethoxazole plus doxycycline as oral eradicative treatment for melioidosis (MERTH): a multicentre, double-blind, non-inferiority, randomised controlled trial. *The Lancet* (2013). doi:10.1016/S0140-6736(13)61951-0

62. Limmathurotsakul, D. *et al.* Risk factors for recurrent melioidosis in northeast Thailand. *Clin. Infect. Dis.* **43,** 979–986 (2006).

63. Galyov, E. E., Brett, P. J. & DeShazer, D. Molecular insights into *Burkholderia pseudomallei* and *Burkholderia mallei* pathogenesis. *Annu. Rev. Microbiol.* **64,** 495–517 (2010).

64. French, C. T. *et al.* Dissection of the *Burkholderia* intracellular life cycle using a photothermal nanoblade. *Proc. Natl. Acad. Sci.* **108,** 12095–12100 (2011).

65. Kespichayawattana, W., Rattanachetkul, S., Wanun, T., Utaisincharoen, P. & Sirisinha, S. *Burkholderia pseudomallei* induces cell fusion and actin-associated membrane protrusion: a possible mechanism for cell-to-cell spreading. *Infect. Immun.* **68,** 5377–5384 (2000).

66. Bernadette M Saunders, W. J. B. Life and death in the granuloma: immunopathology of tuberculosis. *Immunol. Cell Biol.* **85,** 103–111 (2007).

67. Conejero, L. *et al.* Low-dose exposure of C57BL/6 mice to *Burkholderia pseudomallei* mimics chronic human melioidosis. *Am. J. Pathol.* **179,** 270–280 (2011).

68. Wong, K.T, Puthucheary, S.D & Vadivelu, J. The histopathology of human melioidosis. *Histopathology* **26,** 51–55 (1995).

69. Suparak, S. *et al.* Burkholderia pseudomallei-induced cell fusion in U937 macrophages can be inhibited by monoclonal antibodies against host cell surface molecules. *Microbes Infect.* **13,** 1006–1011 (2011).

70. Burtnick, M. N. *et al.* The cluster 1 type VI secretion system is a major virulence determinant in Burkholderia pseudomallei. *Infect. Immun.* **79,** 1512–1525 (2011).

71. Chen, Y. *et al.* Regulation of type VI secretion system during *Burkholderia pseudomallei* infection. *Infect. Immun.* **79,** 3064–3073 (2011).

72. Williams, S. G., Varcoe, L. T., Attridge, S. R. & Manning, P. A. Vibrio cholerae Hcp, a secreted protein coregulated with HlyA. *Infect. Immun.*

64, 283–289 (1996).

73. Das, S. & Chaudhuri, K. Identification of a unique IAHP (IcmF associated homologous proteins) cluster in *Vibrio cholerae* and other proteobacteria through in silico analysis. *In Silico Biol.* **3,** 287–300 (2003).

74. Bladergroen, M., Badelt, K. & Spaink, H. Infection-blocking genes of a symbiotic *Rhizobium leguminosarum* strain that are involved in temperature-dependent protein secretion. *Mol. Plant. Microbe Interact.* **16,** 53–64 (2003).

75. Pukatzki, S. *et al.* Identification of a conserved bacterial protein secretion system in *Vibrio cholerae* using the Dictyostelium host model system. *Proc. Natl. Acad. Sci. U. S. A.* **103,** 1528–1533 (2006).

76. Mougous, J. D. *et al.* A virulence locus of *Pseudomonas aeruginosa* encodes a protein secretion apparatus. *Science* **312,** 1526–1530 (2006).

77. Boyer, F., Fichant, G., Berthod, J., Vandenbrouck, Y. & Attree, I. Dissecting the bacterial type VI secretion system by a genome wide in silico analysis: what can be learned from available microbial genomic resources? *Bmc Genomics* **10,** 104 (2009).

78. Cascales, E. The type VI secretion toolkit. *EMBO Rep.* **9,** 735–741 (2008).

79. Burtnick, M. N., DeShazer, D., Nair, V., Gherardini, F. C. & Brett, P. J. *Burkholderia mallei* cluster 1 type VI secretion mutants exhibit growth and actin polymerization defects in RAW 264.7 murine macrophages. *Infect. Immun.* **78,** 88–99 (2010).

80. Schwarz, S. *et al. Burkholderia* type VI secretion systems have distinct

roles in eukaryotic and bacterial cell interactions. *Plos Pathog.* **6,** e1001068 (2010).

81. Lesic, B., Starkey, M., He, J., Hazan, R. & Rahme, L. Quorum sensing differentially regulates *Pseudomonas aeruginosa* type VI secretion locus I and homologous loci II and III, which are required for pathogenesis. *Microbiology* **155,** 2845–55 (2009).
82. Records, A. R. The type VI secretion system: a multipurpose delivery system with a phage-like machinery. *Mol. Plant. Microbe Interact.* **24,** 751–757 (2011).
83. Russell, A. B. *et al.* Type VI secretion delivers bacteriolytic effectors to target cells. *Nature* **475,** 343–347 (2011).
84. Schell, M. A. *et al.* Type VI secretion is a major virulence determinant in *Burkholderia mallei*. *Mol. Microbiol.* **64,** 1466–1485 (2007).
85. Shalom, G., Shaw, J. G. & Thomas, M. S. *In vivo* expression technology identifies a type VI secretion system locus in *Burkholderia pseudomallei* that is induced upon invasion of macrophages. *Microbiology* **153,** 2689–2699 (2007).
86. Silverman, J. M., Brunet, Y. R., Cascales, E. & Mougous, J. D. Structure and regulation of the type VI secretion system. *Annu. Rev. Microbiol.* **66,** 453–472 (2012).
87. Hood, R. D. *et al.* A type VI secretion system of *Pseudomonas aeruginosa* targets a toxin to bacteria. *Cell Host Microbe* **7,** 25–37 (2010).
88. Bingle, L. E., Bailey, C. M. & Pallen, M. J. Type VI secretion: a

beginner's guide. *Curr. Opin. Microbiol.* **11,** 3–8 (2008).

89. Zheng, J. & Leung, K. Y. Dissection of a type VI secretion system in *Edwardsiella tarda*. *Mol. Microbiol.* **66,** 1192–1206 (2007).

90. Felisberto-Rodrigues, C. *et al.* Towards a structural comprehension of bacterial type VI secretion systems: characterization of the TssJ-TssM complex of an *Escherichia coli* pathovar. *Plos Pathog.* **7,** e1002386 (2011).

91. Aschtgen, M.-S., Gavioli, M., Dessen, A., Lloubès, R. & Cascales, E. The SciZ protein anchors the enteroaggregative *Escherichia coli* type VI secretion system to the cell wall. *Mol. Microbiol.* **75,** 886–899 (2010).

92. Leiman, P. *et al.* Morphogenesis of the T4 tail and tail fibers. *Virol. J.* **7,** 355 (2010).

93. Lossi, N. S., Dajani, R., Freemont, P. & Filloux, A. Structure-function analysis of HsiF, a gp25-like component of the type VI secretion system, in *Pseudomonas aeruginosa*. *Microbiology* **157,** 3292–3305 (2011).

94. Cascales, E. & Cambillau, C. Structural biology of type VI secretion systems. *Philos. Trans. R. Soc. B Biol. Sci.* **367,** 1102–1111 (2012).

95. Bönemann, G., Pietrosiuk, A., Diemand, A., Zentgraf, H. & Mogk, A. Remodelling of VipA/VipB tubules by ClpV-mediated threading is crucial for type VI protein secretion. *Embo J.* **28,** 315–325 (2009).

96. Leiman, P. G. *et al.* Type VI secretion apparatus and phage tail-associated protein complexes share a common evolutionary origin. *Proc. Natl. Acad. Sci.* **106,** 4154–4159 (2009).

97. Browning, C., Shneider, M. M., Bowman, V. D., Schwarzer, D. & Leiman, P. G. Phage pierces the host cell membrane with the iron-loaded spike. *Structure* **20,** 326–339 (2012).

98. Bönemann, G., Pietrosiuk, A. & Mogk, A. Tubules and donuts: a type VI secretion story. *Mol. Microbiol.* **76,** 815–821 (2010).

99. Pukatzki, S., McAuley, S. B. & Miyata, S. T. The type VI secretion system: translocation of effectors and effector-domains. *Curr. Opin. Microbiol.* **12,** 11–17 (2009).

100. Ballister, E. R., Lai, A. H., Zuckermann, R. N., Cheng, Y. & Mougous, J. D. In vitro self-assembly of tailorable nanotubes from a simple protein building block. *Proc. Natl. Acad. Sci.* **105,** 3733–3738 (2008).

101. Osipiuk, J. *et al.* Crystal structure of secretory protein Hcp3 from *Pseudomonas aeruginosa*. *J. Struct. Funct. Genomics* **12,** 21–26 (2011).

102. Jobichen, C. *et al.* Structural basis for the secretion of EvpC: a key type VI secretion system protein from *Edwardsiella tarda*. *Plos One* **5,** e12910 (2010).

103. Pukatzki, S., Ma, A. T., Revel, A. T., Sturtevant, D. & Mekalanos, J. J. Type VI secretion system translocates a phage tail spike-like protein into target cells where it cross-links actin. *Proc. Natl. Acad. Sci.* **104,** 15508–15513 (2007).

104. Hachani, A. *et al.* Type VI secretion system in *Pseudomonas aeruginosa*: secretion and multimerization of VgrG proteins. *J. Biol. Chem.* **286,** 12317–12327 (2011).

105. Kanamaru, S. Structural similarity of tailed phages and pathogenic bacterial secretion systems. *Proc. Natl. Acad. Sci.* **106,** 4067–4068 (2009).

106. Suarez, G., Sierra, J. C., Kirtley, M. L. & Chopra, A. K. Role of Hcp, a type 6 secretion system effector, of *Aeromonas hydrophila* in modulating activation of host immune cells. *Microbiology* **156,** 3678–3688 (2010).

107. Zhou, Y. *et al.* Hcp family proteins secreted via the type VI secretion system coordinately regulate *Escherichia coli* K1 interaction with human brain microvascular endothelial cells. *Infect. Immun.* **80,** 1243–1251 (2012).

108. Suarez, G. *et al.* Molecular characterization of a functional type VI secretion system from a clinical isolate of *Aeromonas hydrophila*. *Microb. Pathog.* **44,** 344–361 (2008).

109. Silverman, J. M. *et al.* Haemolysin Coregulated Protein Is an Exported Receptor and Chaperone of Type VI Secretion Substrates. *Mol. Cell* **51,** 584–593 (2013).

110. Schafer, A. *et al.* Small mobilizable multi-purpose cloning vectors derived from the *Escherichia coli* plasmids pK18 and pK19: selection of defined deletions in the chromosome of *Corynebacterium glutamicum*. *Gene* **145,** 69–73 (1994).

111. Sun, G. W. *et al.* Identification of a regulatory cascade controlling Type III Secretion System 3 gene expression in *Burkholderia pseudomallei. Mol. Microbiol.* **76,** 677–689 (2010).

112. Lefebre, M. D. & Valvano, M. A. Construction and evaluation of plasmid

vectors optimized for constitutive and regulated gene expression in *Burkholderia cepacia* complex isolates. *Appl. Environ. Microbiol.* **68,** 5956–5964 (2002).

113. West, S., Schweizer, H., Dall, C., Sample, A. & Runyen-Janecky, L. Construction of improved *Escherichia-Pseudomonas* shuttle vectors derived from pUC18/19 and sequence of the region required for their replication in *Pseudomonas aeruginosa. Gene* **148,** 81–86 (1994).
114. Liu, B., Ghee, G. K., Eu, H. Y., Chua, K. L. & Gan, Y. H. Model of differential susceptibility to mucosal *Burkholderia pseudomallei* infection. *Infect. Immun.* **70,** 504–511 (2002).
115. Simon, A., Priefer, U. & Pühler, A. A broad range mobilization system for *in vitro* genetic engineering: transposon mutagenesis in gram-negative bacteria. *Nat. Biotechnol.* **1,** 784–791 (1983).
116. Köhler, G. & Milstein, C. Continuous cultures of fused cells secreting antibody of predefined specificity. *Nature* **256,** 495–497 (1975).
117. Ho, S. N., Hunt, H. D., Horton, R. M., Pullen, J. K. & Pease, L. R. Site-directed mutagenesis by overlap extension using the polymerase chain reaction. *Gene* **77,** 51–59 (1989).
118. Doublié, S. Preparation of selenomethionyl proteins for phase determination. *Methods Enzym.* **276,** 523–30 (1997).
119. Terwilliger, T. C. & Berendzen, J. Bayesian correlated MAD phasing. *Acta Crystallogr. D Biol. Crystallogr.* **53,** 571–9 (1997).
120. Otwinowski, Z. & Minor, W. in *Methods Enzymol.* **276,** 307–326

(Academic Press, 1997).

121. Adams, P. D. *et al.* PHENIX: a comprehensive Python-based system for macromolecular structure solution. *Acta Crystallogr. D Biol. Crystallogr.* **66,** 213–221 (2010).
122. Terwilliger, T. C. Automated main-chain model building by template matching and iterative fragment extension. *Acta Crystallogr. D Biol. Crystallogr.* **D59,** 38–44 (2003).
123. Emsley, P. & Cowtan, K. Coot: model-building tools for molecular graphics. *Acta Crystallogr. D Biol. Crystallogr.* **60,** 2126–2132 (2004).
124. Livak, K. & Schmittgen, T. Analysis of relative gene expression data using real-time quantitative PCR and the 2(-Delta Delta C(T)) Method. *Methods* **25,** 402–408 (2001).
125. Suparak, S. *et al.* Multinucleated giant cell formation and apoptosis in infected host cells is mediated by *Burkholderia pseudomallei* type III secretion protein BipB. *J. Bacteriol.* **187,** 6556–6560 (2005).
126. Mori, K. *et al.* The functional interaction between CD98 and CD147 in regulation of virus-induced cell fusion and osteoclast formation. *Med. Microbiol. Immunol. (Berl.)* **193,** 155–162 (2004).
127. Perkins, D.N, Pappin, D.J.C, Creasy, D.M & Cottrell, J.S. Probability-based protein identification by searching sequence database using mass spectrometry data. *Electrophoresis* **20,** 3551–3567 (1999).
128. Pallen, M. J., Chaudhuri, R. R. & Henderson, I. R. Genomic analysis of secretion systems. *Curr. Opin. Microbiol.* **6,** 519–527 (2003).

129. Martin, A.C.R. Accessing the Kabat antibody sequence database by computer. *Proteins Struct. Funct. Genet.* **25,** 130–133 (1996).

130. Messerschmidt, A. in *X-Ray Crystallogr. Biomacromolecules* 47–78 (Wiley-VCH Verlag GmBH & Co. KGaA, 2007).

131. Ramachandran, G., Ramakrishnan, C. & Sasisekharan, V. Stereochemistry of polypeptide chain configuration. *J. Mol. Biol.* **7,** 95–99 (1963).

132. Holm L & Sander C. Removing near-neighbour redundancy from large protein sequence collections. *Bioinformatics* **14,** 423–429 (1998).

133. Larkin, M. *et al.* Clustal W and Clustal X version 2.0. *Bioinformatics* **23,** 2947–2948 (2007).

134. Felgner, P. L. *et al.* A *Burkholderia pseudomallei* protein microarray reveals serodiagnostic and cross-reactive antigens. *Proc. Natl. Acad. Sci.* **106,** 13499–13504 (2009).

135. Tabata, N *et al.* Induction of homotypic cell aggregation and formation of multinucleated giant cells by anti-FRP-1 monoclonal antibodies. *J. Immunol.* **153,** (1994).

136. Kim, J., Chen, J. & Lou, Z. DBC1 is a negative regulator of SIRT1. *Nature* **451,** 2008

137. Zhao, W. *et al.* Negative regulation of the deacetylase SIRT1 by DBC1. *Nature* **451,** 587–590 (2008).

138. Escande, C. *et al.* Deleted in breast cancer-1 regulates SIRT1 activity and contributes to high-fat diet-induced liver steatosis in mice. *J. Clin. Invest.* **120,** 545–558 (2010).

139. Remold-O'Donnell, E., Zimmerman, C., Kenney, D. & Rosen, F. Expression on blood cells of sialophorin, the surface glycoprotein that is defective in Wiskott-Aldrich syndrome. *Blood* **70,** 104–109 (1987).

140. Wu, H.-Y., Chung, P.-C., Shih, H.-W., Wen, S.-R. & Lai, E.-M. Secretome analysis uncovers an Hcp-family protein secreted via a type VI secretion system in *Agrobacterium tumefaciens*. *J. Bacteriol.* **190,** 2841–2850 (2008).

141. Miyata, S., Kitaoka, M., Brooks, T., McAuley, S. & Pukatzki, S. *Vibrio cholerae* requires the type VI secretion system virulence factor VasX to kill *Dictyostelium discoideum*. *Infect. Immun.* **79,** 2941–2949 (2011).

142. Schell, M. A. *et al.* Type VI secretion is a major virulence determinant in *Burkholderia mallei*. *Mol. Microbiol.* **64,** 1466–1485 (2007).

143. Helming, L. & Gordon, S. Molecular mediators of macrophage fusion. *Trends Cell Biol.* **19,** 514–522 (2009).

144. Vignery, A. Macrophage fusion: the making of osteoclasts and giant cells. *J. Exp. Med.* **202,** 337–340 (2005).

145. Namba, K. *et al.* Involvement of ADAM9 in multinucleated giant cell formation of blood monocytes. *Cell. Immunol.* **213,** 104–113 (2001).

146. Muangsombut, V. *et al.* Inactivation of *Burkholderia pseudomallei* bsaQ results in decreased invasion efficiency and delayed escape of bacteria from endocytic vesicles. *Arch. Microbiol.* **190,** 623–631 (2008).

147. Allwood, E.M, Devenish, R.J, Prescott, M, Adler, B & Boyce, J.D.

Strategies for intracellular survival of *Burkholderia pseudomallei*. *Front. Microbiol.* **2,** 170 (2011).

148. Pilatz, S. *et al.* Identification of *Burkholderia pseudomallei* genes required for the intracellular life cycle and in vivo virulence. *Infect. Immun.* **74,** 3576–3586 (2006).
149. Chanchamroen, S., Kewcharoenwong, C., Susaengrat, W., Ato, M. & Lertmemongkolchai, G. Human polymorphonuclear neutrophil responses to *Burkholderia pseudomallei* in healthy and diabetic subjects. *Infect. Immun.* **77,** 456–463 (2009).
150. Stevens, M. P. *et al.* Identification of a bacterial factor required for actin-based motility of *Burkholderia pseudomallei. Mol. Microbiol.* **56,** 40–53 (2005).
151. Golledge, C., Chin, W., Tribe, A., Condon, R. & Ashdown, L. A case of human melioidosis originating in south-west Western Australia. *Med. J. Aust.* **157,** 332–334 (1992).
152. Gouet, P., Courcelle, E., Stuart, D. & Metoz, F. ESPript: analysis of multiple sequence alignments in PostScript. *Bioinformatics* **15,** 305–308 (1999).
153. Galimand, M. & Dodin, A. Focus on melioidosis throughout the world. *Bull. Soc. Pathol. Exot. Filiales* **62,** 259–263 (1969).
154. Laskowski, R., MacArthur, M., Moss, D. & Thorton, J. PROCHECK: a program to check the stereochemical quality of protein structures. *J. Appl. Crystallogr.* **26,** 283–291 (1993).

155. Zanetti, F., De Luca, G. & Stampi, S. Recovery of *Burkholderia pseudomallei* and *B. cepacia* from drinking water. *Int. J. Food Microbiol.* **59,** 67–72 (2000).

156. Delano, W. The PyMOL molecular graphics system. (2002).